國立台灣大學生命科學院分子與細胞生物學研究所

博士論文

Institute of Molecular and Cellular Biology

College of Life Science

National Taiwan University

Doctoral Dissertation

表皮生長因子與 PYR-1 在線蟲中影響特定細胞凋亡的

機制研究

Characterization of EGF signaling and PYR-1 in the death

of specific cells in *C. elegans*

蔣沆祥

Hang-Shiang Jiang
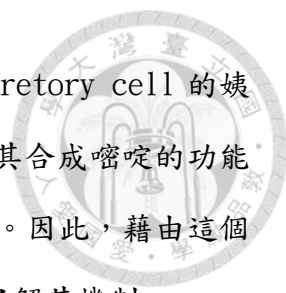
指導教授：吳益群 教授

Advisor: Yi-Chun Wu, Ph.D.

中華民國 103 年 7 月

July, 2014

摘要

計畫性細胞凋亡在生物體發育上扮演重要的角色。儘管執行計畫性細胞凋亡的基因已被發現且研究許多，這些基因如何在生物發育過程中被啟動與調控仍然有待發掘。我們發現在線蟲中，表皮生長因子〈LIN-3/EGF〉會以一種外來訊號的方式促進特定細胞的計畫性細胞凋亡。過少的 EGF 會導致計畫性細胞凋亡的減少；反之，過多的 EGF 會導致計畫性細胞凋亡的增加。這表示在生物體中，EGF 必須保持在一個適當的濃度以確保適度的計畫性細胞凋亡進行。藉由遺傳分析，我們發現 EGF 會藉由上皮生長因子受器〈LET-23/EGFR〉活化下游 Mitogen-Activated Protein Kinase〈MAPK〉路徑以及 ETS 轉錄因子〈LIN-1〉來促進線蟲中的 BH3-only 基因〈*egl-1*〉的轉錄並進一步引起特定細胞中的計畫性細胞凋亡。利用即時定量聚合酶連鎖反應和活體螢光觀測，我們發現在 EGF 的突變株中，*egl-1* 的轉錄量會減少。更進一步地，利用凝膠遷移實驗〈EMSA〉以及異位表現基因的方式，我們證明了 LIN-1 可以直接結合到 *egl-1* 的啟動子上，而且這個結合對於表皮生長因子在活體中促進計畫性細胞凋亡來說是重要的。這些結果說明了表皮生長因子可以藉由提升 *egl-1* 的轉錄來促進特定計畫性細胞凋亡。

為了進一步找出在線蟲中參與計畫性細胞凋亡的調控因子，我們將 *grp-1* 突變株處理突變劑並找尋具有尾巴缺陷的突變株。GRP-1是一種ARF 家族的GTP 交換因子，當其和計畫性細胞凋亡相關基因同時產生突變時，突變株會展現尾巴缺陷的現象。藉由這個方式，我們找到了 182 個突變株，其中含有已知的計畫性細胞凋亡基因，如 *egl-1*、*ced-4*、*ced-3*、*ced-8*和 *ced-11*。除此之外，我們亦發現了 PYR-1 在線蟲中具有促進計畫性細胞凋亡的功能。這些結果顯示此基因掃描是具有其可行性。PYR-1 是 人 類 CAD （carbamoyl phosphate synthetase 、 aspartate transcarbamylase 與 dihydroorotase)的同源基因，參與在合成嘧啶的速率決定
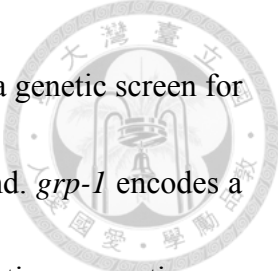
步驟。我們發現 PYR-1 影響到表皮細胞 hyp8/9 及分泌細胞 excretory cell 的姨細胞計畫性細胞凋亡,而且這個促進計畫性細胞凋亡的功能和其合成嘧啶的功能並不相關。除此之外,我們亦發現 PYR-1 是 CED-3 的酶作用物。因此,藉由這個基因掃描,我們找到了新的計畫性細胞凋亡相關基因並且初步了解其機制。

ABSTRACT

Programmed cell death (PCD) is the physiological death of a cell mediated by an intracellular suicide program. Although key components of the PCD execution pathway have been identified, how PCD is regulated during development is poorly understood. We found that the epidermal growth factor (EGF)-like ligand LIN-3 acts as an extrinsic signal to promote the death of specific cells in *Caenorhabditis elegans*. The loss of LIN-3 or its receptor LET-23 reduced the death of these cells, while excess LIN-3 or LET-23 signaling resulted in an increase in cell deaths. Our molecular and genetic data support the model that the LIN-3 signal is transduced through LET-23 to activate the LET-60/RAS-MPK-1/ERK MAPK pathway and the downstream ETS domain-containing transcription factor LIN-1. LIN-1 binds to, and activates transcription of, the key pro-apoptotic gene *egl-1*, which leads to the death of specific cells. Our results provide the first evidence that EGF induces PCD at the whole organism level and reveal the molecular basis for the death-promoting function of LIN-3/EGF. In addition, the level of LIN-3/EGF signaling is important for the precise fine-tuning of the life-versus-death fate. Our data and the previous cell culture studies that EGF triggers apoptosis in some cell lines suggest that the EGF-mediated modulation of PCD is likely conserved in *C. elegans* and humans.

To identify new genes involved in PCD in *C. elegans*, we conducted a genetic screen for mutants with a high penetrance of tail defects in the *grp-1* background. *grp-1* encodes a GTP exchange factor for ARFs and mutations defective in the activation, execution, or kinetics of PCD act synergistically with the *grp-1* mutation to cause abnormal tail morphology. From this screen, we isolated 182 mutants. These mutants are classified into three subgroups, depending on their cell-corpse profiles: reduced/delayed, elevated and unchanged cell corpse numbers during embryogenesis. By SNP mapping and complementation tests, 22 mutations isolated were localized in known *ced* genes. This result showed that this screen is feasible to identify genes important for PCD. In addition, we have isolated *pyr-1*, encoding *C. elegans* CAD (carbamoyl phosphate synthetase, aspartate transcarbamylase, and dihydroorotase). In mammals, CAD has been reported to control the rate-limiting step during pyrimidine biosynthesis. We found that *pyr-1* promotes the PCD of the aunt cells of hyp8/9 and excretory cell and this cell death-promoting function is independent of its CAD activity. Moreover, we showed that PYR-1 is a substrate of CED-3 in *vitro*. Therefore, we identified a previously unassigned pro-apoptotic function of PYR-1.

TABLE OF CONTENTS

Chapter 1

LIN-3/EGF Promotes the Programmed Cell Death of

Specific Cells in *C. elegans* by

Transcriptional Activation of the Pro-apoptotic Gene *egl-1*
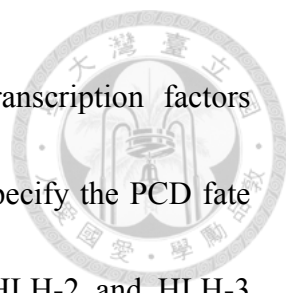
INTRODUCTION
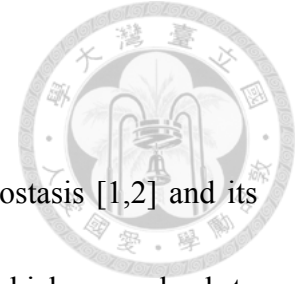
PCD is important for proper animal development and tissue homeostasis [1,2] and its

dysregulation can cause aberrant death or survival of cells, which may lead to

developmental defects, degenerative diseases, or cancers [1,2].

C. elegans is an excellent model for studying PCD because of its invariant cell lineage

and the conserved cell death pathway [3,4]. Throughout the development of the *C.*

elegans adult hermaphrodite, 131 somatic cells undergo PCD in an essentially invariant

temporal and spatial pattern [5,6]. Genetic and molecular studies have identified four

genes, *egl-1* (BH3-only gene), *ced-9* (*bcl-2*), *ced-4* (*apaf-1*), and *ced-3* (caspase), that

function in the core PCD pathway [7-12]. In living cells, CED-9 interacts with, and

sequesters, CED-4 at the surface of mitochondria to prevent the cells undergoing PCD

[13]. In cells destined to die, EGL-1 binds to CED-9, resulting in a conformational

change in CED-9 and the release of bound CED-4 [14]. The released CED-4

translocates from the mitochondrion to the perinuclear membrane and interacts with,

and activates, the caspase CED-3, leading to the eventual demise of the cell [15]. A

recent study in mid-embryos and the germline suggested the existence of an alternative

cell death activation mechanism that does not involve a direct interaction between

CED-4 and CED-9 [16]. The transcriptional regulation of *egl-1* is a critical step in the

induction of most PCD events in the embryo [17]. Several transcription factors

controlling *egl-1* transcription have been identified and shown to specify the PCD fate

of specific cells [4,18]. For example, two transcription factors HLH-2 and HLH-3

activate *egl-1* transcription by direct binding to the *egl-1* cis-regulatory region during

the specification of the death fate of NSM sister cells [18, 19]. Like HLH-2 and HLH-3,

cell death specification genes have been shown to transcriptionally regulate the

components of the core PCD machinery in a cell-autonomous manner. It is unclear

whether the PCD fate, like many other cell fates, may be regulated by an extrinsic

signal.

Extrinsic signals are crucial for a variety of developmental processes and act through

receptors to elicit specific biological functions in a cell-nonautonomous manner. One

example of such a signal-receptor pair is epidermal growth factor (EGF) and the EGF

receptor (EGFR), which are involved in cell proliferation, differentiation, migration,

survival, and death [20-22]. EGF has long been considered as a growth factor, since it

stimulates proliferation in cultured cells, animals, and humans [23]. It also protects cells

from apoptosis, as shown in cultured cells and Drosophila [24-29]. EGF can signal

through the RAS-ERK-mediated and/or PI3K-mediated pathway(s) to activate

transcription of various anti-apoptotic proteins, such as Bcl-X_L and Mcl-1 [25-27], and

also regulates post-transcriptional modifications, such as phosphorylation of BAD and caspase-9, to prevent apoptosis [28,29]. However, in contrast to this cytoprotective function, it has also been shown to promote apoptosis, as exogenous EGF induces apoptosis in several cell lines, such as A431, MDA-MB-468, and MCF-7 [30-32]. It is not clear how it exerts different functions in different cells under different conditions or whether the apoptosis-promoting function plays a physiological role during animal development.

In *C. elegans, lin-3* and *let-23* encode, respectively, the sole EGF-like ligand and the EGFR and control many aspects of development, including ovulation, vulval differentiation, cell specification, and behavioral quiescence [33-38]. Activated LET-23 can recruit SEM-5 (orthologous to human Grb2) from the cytosol to the plasma membrane to activate LET-60, a member of the GTP-binding RAS family [39,40]. LET-60 then triggers a kinase cascade involving the sequential phosphorylation of LIN-45 (a Raf ortholog), MEK-2 (a MAPK kinase kinase), and MPK-1 (an ERK ortholog) [41-45]. Once MPK-1 is phosphorylated, it translocates to the nucleus and regulates the transcription of numerous target genes by phosphorylation of specific transcription factors [46]. Besides activating the LET-60-MPK-1 pathway, LET-23 activates the PLC-γ-mediated signaling pathway to regulate ovulation and behavioral

quiescence [36,38]. In addition, the SEM-5-binding protein SOC-1 is involved in both

the PLC-γ- and PI3K-mediated signaling pathways [47]. The LET-60-MPK-1- and

PI3K-mediated signaling pathways have been shown to be involved in physiological

and genotoxic stress-induced germline cell death [48-51]. However, how these

pathways are regulated by upstream signals, how they are linked to the intrinsic PCD

machinery to control germline cell death, and whether they play a role in somatic PCD

remain unknown.

We now report that LIN-3 acts as an extrinsic signal to promote specific somatic PCDs

and the identification of components that transmit the LIN-3 signal to the intrinsic PCD

machinery. Our data indicate that secreted LIN-3 induces cell death through the receptor

LET-23, which acts in a cell-autonomous manner during PCD. Our genetic and

biochemical data suggest that the LET-60-MPK-1 pathway transmits the LIN-3 signal

from LET-23 to the transcription factor LIN-1 for transcriptional up-regulation of *egl-1,*

which leads to activation of PCD.

MATERIALS AND METHODS

General Methods and Strains

Unless otherwise stated, *C. elegans* strains were maintained at 20°C as described

previously [52]. The N2 Bristol strain was used as the wild-type strain. Alleles used:

Linkage group (LG)I: *aap-1(m889)*, *aap-1(ok282)*, *age-2(yw23)*, *daf-16(m26)*, and

mek-2(ku114).

LGII: *age-1(hx546)*, *age-1(m333)*, *let-23(n1045)*, *let-23(sy1)*, *let-23(sy97)*,

lin-31(gk569), *lin-31(n301)*, *lin-31(n1053)*, *plc-3(tm1340)*, and *rrf-3(pk1426)*.

LGIII: *ced-4(n1162)*, *ced-9(n1950)*, *mpk-1(ku1)*, *mpk-1(n2521)*, *unc-32(e189)*,

unc-79(e1068), and *syIs107[P$_{lin-3}$::pes-10::gfp]*.

LGIV: *ced-3(n717)*, *let-60(n1046)*, *let-60(sy93)*, *lin-1(n1761)*, *lin-1(n303)*, *lin-1(n1047)*,

lin-1(sy254), *lin-3(e1417)*, *lin-3(n378)*, *lin-45(n2506)*, and *plc-4(ok1215)*.
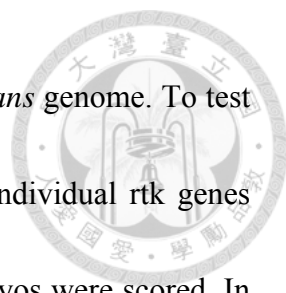
LGV: *egl-1(n1084n3082)*, *plc-2(ok1761)*, *sos-1(cs41)*, and *bcIs37[P$_{egl-1}$::his-24::gfp]*.

LGX: *plc-1(rx1)*, *sem-5(n1779)*, and *syIs1[lin-3(+)]*.

All alleles are described in WormBase (http://www.wormbase.org/). *tpIs8* is an

integrated version of *tpEx270[P$_{B0280.7}$::4Xnls::mrfp; unc-119(+)]* (this report).

P$_{B0280.7}$::4Xnls::mrfp is expressed in g1 and g2 gland cells [53].
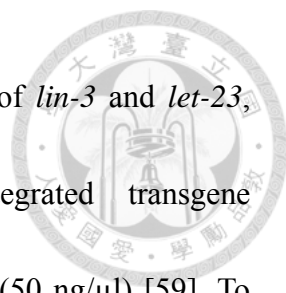
RNA interference (RNAi)

There are about 40 receptor tyrosin kinase (rtk) genes in the *C. elegans* genome. To test the involvement of these genes in promoting PCD, RNAi of the individual rtk genes was performed by feeding [54], and the cell corpses of treated embryos were scored. In this screen, only *let-23* RNAi significantly decreased cell corpse numbers at the comma and 1.5-fold stages. To characterize the effect of the *lin-3* signaling pathway on the number of embryonic cell corpses, the *rrf-3(pk1426)* mutant, which is sensitive to RNAi [55], was treated by feeding RNAi at 20°C, as previously described [56]. In other RNAi experiments, animals were treated with RNAi without the *rrf-3(pk1426)* mutation. The *lin-3* or *let-23* RNAi treatment caused more than 50 % rod-like larval lethality both in the wild-type and *rrf-3(pk1426)* mutant, confirming that *lin-3* and *let-23* RNAi works well in these experiments. RNAi plasmids were obtained from the J. Ahringer RNAi library. L4 hermaphrodites were put onto the RNAi plates, and F1 were scored for the number of embryonic cell corpses, surviving ABpl/rpppapp, or extra gland cells. The empty vector L4440 was used as negative control.

Transgenic animals

Germline transformation experiments were performed as described previously [57]. To observe the expression pattern of *let-23*, $P_{let-23}::4Xnls::gfp$ (50 ng/µl) was injected into *unc-119(ed3)* worms with the coinjection markers *unc-119* [58] (50 ng/µl) and

P_{ced-1}::1Xnls::mrfp (50 ng/µl). To examine the expression pattern of *lin-3* and *let-23*,

P_{let-23}::4Xnls::mrfp (200 ng/µl) was injected into an integrated transgene

syIs107[P_{lin-3}::pes-10::gfp] with the coinjection markers P_{elt-2}::gfp (50 ng/µl) [59]. To

test whether secreted LIN-3 rescued the cell death defect of the *lin-3* mutant and caused

ectopic cell deaths, P_{elt-2}::gfp or P_{elt-2}::lin-3::gfp (50 ng/µl) was injected into the

lin-3(e1417) mutant and wild-type with the coinjection marker *sur-5::gfp* (50 ng/µl). To

test the effect of LIN-1 overexpression on PCD, plasmids pPD49.78 and pPD49.83

(containing P_{hsp} without an insert) or P_{hsp}::lin-1 (50 ng/µl) was co-injected with the

coinjection marker *sur-5::gfp* (50 ng/µl) into animals carrying the integrated transgene

tpIs8. To examine the importance of the LIN-1 binding site in the *egl-1* promoter,

wild-type (pBC08) [7] or mutant *egl-1* (2 ng/µl) was injected into either

egl-1(n1084n3082) or *lin-3(e1417); egl-1(n1084n3082)* mutants with the coinjection

marker *sur-5::gfp* (50 ng/µl).
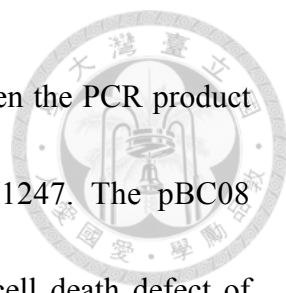
Heat shock treatment

Embryos were incubated at 20°C or heat shocked at 33°C for 10-60 min and then

moved to 20°C. The number of g1 and g2 gland cells was scored at the L4 stage using

the *tpIs8* transgene after three days.
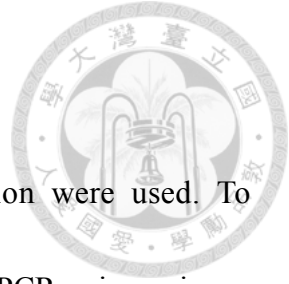
Molecular biology
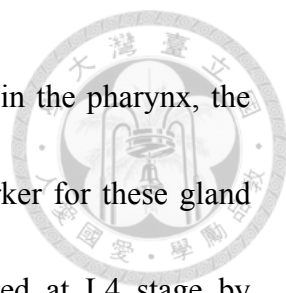
Standard methods of cloning, sequencing, and PCR amplification were used. To generate *P_{let-23}::4xnls::gfp*, the *let-23* promoter was amplified by PCR using primers 5'-gtctagagcatctgcacttggg-3' and 5'-gggatccgcctcccag-3' and the resulting PCR fragment was inserted into the pPD122.56 vector to generate pYW1242. Full-length *lin-3* cDNA was obtained by RT-PCR using worm total RNA and the primers 5'-CCACCGGTATGCGGAAAATGCTAC-3' and 5'-CCACCGGTTTTGTGTGTCGAATCATTGG-3'. To obtain *P_{elt-2}::lin-3::gfp*, the *elt-2* promoter, previously amplified by PCR using 5'-TTGGATCCCGGTGAAACTCTCTTGG-3' and 5'-CCGGATCCCAGTGGCACCTAAAACATC-3', was cloned into the BamHI site of pPD95.75 and *lin-3* cDNA was cloned into the AgeI site to generate pYW1243. To generate *P_{hsp}::lin-1*, a full-length *lin-1* cDNA was amplified from the yk1150h12 plasmid by PCR using 5'-ccggatccatgaatcacattgaccttttg-3' and 5'-ttccatggctacaaagttggcattttttatg-3', and the resulting PCR fragment was inserted into the heat-shock vectors pPD49.78 and pPD49.83 to generate pYW1245 and pYW1246, respectively. The DNA fragment corresponding to the LIN-1 DNA binding domain was amplified by PCR using the yk1150h12 plasmid as template and 5'-CCGGATCCATGAATCACATTGACCTTTTG-3' and

5'-TTGGATCCTTTCGTTGGCGGCTGCGG-3' as primers [60], then the PCR product was inserted into vector pGEX-4T-1 to generate plasmid pYW1247. The pBC08 plasmid contains the *egl-1* genomic fragment, which rescues the cell death defect of *egl-1* mutants [7]. To generate mutant *egl-1* with a defect in the LIN-1 binding site, two partial fragments of *egl-1* from pBC08 were first amplified by PCR using primer pairs 5'-caatttatagtaaagttaacttca-3' plus 5'-cacatacagtagcttgaattcaactatacatctg-3' and 5'-aattcaagctactgtatgtgtcacttccaccacc-3' plus 5'-ggccgctctagaactagtgg-3'. The products were then used as templates for fusion PCR to generate a larger fragment to replace the corresponding region in pBC08 to generate pYW1248. This mutant *egl-1* was identical to wild-type *egl-1* except that the core LIN-1 binding motif was changed from CAGGAA to GCTACT.

Cell death assays

Cell corpses were counted at the indicated developmental stages and the number of extra cells in the anterior and posterior pharynx of L4 hermaphrodites was scored using Nomarski optics as described previously [61]. To analyze the first 13 cell deaths that occur in the AB lineage during embryogenesis, embryos were mounted onto 4% agar pads and recorded using a four-dimensional DIC microscopy analysis as described previously [62]. The survival of ABpl/rpppapp was examined by its localization in the

11
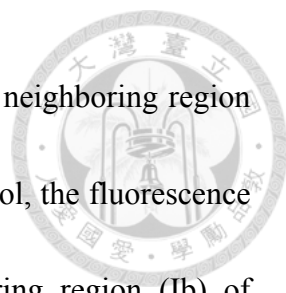
tail with the aid of *sur-5::gfp*. To count the number of gland cells in the pharynx, the integrated transgene *tpIs8[P$_{B0280.7}$::4Xnls::mrfp]* was used as a marker for these gland cells [53], and the number of the mRFP-positive cells was scored at L4 stage by fluorescence microscopy.

Quantitative real-time reverse transcriptase (RT)-PCR

Total RNA was isolated from embryos developing up to the comma stage and purified by chloroform extraction and isopropanol precipitation, then 500 ng was reverse transcribed into cDNA using RevertAid H Minus First Strand cDNA Synthesis Kits (Fermentas). Equal amounts of the different cDNAs were used as the template for gene-specific PCR with appropriate primers. Water was used as negative control and *tbg-1* RT-PCR was performed as an internal control. The CT values of the test genes were normalized to that of *tbg-1* and relative expression levels were derived using the comparative CT method [63].

Quantification of P_{egl-1}::*gfp* intensity in ABprpppapp

To measure the P_{egl-1}::*gfp* expression within ABprpppapp, fluorescence micrographs were captured using a Zeiss AxioImager M2 microscope (Zeiss) equipped with a charge-coupled device camera. GFP intensity was determined using Image J by

measuring the fluorescence signals within ABprpppapp (Ia) and its neighboring region

(Ib) of *ced-3(717)* and *lin-3(e1417) ced-3(n717)* mutants. As a control, the fluorescence

signals within two cells near ABprpppapp (Ia) and its neighboring region (Ib) of

ced-3(717) and *lin-3(e1417) ced-3(n717)* mutants was determined. The value of Ia

minus the value of Ib was used as the value for relative GFP intensity, and the relative

GFP intensity of the *ced-3(n717)* mutant was used for normalization.

Prediction of potential LIN-1 binding sites

The prediction of potential LIN-1 binding sites was performed at

http://www.cbrc.jp/research/db/TFSEARCH.html by submitting the sequence from

+174 to +5820 (5′-3′) downstream of the stop codon of the *egl-1* gene and the sequence

from −1914 to −837 (5′-3′) upstream of the stop codon [64]. Four binding sites for Elk-1,

the mammal LIN-1 ortholog, were predicted; these were AGCTTTCCGGCTCA (P1),

CGATCCGGAAATCC (P2), TAGTTGAATTCAACAGGAAGTATGTGTCACTTCC

(P3), and CAATTTCCGGTAAT (P4). P2 and P3, but not P1 or P4, are conserved in *C.*

briggsae. P2 has been shown to be important for the PCD of the neurosecretory-motor

(NSM) neuron [19], but *lin-3* and *let-23* do not seem to be involved in the death of

NSM sister cell (Figure 1D), we therefore focused on P3 in this study.

Electrophoretic mobility shift assay (EMSA)

Expression of GST and GST::LIN-1(DBD) was induced in *Escherichia coli* strain BL21

carrying the respective plasmids pGEX-4T-1 and pYW1247 by addition of 0.4 mM

isopropyl thiogalactoside and incubation for 1h at 37°C. The cells were then harvested

and disrupted by sonication in phosphate-buffered saline containing protease inhibitor

cocktail (Calbiochem) and 1% Triton X-100, and the proteins were purified on

glutathione Sepharose (Amersham Biosciences) according to the manufacturer's

protocol. The amount of protein was measured by the Bradford method (Biorad). The

sense and antisense oligonucleotides containing the predicted LIN-1 binding sequences,

which were synthesized and biotinylated at the 3' end (Genomics), were mixed in

annealing buffer (5 mM NaCl, 1 mM Tris-HCl, 1 mM $MgCl_2$, and 0.1 mM dithiothreitol,

pH 7.9) at a final concentration of 1μM, denatured at 98°C for 2 min, and allowed to

anneal by slowly cooling the mixture to 25°C. Unlabeled probes were used as

competitors in competition experiments. The sequences of the probes were: wild-type:

5'-gaattcaacaggaagtatgtgtcacttccaccac-3' and 5'-gtggtggaagtgacacatacttcctgttgaattc-3';

mutant: 5'- gaattcaagctactgtatgtgtcacttccaccac-3' and

5'-gtggtggaagtgacacatacagtagcttgaattc-3'. EMSA were performed using LightShift

Chemiluminescent EMSA kits (Pierce), following the manufacturer's instruction. The

mixture was separated at 100 V at 4°C on a 5.5% non-denaturing polyacrylamide gel,

then the DNA was transferred to a charged nylon membrane (Millipore) at 150 mA for 30 min and cross-linked with UV light using the auto crosslink option on a UV Stratalinker 1800 (Stratagene). The membrane was then blocked, washed, and exposed to X-ray film following the manufacturer's protocol.

Statistical analysis

In histograms, the values are shown as the mean and standard deviation (SD). Data derived from different genetic backgrounds at a specific developmental stage were compared using Student's two-tailed unpaired t-test. Data were considered statistically different at $P<0.05$. Fisher's exact test was used when comparing the percentages of surviving or missing cells in different genetic backgrounds. Data were considered statistically different at $P<0.05$.
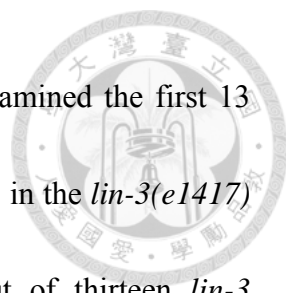
RESULTS

lin-3 and *let-23* promote specific PCDs in *C. elegans*

While screening to test the potential involvement of receptor tyrosine kinase genes in

PCD (see Materials and Methods), we found that several *let-23* mutants have reduced

numbers of cell corpses (Figure 1A). The *let-23* gene encodes EGFR [34], raising the

intriguing possibility that LET-23 might mediate an outside-in signal to affect PCD.

lin-3 encodes the only EGF in *C. elegans* [33] and we found that *lin-3* mutants had a

similar reduction in numbers of cell corpses as *let-23* single mutants or the *let-23; lin-3*

double mutant at the same embryonic stages (Figure 1A). This shows that *lin-3* and

let-23 function in the same pathway to affect cell corpse number, probably by acting as

a ligand-receptor pair. Inactivation of *lin-3* or *let-23* by RNA interference (RNAi)

reduced the numbers of cell corpses to a similar extent as the *lin-3* or *let-23* mutations

(Figure 1A). Because the *lin-3* or *let-23* RNAi treatment caused more than 50 %

rod-like larval lethality, phenocopying the strong loss-of-function *lin-3* or *let-23*

mutants [65], the reduced numbers of cell corpses observed in the *lin-3* or *let-23*

mutants mentioned above likely represented the phenotype caused by nearly complete

elimination of *lin-3* or *let-23,* respectively. Interestingly, in these mutants, only a partial

reduction of cell corpse numbers from the comma stage to the 2-fold stage was observed,

suggesting that *lin-3* and *let-23* may be essential for some but not all cell deaths.
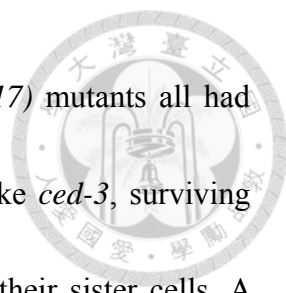
To investigate whether *lin-3* may affect specific cell deaths, we examined the first 13 cell deaths that occur in the AB lineage during embryogenesis [6,66] in the *lin-3(e1417)* mutant by using four-dimensional DIC microscopy. In three out of thirteen *lin-3* embryos we analyzed, only ABplpppapp or its lineal homolog ABprpppapp failed to die, and the other cell deaths occurred normally (Figure 1B and Appendix 1). ABplpppapp and ABprpppapp (these cells are collectively termed ABpl/rpppapp hereafter), which are aunt cells of hypodermal cells hyp8/9, are generated at approximately 270 min after fertilization and undergo PCD soon after birth [6]. Consistent with the DIC four-dimensional microscopy data, approximately 20% of surviving ABpl/rpppapp were observed in the tail of the *lin-3(e1417)* mutant (Figure 1C and D), indicating that the disappearance of ABpl/rpppapp corpses is due to the survival of these cells. A similar result was observed in the *let-23(sy1)* mutant and in the *lin-3(e1417)* mutant feeding *let-23* RNAi (Figure 1D), showing that *lin-3* and *let-23* act in the same pathway to promote the death of ABpl/rpppapp.

We also measured the duration time of the first 13 cell corpses derived from the AB lineage in the wild-type and *lin-3(e1417)* mutant embryos and found that the corpse duration time was statistically undistinguishable in the wild-type and *lin-3* embryos (Appendix 2, *P*=0.24, two-tailed *t* test). This result indicates that the kinetics of corpse

removal is normal in the *lin-3(e1417)* mutant, and rules out the possibility that the decrease of cell corpse numbers in the *lin-3* mutants may be attributed to enhanced cell corpse removal.
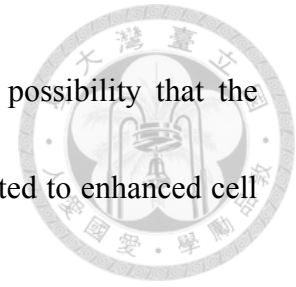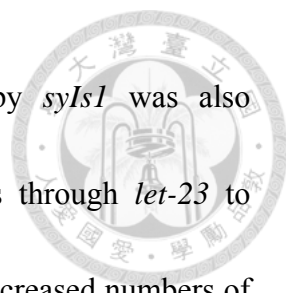
We next examined whether *lin-3* or *let-23* may also be important for the death of other PCDs. We scored the extra surviving cells in the pharynx of the *lin-3* or *let-23* mutant at the L3 and L4 stages. In wild-type animals, 16 cells in the anterior pharynx and 6 in the posterior pharynx undergo PCD during mid-embryogenesis. Eight out of these 22 cells (NSML/R, I2L/R, g1AL/R and g2L/R) undergo PCD during the comma to 2-fold stage. In virtually all wild-type embryos, no extra surviving cells are observed in these regions at the late larval stages [6,11,61]. In *lin-3* and *let-23* mutants, about 10 % of the sister cells of g1A gland cells and I1 interneurons survived, and the death of other 18 cells in the pharynx region was essentially normal (Figure 1E). Furthermore, the percentage of animals with surviving g1A and I1 sisters was enhanced by the weak *ced-3(n2427)* mutation; however, essentially no enhancement was observed in other 18 cells examined (Appendix 3). This result shows that *lin-3* and *let-23* are important for the death of specific cells. Consistently, using an integrated transgene *tpIs8*, which expresses monomeric red fluorescent protein (mRFP) in the g1A, g1P, and g2 gland cells [53], we found that 10 % of the *lin-3* animals had extra gland cells, whereas

19

wild-type worms had no extra gland cell and the strong *ced-3(n717)* mutants all had

extra gland cell(s) (Figure 1F and G). This result indicates that, like *ced-3*, surviving

cells in the *lin-3* mutant adopt the terminal differentiation fate of their sister cells. A

similar result was observed in the wild-type or *lin-3(e1417)* mutant feeding *let-23* RNAi

(Figure 1G), showing that *lin-3* and *let-23* also act in the same pathway to promote the

death of gland cells. Our data show that *lin-3* and *let-23* are important for the death of

specific cells, including g1A and I1 sister cells and ABpl/rpppapp and that these genes

are dispensable for most cell deaths analyzed in this work.

Overexpression of *lin-3* cause ectopic cell deaths

We next examined whether over-activation of *lin-3* signaling could cause ectopic cell

deaths during embryogenesis. We found that overexpression of *lin-3* genomic DNA

from the integrated transgene *syIs1* [33] increased embryonic cell corpse numbers

(Appendix 4). Using the integrated transgene *tpIs8* to label g1 and g2 gland cells, we

found that *syIs1* caused the loss of one or two gland cells in 19% of transgenic worms

(Figure 2A and B). This phenotype of gland cell loss was suppressed by the

loss-of-function mutation in *egl-1* or *ced-3* (Figure 2A and B). This result shows that

lin-3 overexpression induces ectopic gland cell death rather than alters gland cell fate,

and that the cell death-promoting activity of *lin-3* requires the core PCD pathway. In

addition, the phenotype of ectopic gland cell death induced by *syIs1* was also suppressed by *let-23* RNAi (Figure 2B), showing that *lin-3* acts through *let-23* to promote the ectopic cell death of the gland cells. Consistently, the increased numbers of embryonic cell corpses induced by *syIs1* was also suppressed by loss-of-function mutations in *let-23* or in components of the core PCD pathway (Appendix 4).

let-23 is expressed in dying cells, including ABpl/rpppapp
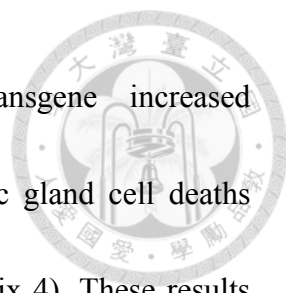
Next, we examined whether there was a correlation between *let-23* expression and PCD using the transgene *syEx234[P_{let-23}::let-23::gfp]* [67]. As shown in Figure 3A, the LET-23::GFP fusion protein was detected as a crescent on the surface of some dying cells (indicated by arrowheads). The cause and physiological significance of this crescent-shaped localization pattern is not clear. To be sure that *let-23* was expressed in dying cells and not on the membranes of adjacent living cells, we generated the construct *P_{let-23}::4Xnls::gfp* and microinjected it into the wild-type to generate transgenic worms. *P_{let-23}::4Xnls::gfp* contains the *let-23* promoter *P_{let-23}* fused to the GFP cDNA containing four copies of the nuclear localization signal (4XNLS). The GFP signal was detected in the nuclei of the dying cells (Figure 3B), clearly showing that *let-23* is expressed in dying cells. Notably, the GFP signal was observed in the ABpl/rpppapp corpses (Figure 3C).

21

LIN-3 can act as an extrinsic signal to promote PCD

Like its *Drosophila* and vertebrate homologs, *lin-3* encodes a transmembrane precursor protein, consisting of an extracellular domain containing one EGF motif, a transmembrane domain, and a cytoplasmic domain [33,68]. Genetic and laser ablation studies have suggested that the LIN-3 precursor protein can be cleaved to form a secreted product [33,69,70]. Using the transcriptional reporter $P_{lin-3}::gfp$ [71] and $P_{let-23}::4Xnls::mrfp$, no $P_{lin-3}::gfp$-expressing cell was located adjacent to the $P_{let-23}::4xnls::rfp$-expressing cell corpses, as shown in Figure 3D. In addition, no $P_{lin-3}::gfp$ signal was detected near ABpl/rpppapp corpses (Figure 3E). These observations raise a possibility that *lin-3* may be secreted and act at a distance to promote PCD.
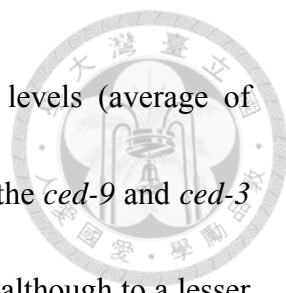
To test this hypothesis, we generated a DNA construct $P_{elt-2}::lin-3::gfp$, in which a *lin-3::gfp* fusion cDNA was expressed under the control of the *elt-2* promoter P_{elt-2} and introduced it to the wild-type and *lin-3* mutant. P_{elt-2} is used here because it is exclusively expressed in intestinal cells and their precursor cells [59] and no PCD occurs in these cells [6]. We found that, in the *lin-3* mutant, the $P_{elt-2}::lin-3::gfp$ transgene not only increased the number of embryonic cell corpses to the wild-type level (Figure 3F) but also rescued the inappropriate survival of gland cells (Figure 3G).

Moreover, when introduced to the wild-type, the $P_{elt-2}::lin-3::gfp$ transgene increased

the embryonic cell corpse number (Figure 3F) and caused ectopic gland cell deaths

(Figure 3H), as the transgene *syIs1* did (Figure 2A, B and Appendix 4). These results

show that LIN-3::GFP secreted from the intestine can act at a distance to induce cell

death in other parts of the embryo, e.g. gland cells in the head region. In our study, the

adult worms transgenic for $P_{elt-2}::lin-3::gfp$ had a multi-vulva phenotype, resembling

worms carrying *syIs1* [33], reinforcing the notion that LIN-3::GFP expressed in the

intestine is secreted and active.
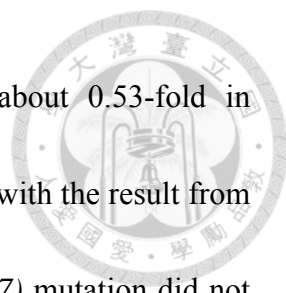
lin-3 signaling up-regulates egl-1 transcription

Because the cell death-promoting activity of *lin-3* requires the core PCD pathway

(Figure 2A, B, and Appendix 4), we next examined whether *lin-3* signaling promotes

PCD by regulating the expression of *egl-1, ced-9, ced-4*, or *ced-3*. To this end, we

measured the transcript levels of *egl-1, ced-9, ced-4*, or *ced-3* in worms with different

levels of *lin-3* activity by quantitative real-time reverse transcription (RT)-PCR. As

shown in Figure 4A, the abundance of *egl-1* transcripts correlated well with the level of

lin-3 activity, which, in turn, correlated well with the number of cell deaths. *egl-1*

transcripts were less abundant in *lin-3* and *let-23* mutants than in wild-type animals

(average of 0.53-fold and 0.57-fold, respectively), while *lin-3* overexpression using the

integrated transgene *syIs1* caused an increase in *egl-1* transcript levels (average of

2.15-fold). Similarly, levels of the *ced-4* transcript, but not those of the *ced-9* and *ced-3*

transcripts, also showed a correlation with the level of *lin-3* activity, although to a lesser

extent than the *egl-1* transcript. These data show that LIN-3 and LET-23 signaling

activates transcription of *egl-1* and, to a lesser extent, *ced-4, in vivo*. Interestingly, we

found that the *lin-3(e1417)* mutation reduced the *egl-1* transcript level in the *ced-3(n717)*

mutant (average of 0.61-fold) to a similar extent as the *lin-3(e1417)* mutation did in the

wild-type (Figure 4A). This result supports the model that the LIN-3-mediated

up-regulation of *egl-1* transcription occurs before *ced-3* activation during PCD.
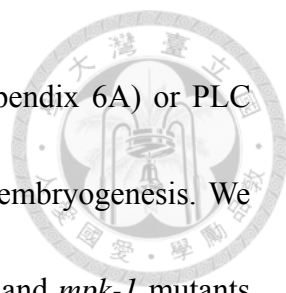
Next, we examined the effect of *lin-3* on the *egl-1* transcription activity in ABprpppapp

using the transcriptional fusion reporter $P_{egl-1::}gfp$ [64]. The *egl-1(n1084n3082)*

mutation caused frequent survival of ABpl/rpppapp, showing that *egl-1* is required for

the death of ABprpppapp (Figure 1C and D). We measured and compared the

fluorescence intensity of GFP in ABprpppapp of the *ced-3* and *lin-3 ced-3* mutants. The

ced-3(n717) mutation blocks the death of ABprpppapp, hence allowing the observation

of the $P_{egl-1}::gfp$ transgene in the surviving ABprpppapp, and has no effect on the

lin-3-mediated *egl-1* transcription (Figure 4A). In the *ced-3(n717)* mutant, ABprpppapp

survived and expressed $P_{egl-1::}gfp$ at the comma stage (Figure 4B). The *lin-3(e1417)*

mutation significantly decreased the intensity of $P_{egl-1}::gfp$ to about 0.53-fold in

ABprpppapp of the *ced-3* mutant (Figure 4B, *P*=0.0004), consistent with the result from

quantitative real-time RT-PCR (Figure 4A). Notably, the *lin-3(e1417)* mutation did not

affect the *egl-1* transcription in two adjacent cells that also express *egl-1* (Figure 4B,

control experiment, *P*=0.6839). Therefore, loss of *lin-3* reduces the *egl-1* transcription

level in a cell-specific manner. These data and the aforementioned observation that the

egl-1(lf) mutation blocked the *syIs1*-induced cell death (Figure 2A, B, and Appendix 4)

together support the notion that *lin-3* signaling promotes the death of ABprpppapp by

transcriptional activation of *egl-1*.

LET-23 transduces the cell death-promoting signal via the LET-60-MPK-1

pathway
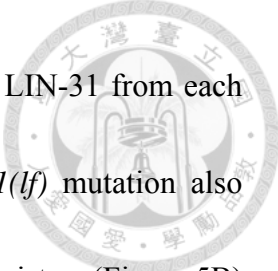
We next investigated how *lin-3* and *let-23* signaling may up-regulate *egl-1* to promote

PCD. Activated LET-23 has been shown to act via multiple signaling pathways,

including the LET-60-MPK-1- and PLC-γ-mediated pathways, to control *C. elegans*

development [36,38-45]. SOC-1, a SEM-5-binding protein, has been reported to act not

only in the LET-60-MPK-1 pathway, but also in the PLC-γ- and PI3K-mediated

signaling pathways [47]. We found that mutants defective in the LET-60-MPK-1

pathway had reduced cell corpse numbers during mid-embryogenesis (Appendix 5),

while mutants defective in either the PI3K-mediated pathway (Appendix 6A) or PLC genes (Appendix 6B) had normal cell corpse numbers throughout embryogenesis. We further analyzed whether specific PCDs were affected in the *let-60* and *mpk-1* mutants using the assays described above. We found that *let-60* and *mpk-1* are required for the death of ABpl/rpppapp (Figure 5A), glA sisters, and I1 sisters (Figure 5B) but essentially dispensable for most cell deaths examined in this work. These data show that mutants defective in the LET-60-MPK-1 pathway have a PCD-defective phenotype similar to *lin-3* and *let-23* mutants. Furthermore, the *lin-3* RNAi treatment did not enhance the survival of ABpl/rpppapp in the *let-60* or *mpk-1* mutant (Figure 5A), showing that, at least in ABpl/rpppapp, *lin-3* and *let-23* transduce the cell death-promoting signal through the LET-60-MPK-1 pathway.

LET-23 transduces the cell death-promoting signal via the transcription factor LIN-1, but not LIN-31
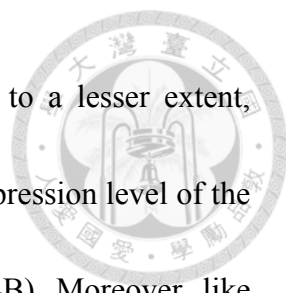
Two transcription factors, the ETS domain-containing protein LIN-1 and the WH domain-containing protein LIN-31, transduce LET-60-MPK-1 signaling to control vulval differentiation [72,73]. In the absence of the LET-60-MPK-1 signaling pathway, LIN-1 forms a complex with LIN-31 and inhibits vulval induction [46]. Activation of the LET-60-MPK-1 pathway leads to phosphorylation of LIN-1 and LIN-31 by MPK-1,

and phosphorylation of LIN-31 results in dissociation of LIN-1 and LIN-31 from each

other and subsequent vulval induction [46]. Interestingly, the *lin-1(lf)* mutation also

caused the survival of ABpl/rpppapp (Figure 5A), g1A sisters, and I1 sisters (Figure 5B),

whereas the *lin-31(lf)* mutation did not (Figure 5A and B). These results show that *lin-1*,

but not *lin-31*, affects specific PCD, despite both genes being necessary for vulval

differentiation. *lin-1* mutants also displayed a reduction of embryonic cell corpse

numbers to a similar extent as mutants defective in the LET-60-MPK-1 pathway,

whereas *lin-31* mutants had a normal cell corpse profile during embryogenesis

(Appendix 7). The *lin-3* RNAi treatment did not enhance the penetrance of

ABpl/rpppapp survival in the *lin-1* mutant, showing that *lin-3* and *lin-1* act in the same

pathway to promote the death of ABpl/rpppapp (Figure 5A). Consistently, the cell

corpse numbers of the *lin-1(sy254) lin-3(e1417)* double mutant showed no significant

difference when compared to the *lin-1(sy254)* or *lin-3(e1417)* single mutant (Appendix

7). These data and the aforementioned genetic results support the notion that LIN-3 and

LET-23 act through the LET-60-MPK-1 pathway and transcription factor LIN-1 to

promote PCD.
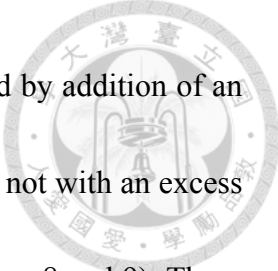
LIN-1 activates *egl-1* transcription by direct binding to the *egl-1* promoter

We next studied the mechanism by which LIN-1 promotes PCD. As mentioned above,

LIN-3 and LET-23 signaling activates transcription of *egl-1* and, to a lesser extent,

ced-4, in vivo (Figure 4A). This was confirmed by examining the expression level of the

transcriptional fusion reporter $P_{egl-1}::gfp$ in ABprpppapp (Figure 4B). Moreover, like

lin-3 overexpression, heat shock-induced *lin-1* overexpression in the wild-type caused

the phenotype of gland cell loss, and this phenotype can be suppressed by an *egl-1(lf)*

mutation (Figure 5C). These results support the model that LIN-1 acts upstream of *egl-1*

to promote the death of gland cells.

LIN-1 contains a highly conserved ETS domain [73], which binds to DNA with the

minimal recognition sequence GGAA/T [60]. A potential LIN-1 binding sequence was

found in the promoter region of *egl-1*, but not that of *ced-4* (Figure 6A, see Materials

and Methods for details), supporting the possibility that LIN-1 binds directly to *egl-1*.

We therefore generated the GST::LIN-1(DBD) fusion protein, in which the DNA

binding domain of LIN-1 was fused to glutathione S-transferase (GST), and tested its

ability to bind to a 34 bp DNA fragment (named P3) containing the LIN-1 binding

sequence in the electrophoretic mobility shift assay (EMSA). The results are shown in

Figure 6B. The P3 fragment displayed similar mobility in the presence or absence of

GST (lanes 1 and 2), confirming that GST does not bind to the DNA fragment. In

contrast, the presence of GST::LIN-1(DBD) resulted in the dose-dependent appearance

of a slowly migrating band (lanes 3-5), and this effect was eliminated by addition of an

excess of non-labeled wild-type DNA competitor (lanes 6 and 7), but not with an excess

of a DNA competitor with a mutation in the core GGAA/T motif (lanes 8 and 9). These

results show that the slowly migrating band is a complex of GST::LIN-1(DBD) and P3

and that LIN-1 binds to the P3 region of *egl-1 in vitro*.

To test the physiological importance of the interaction between LIN-1 and the *egl-1*

promoter, we mutated the P3 sequence in *egl-1* genomic DNA and assessed the ability

of the mutant *egl-1* gene to rescue the cell death defect of the *egl-1* mutant. Specifically,

we examined the cell death phenotype by scoring the surviving ABpl/rpppapp in the L1

tail (Figure 6C) and by counting the number of cell corpses at the 1.5-fold stage (Figure

6D). In the control experiment, *egl-1* mutants carrying the wild-type *egl-1* transgene

showed no surviving ABpl/rpppapp (Figure 6C), indicating that the wild-type *egl-1*

transgene *Ex[egl-1(+)]* fully rescued the *egl-1* cell death defect. When the LIN-1

recognition sequence CAGGAA in the P3 region of the *egl-1* promoter was mutated into

GCTACT [60], the mutant *egl-1* transgene *Ex[egl-1(mut)]* only partially rescued the

egl-1 cell death defect. In the two transgenic lines, the percentages of ABpl/rpppapp

survival were 15 % and 25 %, similar to that of the *lin-3* mutant (Figure 6C). The *egl-1;*

Ex[egl-1(mut)] transgenic worms also had a similar number of embryonic cell corpses

as the *lin-3* mutant at the 1.5-fold stage (Figure 6D). These results show that the binding

of LIN-1 to the *egl-1* promoter is important for the cell-killing activity of *egl-1*.

To test whether this LIN-1-mediated cell-killing activity of *egl-1* may depend on LIN-3

signaling, we examined whether a *lin-3(lf)* mutation may reduce the rescuing activity of

the mutant *egl-1* transgene by scoring surviving ABpl/rpppapp (Figure 6C) and

embryonic cell corpses (Figure 6D). As shown in Figure 6C and 6D, the *lin-3(lf)*

mutation reduced the rescuing activity of the wild-type *egl-1* transgene, but failed to

reduce the rescuing activity of the mutant *egl-1* transgene. These results show that

binding of LIN-1 to the *egl-1* promoter is critical for LIN-3 signaling to promote PCD.

These data support the idea that LIN-3 acts through LIN-1 to promote PCD by

transcriptional activation of *egl-1*.
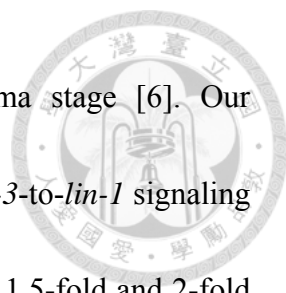
DISCUSSION

LIN-3 signaling promotes PCD through LET-60-MPK-1 signaling and LIN-1 to

activate egl-1 transcription
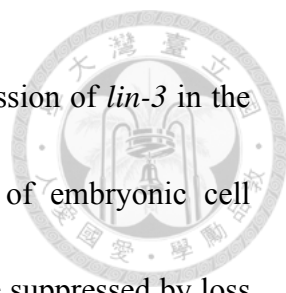
LIN-3-induced LET-60-MPK-1 signaling is important in multiple aspects of

development in *C. elegans* [39-45]. In this study, we provide evidence that it is also

essential for specific somatic PCD. Mutants defective in genes coding for proteins in

this pathway showed reduced PCD in specific cells, ABpl/rpppapp, g1A sisters, and I1

sisters. In contrast, over-activation of this pathway resulted in ectopic deaths of specific

cells, such as gland cells. These results show that LIN-3-induced LET-60-MPK-1

signaling is crucial for the death-versus-life fate of specific cells. In addition, the

downstream transcription factor LIN-1, but not LIN-31, was shown to act in the

LIN-3-induced LET-60-MPK-1 signaling pathway to regulate PCD via the target gene

egl-1. Furthermore, we showed that LIN-1 bound directly to the *egl-1* promoter *in vitro*

and that the LIN-1 binding site of the *egl-1* promoter was important for the cell

death-promoting function of LIN-3 *in vivo*.

Out of 35 embryonic PCDs we analyzed, including the first 13 PCDs in the AB lineage

and 22 pharyngeal PCDs, the *lin-3*-to-*lin-1* signaling pathway is important for the death

of ABpl/rpppapp, g1A sisters, and I1 sisters. ABpl/rpppapp and I1 sisters undergo PCD

31
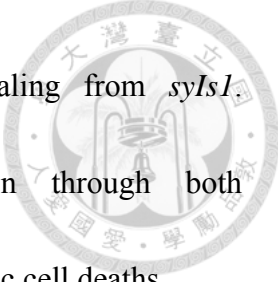
before the comma stage, and g1A sisters die during the comma stage [6]. Our

embryonic cell corpse data revealed that mutants defective in the *lin-3*-to-*lin-1* signaling

pathway had less cell corpses at not only the comma stage, but also 1.5-fold and 2-fold

stages. However, the identities of dying cells affected at the latter two stages have not

yet been determined, partly because no cell-specific markers are available to test for

their survival in the mutants. It is possible that those lineages where PCDs might be more

severely affected have not yet been analyzed in our work and, if so, the *lin-3* signaling

pathway might play a predominant role in these PCDs as compared to the death of

ABpl/rpppapp, g1A sisters, and I1 sisters. Since the mutants defective in the *lin-3* signaling

pathway showed a partially penetrant phenotype in the survival of ABpl/rpppapp, g1A

sisters, and I1 sisters, other genes or pathways, in addition to the *lin-3* signaling pathway,

are required to efficiently promote the death of, at least, ABpl/rpppapp, g1A sisters, and I1

sisters.

Although we have not yet characterized all affected embryonic PCDs, the data obtained

using either the specific cell death assays or the embryonic cell corpse counting assays were

similar. For example, the *lin-3, let-23, let-60, mpk-1* and *lin-1* single mutants had the

same phenotype as their respective single mutants in the *lin-3* or *let-23* mutant

background or feeding *lin-3* or *let-23* RNAi (Figure 1A, 1D, 1G, 5A, and Appendix 7).

Overexpression of *lin-3* using its endogenous promoter or misexpression of *lin-3* in the

intestine resulted in ectopic gland cells and increased numbers of embryonic cell

corpses during comma to two-fold stages. Both phenotypes could be suppressed by loss

of *let-23* or components of the core PCD pathway (Figure 2 and Appendix 4). In

addition, the wild-type *egl-1* genomic DNA fully rescued the *egl-1* cell death defect, but

the mutant *egl-1* genomic DNA with a mutation in the LIN-1 binding site could only

rescue the *egl-1* cell death defect to a similar extent as the *lin-3* mutant (Figure 6C and

6D). Furthermore, loss of *lin-3* did not aggravate the PCD defect of the *egl-1;*

Ex[egl-1(mut)] transgenic animals (Figure 6C and 6D). Therefore, the *lin-3*-to-*lin-1*

signaling pathway may promote the death of ABpl/rpppapp and g1A sisters as well as

other yet uncharacterized doomed cells by the same molecular mechanism. However,

we cannot rule out the possibility that *let-23, mpk-1, let-60* or *lin-1* may affect other

aspects of PCD, rather than promoting the PCD fate, in the yet unidentified doomed

cells.

In the genetic interaction experiments, the *let-23(n1045)* mutation does not completely

eliminate the cell death-promoting function of *syIs1*: the mutation reduced the numbers

of ectopic embryonic cell deaths (Appendix 4) to the wild-type level, but not to the

let-23(n1045) mutant level. The *let-23(n1045)* allele may still have a residual *let-23*

activity [65] and therefore cannot fully block the *lin-3* signaling from *syIs1*.

Alternatively, *syIs1* may exert its PCD-promoting function through both

LET-23-dependent and LET-23 independent pathways to cause ectopic cell deaths.

Previous studies showed that LIN-1 is negatively regulated by the upstream

LIN-3-induced LET-60-MPK-1 signaling pathway during vulval induction [46]. We

found that the LIN-1 function is positively regulated by this signaling pathway to

promote the PCD fate of specific cells. During vulval development, although *lin-1*

inhibits most target gene expression downstream of the LET-60-MPK-1 pathway, *lin-1*

is also required positively for the expression of several downstream genes, such as

egl-17 [74]. Our data indicated that *lin-1* activates *egl-1* expression in promoting PCD

of specific cells. Interestingly, both of these *lin-1*-mediated gene expression processes

are positively regulated by the LET-60-MPK-1 pathway and do not require *lin-31*. It

appears that LIN-1 could have either a positive or negative function on gene expression,

depending on the cellular context and target genes.

LIN-3 signaling was also found to activate *ced-4* transcription, but *egl-1* transcription

probably accounted for most of the LIN-3 signaling-mediated cell death, as, in the *egl-1*

mutant, the mutant *egl-1* transgene lacking the LIN-1 binding site could only restore the

penetrance of ABpl/rpppapp death and the embryonic cell corpse number to the levels

seen in the *lin-3* mutant.

A previous study showed that dying cells that inappropriately survive generally adopt

the fate of the sister or lineal homolog if the latter cells are terminally differentiated [11].

We observed that the g1A sister, when survived in the *lin-3* or *ced-3* mutant, expressed

the gland cell marker $P_{B0280.7}::4Xnls::mrfp$, indicating that the g1A sister adopted its

sister cell fate. To rule out the possibility that the *lin-3* mutation may cause cell fate

transformation and hence block cell death, we examined surviving ABpl/rpppapp in

detail in the *lin-3* mutant. ABpl/rpppapp was chosen because the sister of ABpl/rpppapp

divides once and generates a hypodermal cell and a phasmid sheath cell [6]. It has been

shown that dying cells that inappropriately survive do not adopt their sister cell fates, if

the latter cells undergo cell division and the resulting descendent cells then differentiate

[11]. The observation that surviving ABpl/rpppapp in the *lin-3* or *egl-1* mutant did not

express the hypodermal cell-specific genes *dpy-7* and *ajm-1* (data not shown), as

assayed by their respective reporters $P_{dpy-7}::yfp$ and *ajm::gfp*, suggesting that surviving

ABpl/rpppapp did not further divide or differentiate to generate a hypodermal cell. This

result argues against the possibility that the *lin-3* mutation affects ABpl/rpppapp

survival indirectly through cell fate transformation to its sister or niece cell.

An appropriate level of extrinsic LIN-3 signaling is important for the precise fine-tuning of the life-versus-death fate of cells

Our data support the following model explaining how different levels of LIN-3 expression or activity might regulate PCD (Figure 6E). In the wild-type, after binding LIN-3, LET-23 transduces the cell death-promoting signal through the LET-60-MPK-1 pathway, leading to LIN-1 activation, followed by *egl-1* transcription, and the demise of specific cells. However, mutations in either the LIN-3-induced LET-60-MPK-1 signaling pathway or LIN-1 or a defect in the LIN-1-binding site of the *egl-1* promoter reduces *egl-1* transcription and thus the probability that a cell undergoes PCD. In contrast, overexpression of *lin-3* enhances *egl-1* transcription and leads to ectopic cell deaths. Therefore, LIN-3 signaling may act to specify the death of specific cells and fine-tunes the life-versus-death fate of these cells by modulating transcription of *egl-1*.
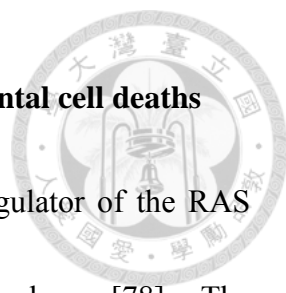
Although EGF has long been known to function in the process of cell proliferation and survival, some reports showed that it also promotes apoptosis [30-32]. In some cases, the difference in cellular outcome appears to depend on its concentration, with a low EGF concentration promoting cell proliferation and a high concentration inducing apoptosis [75,76]. Cells expressing different levels of EGFR also show different responses to the same amount of EGF, as it has been reported that exogenous EGF

attenuates cell death in rats, which express low levels of EGFR, but promotes cell death in mice, which express high levels of EGFR [77]. Thus, it is likely that overactivation of EGF signaling triggers apoptosis. This may be a conserved physiological mechanism for preventing unrestricted proliferation when cells respond to persistent or hyperactivated EGF signaling. In *C. elegans*, cells may use this strategy to fine-tune PCD: cells that are doomed to die may express a high level of LET-23 or its downstream signaling components. This may either avoid inappropriate survival of cells that occasionally escape from the cell death machinery or preset a cell in a sensitized stage to respond quickly when it receives the death signal. This may also explain why some cells are more sensitive to apoptotic stimuli than others.

Our data show that different cells appear to show different susceptibility to *lin-3* signaling in PCD at, at least, three different levels. First, ABpl/rpppapp, g1A sisters, and I1 sisters require *lin-3* signaling for PCD and are sensitive to the wild-type level of *lin-3* signaling. Second, g1 and g2 cells are sensitive to a high level of *lin-3* signaling in PCD, since they survive in the wild-type but can be induced to undergo PCD by the *syIs1* transgene. Third, cells, such as PLM (data not shown), survive even in the presence of the transgene *syIs1* and are therefore insensitive to *lin-3* signaling for their life vs death fate. These results together show a complexity of extrinsic signaling in PCD regulation.

The LET-60-MPK-1 pathway promotes germline and developmental cell deaths

Consistent with our data, mutants defective in *ksr-1*, a positive regulator of the RAS signaling pathway, have reduced embryonic cell corpse numbers [78]. The LET-60-MPK-1- and PI3K-mediated signaling pathways are also known to be involved in physiological or genotoxic stress-induced germ cell death in *C. elegans* [48-51], although the ligand and receptor for these pathways have not yet been identified. The LET-60-MPK-1 pathway regulates the apoptotic process of irradiation-induced germ cell death by restricting CEP-1 protein expression to cells in late pachytene. More importantly, MPK-1, the *C. elegans* ERK, is activated following irradiation and is required for *egl-1* transcription in irradiation-induced germ cell death [50]. This result and our present findings show that the LET-60-MPK-1 pathway regulates *egl-1* transcription to promote both physiological somatic PCD and genotoxic stress-induced germline cell death. In mammalian cells, activation of the RAS-ERK pathway upregulates Bcl-X$_L$ transcription [26]. It has also been shown that EGF regulates the expression of Mcl-1, a member of the anti-apoptotic Bcl-2 family, through activation of MAPK signaling and the direct binding of Elk-1, a member of the ETS gene family, to the Mcl-1 promoter [79]. Thus, the interaction of the RAS-ERK pathway and Bcl-2 family members, such as *egl-1*, Bcl-X$_L$, and Mcl-1, may be a conserved strategy for regulating cell death or survival in evolution.

Pathological and physiological roles of EGFR in promoting cell death

It has been reported that cisplatin, a widely used chemotherapeutic agent for human cancers, causes nephrotoxicity in patients and induces extensive death of the proximal tubules in mice or cultured proximal tubule cells [80-82]. Cisplatin activates EGFR and ERK to trigger apoptosis in cultured proximal tubule cells [82]. In addition, in the autoimmune cutaneous disease pemphigus vulgaris, the body produces autoantibodies that can induce EGFR activation and ERK phosphorylation, leading to activation of caspase-3 [83]. EGFR activation-induced RAS signaling has also been implicated in age-related brain degeneration in *Drosophila* [84]. Taken together, these results and our data show that EGFR activation-induced cell death is a conversed phenomenon and plays an important role in pathological and physiological conditions.

Mutations that cause constitutive activation of EGFR are commonly observed in human cancers. Specific antibodies or inhibitors against activated EGFR have been developed and used as targeted therapeutics [85]. However, previous studies in human cell lines [30-32] and our present results show that overactivation of EGF signaling can promote apoptosis, raising the concern that drugs that antagonize EGFR signaling might have an anti-apoptotic effect and thus a potential tumor-promoting side-effect, depending on the cellular context. Further information on the molecular basis of the distinct divergent

cellular responses of cell proliferation, cell survival, and death to EGF signaling is important for our understanding of the physiological roles of EGF and EGFR signaling during development and homeostasis and for providing perspectives for optimizing the strategy of anticancer drug design.

REFERENCES

1. Fuchs Y, Steller H (2011) Programmed cell death in animal development and disease. Cell 147: 742-758.

2. Baehrecke EH (2002) How death shapes life during development. Nat Rev Mol Cell Biol 3: 779-787.

3. Lettre G, Hengartner MO (2006) Developmental apoptosis in *C. elegans*: a complex CEDnario. Nat Rev Mol Cell Biol 7: 97-108.

4. Potts MB, Cameron S (2011) Cell lineage and cell death: *Caenorhabditis elegans* and cancer research. Nat Rev Cancer 11: 50-58.

5. Sulston JE, Horvitz HR (1977) Post-embryonic cell lineages of the nematode, *Caenorhabditis elegans*. Dev Biol 56: 110-156.

6. Sulston JE, Schierenberg E, White JG, Thomson JN (1983) The embryonic cell lineage of the nematode *Caenorhabditis elegans*. Dev Biol 100: 64-119.

7. Conradt B, Horvitz HR (1998) The *C. elegans* protein EGL-1 is required for programmed cell death and interacts with the Bcl-2-like protein CED-9. Cell 93: 519-529.

8. Hengartner MO, Horvitz HR (1994) *C. elegans* cell survival gene *ced-9* encodes a functional homolog of the mammalian proto-oncogene *bcl-2*. Cell 76: 665-676.

9. Yuan J, Shaham S, Ledoux S, Ellis HM, Horvitz HR (1993) The *C. elegans* cell

death gene *ced-3* encodes a protein similar to mammalian interleukin-1 beta-converting enzyme. Cell 75: 641-652.

10. Zou H, Henzel WJ, Liu X, Lutschg A, Wang X (1997) Apaf-1, a human protein homologous to *C. elegans* CED-4, participates in cytochrome c-dependent activation of caspase-3. Cell 90: 405-413.

11. Ellis HM, Horvitz HR (1986) Genetic control of programmed cell death in the nematode *C. elegans*. Cell 44: 817-829.

12. Hengartner MO, Ellis RE, Horvitz HR (1992) *Caenorhabditis elegans* gene *ced-9* protects cells from programmed cell death. Nature 356: 494-499.

13. Chen F, Hersh BM, Conradt B, Zhou Z, Riemer D, et al. (2000) Translocation of *C. elegans* CED-4 to nuclear membranes during programmed cell death. Science 287: 1485-1489.

14. Yan N, Gu L, Kokel D, Chai J, Li W, et al. (2004) Structural, biochemical, and functional analyses of CED-9 recognition by the proapoptotic proteins EGL-1 and CED-4. Mol Cell 15: 999-1006.

15. Yang X, Chang HY, Baltimore D (1998) Essential role of CED-4 oligomerization in CED-3 activation and apoptosis. Science 281: 1355-1357.

16. Pourkarimi E, Greiss S, Gartner A (2012) Evidence that CED-9/Bcl2 and CED-4/Apaf-1 localization is not consistent with the current model for *C. elegans*

apoptosis induction. Cell Death Differ 19: 406-415.

17. Nehme R, Conradt B (2008) *egl-1*: a key activator of apoptotic cell death in *C. elegans*. Oncogene 27 Suppl 1: S30-40.

18. Peden E, Killian DJ, Xue D (2008) Cell death specification in *C. elegans*. Cell Cycle 7: 2479-2484.

19. Thellmann M, Hatzold J, Conradt B (2003) The Snail-like CES-1 protein of *C. elegans* can block the expression of the BH3-only cell-death activator gene *egl-1* by antagonizing the function of bHLH proteins. Development 130: 4057-4071.

20. Grant S, Qiao L, Dent P (2002) Roles of ERBB family receptor tyrosine kinases, and downstream signaling pathways, in the control of cell growth and survival. Front Biosci 7: d376-389.

21. Danielsen AJ, Maihle NJ (2002) The EGF/ErbB receptor family and apoptosis. Growth Factors 20: 1-15.

22. Wieduwilt MJ, Moasser MM (2008) The epidermal growth factor receptor family: biology driving targeted therapeutics. Cell Mol Life Sci 65: 1566-1584.

23. Xian CJ, Zhou XF (2004) EGF family of growth factors: essential roles and functional redundancy in the nerve system. Front Biosci 9: 85-92.

24. Bergmann A, Tugentman M, Shilo BZ, Steller H (2002) Regulation of cell number by MAPK-dependent control of apoptosis: a mechanism for trophic survival

signaling. Dev Cell 2: 159-170.

25. Henson ES, Gibson EM, Villanueva J, Bristow NA, Haney N, et al. (2003) Increased expression of Mcl-1 is responsible for the blockage of TRAIL-induced apoptosis mediated by EGF/ErbB1 signaling pathway. J Cell Biochem 89: 1177-1192.

26. Jost M, Huggett TM, Kari C, Boise LH, Rodeck U (2001) Epidermal growth factor receptor-dependent control of keratinocyte survival and Bcl-xL expression through a MEK-dependent pathway. J Biol Chem 276: 6320-6326.

27. Leu CM, Chang C, Hu C (2000) Epidermal growth factor (EGF) suppresses staurosporine-induced apoptosis by inducing mcl-1 via the mitogen-activated protein kinase pathway. Oncogene 19: 1665-1675.

28. Allan LA, Morrice N, Brady S, Magee G, Pathak S, et al. (2003) Inhibition of caspase-9 through phosphorylation at Thr 125 by ERK MAPK. Nat Cell Biol 5: 647-654.

29. Fang X, Yu S, Eder A, Mao M, Bast RC, Jr., et al. (1999) Regulation of BAD phosphorylation at serine 112 by the Ras-mitogen-activated protein kinase pathway. Oncogene 18: 6635-6640.

30. Gulli LF, Palmer KC, Chen YQ, Reddy KB (1996) Epidermal growth factor-induced apoptosis in A431 cells can be reversed by reducing the tyrosine kinase activity. Cell

Growth Differ 7: 173-178.

31. Armstrong DK, Kaufmann SH, Ottaviano YL, Furuya Y, Buckley JA, et al. (1994) Epidermal growth factor-mediated apoptosis of MDA-MB-468 human breast cancer cells. Cancer Res 54: 5280-5283.

32. Garcia R, Franklin RA, McCubrey JA (2006) Cell death of MCF-7 human breast cancer cells induced by EGFR activation in the absence of other growth factors. Cell Cycle 5: 1840-1846.

33. Hill RJ, Sternberg PW (1992) The gene *lin-3* encodes an inductive signal for vulval development in *C. elegans*. Nature 358: 470-476.

34. Aroian RV, Koga M, Mendel JE, Ohshima Y, Sternberg PW (1990) The *let-23* gene necessary for *Caenorhabditis elegans* vulval induction encodes a tyrosine kinase of the EGF receptor subfamily. Nature 348: 693-699.

35. Chamberlin HM, Sternberg PW (1994) The *lin-3/let-23* pathway mediates inductive signalling during male spicule development in *Caenorhabditis elegans*. Development 120: 2713-2721.

36. Clandinin TR, DeModena JA, Sternberg PW (1998) Inositol trisphosphate mediates a RAS-independent response to LET-23 receptor tyrosine kinase activation in *C. elegans*. Cell 92: 523-533.
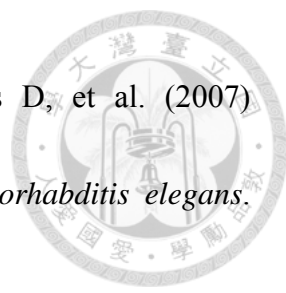
37. Jiang LI, Sternberg PW (1998) Interactions of EGF, Wnt and HOM-C genes specify

the P12 neuroectoblast fate in *C. elegans*. Development 125: 2337-2347.

38. Van Buskirk C, Sternberg PW (2007) Epidermal growth factor signaling induces behavioral quiescence in *Caenorhabditis elegans*. Nat Neurosci 10: 1300-1307.

39. Han M, Sternberg PW (1990) *let-60*, a gene that specifies cell fates during *C. elegans* vulval induction, encodes a *ras* protein. Cell 63: 921-931.

40. Clark SG, Stern MJ, Horvitz HR (1992) *C. elegans* cell-signalling gene *sem-5* encodes a protein with SH2 and SH3 domains. Nature 356: 340-344.

41. Han M, Golden A, Han Y, Sternberg PW (1993) *C. elegans lin-45 raf* gene participates in *let-60 ras*-stimulated vulval differentiation. Nature 363: 133-140.

42. Wu Y, Han M, Guan KL (1995) MEK-2, a *Caenorhabditis elegans* MAP kinase kinase, functions in Ras-mediated vulval induction and other developmental events. Genes Dev 9: 742-755.

43. Kornfeld K, Guan KL, Horvitz HR (1995) The *Caenorhabditis elegans* gene *mek-2* is required for vulval induction and encodes a protein similar to the protein kinase MEK. Genes & Development 9: 756-768.

44. Lackner MR, Kornfeld K, Miller LM, Horvitz HR, Kim SK (1994) A MAP kinase homolog, *mpk-1*, is involved in *ras*-mediated induction of vulval cell fates in *Caenorhabditis elegans*. Genes & development 8: 160-173.

45. Wu Y, Han M (1994) Suppression of activated Let-60 *ras* protein defines a role of

Caenorhabditis elegans Sur-1 MAP kinase in vulval differentiation. Genes Dev 8: 147-159.

46. Tan PB, Lackner MR, Kim SK (1998) MAP kinase signaling specificity mediated by the LIN-1 Ets/LIN-31 WH transcription factor complex during *C. elegans* vulval induction. Cell 93: 569-580.

47. Hopper NA (2006) The adaptor protein *soc-1*/Gab1 modifies growth factor receptor output in *Caenorhabditis elegans*. Genetics 173: 163-175.

48. Gumienny TL, Lambie E, Hartwieg E, Horvitz HR, Hengartner MO (1999) Genetic control of programmed cell death in the *Caenorhabditis elegans* hermaphrodite germline. Development 126: 1011-1022.

49. Perrin AJ, Gunda M, Yu B, Yen K, Ito S, et al. (2013) Noncanonical control of *C. elegans* germline apoptosis by the insulin/IGF-1 and Ras/MAPK signaling pathways. Cell Death Differ 20: 97-107.

50. Rutkowski R, Dickinson R, Stewart G, Craig A, Schimpl M, et al. (2011) Regulation of *Caenorhabditis elegans* p53/CEP-1-dependent germ cell apoptosis by Ras/MAPK signaling. PLoS Genet 7: e1002238.

51. Quevedo C, Kaplan DR, Derry WB (2007) AKT-1 regulates DNA-damage-induced germline apoptosis in *C. elegans*. Curr Biol 17: 286-292.

52. Brenner S (1974) The genetics of *Caenorhabditis elegans*. Genetics 77: 71-94.

53. Hunt-Newbury R, Viveiros R, Johnsen R, Mah A, Anastas D, et al. (2007) High-throughput *in vivo* analysis of gene expression in *Caenorhabditis elegans*. PLoS Biol 5: e237.

54. Timmons L, Court DL, Fire A (2001) Ingestion of bacterially expressed dsRNAs can produce specific and potent genetic interference in *Caenorhabditis elegans*. Gene 263: 103-112.

55. Simmer F, Tijsterman M, Parrish S, Koushika SP, Nonet ML, et al. (2002) Loss of the putative RNA-directed RNA polymerase RRF-3 makes *C. elegans* hypersensitive to RNAi. Curr Biol 12: 1317-1319.

56. Kamath RS, Fraser AG, Dong Y, Poulin G, Durbin R, et al. (2003) Systematic functional analysis of the *Caenorhabditis elegans* genome using RNAi. Nature 421: 231-237.

57. Mello C, Fire A (1995) DNA transformation. Methods Cell Biol 48: 451-482.

58. Maduro M, Pilgrim D (1995) Identification and cloning of *unc-119*, a gene expressed in the *Caenorhabditis elegans* nervous system. Genetics 141: 977-988.

59. Fukushige T, Hawkins MG, McGhee JD (1998) The GATA-factor *elt-2* is essential for formation of the *Caenorhabditis elegans* intestine. Dev Biol 198: 286-302.

60. Miley GR, Fantz D, Glossip D, Lu X, Saito RM, et al. (2004) Identification of residues of the *Caenorhabditis elegans* LIN-1 ETS domain that are necessary for

DNA binding and regulation of vulval cell fates. Genetics 167: 1697-1709.

61. Ellis RE, Jacobson DM, Horvitz HR (1991) Genes required for the engulfment of cell corpses during programmed cell death in *Caenorhabditis elegans*. Genetics 129: 79-94.

62. Schnabel R, Hutter H, Moerman D, Schnabel H (1997) Assessing normal embryogenesis in *Caenorhabditis elegans* using a 4D microscope: variability of development and regional specification. Dev Biol 184: 234-265.

63. Livak KJ, Schmittgen TD (2001) Analysis of relative gene expression data using real-time quantitative PCR and the 2(-Delta Delta C(T)) Method. Methods 25: 402-408.

64. Conradt B, Horvitz HR (1999) The TRA-1A sex determination protein of *C. elegans* regulates sexually dimorphic cell deaths by repressing the *egl-1* cell death activator gene. Cell 98: 317-327.

65. Ferguson EL, Horvitz HR (1985) Identification and characterization of 22 genes that affect the vulval cell lineages of the nematode *Caenorhabditis elegans*. Genetics 110: 17-72.

66. Hoeppner DJ, Hengartner MO, Schnabel R (2001) Engulfment genes cooperate with *ced-3* to promote cell death in *Caenorhabditis elegans*. Nature 412: 202-206.

67. Chang C, Newman AP, Sternberg PW (1999) Reciprocal EGF signaling back to the
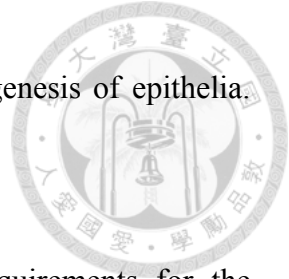
uterus from the induced *C. elegans* vulva coordinates morphogenesis of epithelia. Curr Biol 9: 237-246.

68. Liu J, Tzou P, Hill RJ, Sternberg PW (1999) Structural requirements for the tissue-specific and tissue-general functions of the *Caenorhabditis elegans* epidermal growth factor LIN-3. Genetics 153: 1257-1269.

69. Katz WS, Hill RJ, Clandinin TR, Sternberg PW (1995) Different levels of the *C. elegans* growth factor LIN-3 promote distinct vulval precursor fates. Cell 82: 297-307.

70. Sternberg PW, Horvitz HR (1986) Pattern formation during vulval development in *C. elegans*. Cell 44: 761-772.

71. Hwang BJ, Sternberg PW (2004) A cell-specific enhancer that specifies *lin-3* expression in the *C. elegans* anchor cell for vulval development. Development 131: 143-151.

72. Miller LM, Gallegos ME, Morisseau BA, Kim SK (1993) *lin-31*, a *Caenorhabditis elegans* HNF-3/fork head transcription factor homolog, specifies three alternative cell fates in vulval development. Genes Dev 7: 933-947.

73. Beitel GJ, Tuck S, Greenwald I, Horvitz HR (1995) The *Caenorhabditis elegans* gene *lin-1* encodes an ETS-domain protein and defines a branch of the vulval induction pathway. Genes Dev 9: 3149-3162.

74. Tiensuu T, Larsen MK, Vernersson E, Tuck S (2005) *lin-1* has both positive and negative functions in specifying multiple cell fates induced by Ras/MAP kinase signaling in *C. elegans*. Dev Biol 286: 338-351.

75. Chiu B, Mirkin B, Madonna MB (2006) Mitogenic and apoptotic actions of epidermal growth factor on neuroblastoma cells are concentration-dependent. J Surg Res 135: 209-212.

76. Wang H, Guo D, Ye F, Xi G, Wang B, et al. (2006) Effect and mechanism of epidermal growth factor on proliferation of GL15 gliomas cell line. J Huazhong Univ Sci Technolog Med Sci 26: 604-606.

77. Kiley SC, Chevalier RL (2007) Species differences in renal Src activity direct EGF receptor regulation in life or death response to EGF. Am J Physiol Renal Physiol 293: F895-903.

78. Sugimoto A, Kusano A, Hozak RR, Derry WB, Zhu J, et al. (2001) Many genomic regions are required for normal embryonic programmed cell death in *Caenorhabditis elegans*. Genetics 158: 237-252.

79. Booy EP, Henson ES, Gibson SB (2011) Epidermal growth factor regulates Mcl-1 expression through the MAPK-Elk-1 signalling pathway contributing to cell survival in breast cancer. Oncogene 30: 2367-2378.

80. Berns JS, Ford PA (1997) Renal toxicities of antineoplastic drugs and bone marrow
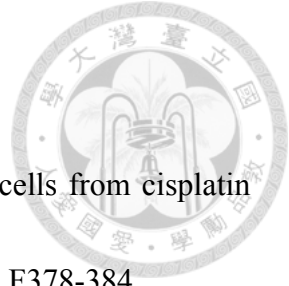
transplantation. Semin Nephrol 17: 54-66.

81. Price PM, Safirstein RL, Megyesi J (2004) Protection of renal cells from cisplatin toxicity by cell cycle inhibitors. Am J Physiol Renal Physiol 286: F378-384.

82. Arany I, Megyesi JK, Kaneto H, Price PM, Safirstein RL (2004) Cisplatin-induced cell death is EGFR/src/ERK signaling dependent in mouse proximal tubule cells. Am J Physiol Renal Physiol 287: F543-549.

83. Frusic-Zlotkin M, Raichenberg D, Wang X, David M, Michel B, et al. (2006) Apoptotic mechanism in pemphigus autoimmunoglobulins-induced acantholysis--possible involvement of the EGF receptor. Autoimmunity 39: 563-575.

84. Botella JA, Kretzschmar D, Kiermayer C, Feldmann P, Hughes DA, et al. (2003) Deregulation of the Egfr/Ras signaling pathway induces age-related brain degeneration in the *Drosophila* mutant *vap*. Mol Biol Cell 14: 241-250.

85. Pao W, Chmielecki J (2010) Rational, biologically based treatment of EGFR-mutant non-small-cell lung cancer. Nat Rev Cancer 10: 760-774.

86. Gu T, Orita S, Han M (1998) *Caenorhabditis elegans* SUR-5, a novel but conserved protein, negatively regulates LET-60 Ras activity during vulval induction. Mol Cell Biol 18: 4556-4564.

FIGURES AND TABLES

A

Genotype	Number of embryonic cell corpses				
	Comma	1.5-fold	2-fold	3-fold	4-fold
Wild-type	10.0 ± 1.6	11.4 ± 1.5	10.0 ± 1.9	2.1 ± 1.7	0.5 ± 0.7
let-23(n1045)	7.3 ± 1.9**	9.0 ± 2.1**	6.3 ± 2.1**	1.7 ± 1.5	0.4 ± 0.6
let-23(sy1)	6.9 ± 2.4**	7.5 ± 2.3**	6.4 ± 2.2**	2.6 ± 1.8	0.3 ± 0.5
let-23(sy97)	6.9 ± 1.9**	8.6 ± 2.2**	7.2 ± 2.7**	2.5 ± 1.8	0.5 ± 0.6
lin-3(e1417)	6.8 ± 2.0**	8.8 ± 2.3**	6.3 ± 2.4**	1.5 ± 1.8	0.2 ± 0.6
lin-3(n378)	6.0 ± 1.7**	9.5 ± 1.6**	7.0 ± 2.2**	2.4 ± 1.6	0.4 ± 0.6
let-23(n1045); lin-3(e1417)	7.2 ± 1.6**	8.9 ± 2.5**	6.8 ± 1.5**	2.0 ± 1.9	0.4 ± 0.5
Control RNAi	9.2 ± 2.9	10.2 ± 3.7	9.7 ± 1.8	2.1 ± 1.8	0.5 ± 0.7
let-23 RNAi	6.8 ± 2.1**	8.2 ± 2.3*	6.9 ± 2.9**	2.0 ± 1.8	0.6 ± 0.7
lin-3 RNAi	7.0 ± 1.7*	8.0 ± 2.5*	6.7 ± 3.0**	1.8 ± 1.7	0.4 ± 0.6

B

C

D

E

Genotype	% of extra surviving cells in the pharyngeal region											
	% g1A sister	% l1 sister	% M1 sister	% m7 sister	% M4 sister	% g2 sister	% m1 sister	% MC sister	% l2 aunt/sister	% e1 aunt/sister	% m2 sister	% NSM sister
Wild-type	0	0	0	0	0	0	5	5	0	0	0	0
lin-3	10	10	0	0	0	0	5	10	0	0	0	0
let-23	15	5	0	0	0	0	0	10	0	0	0	0

F

G

Figure 1. lin-3 and let-23 promote specific PCDs in C. elegans.

(A) The number of cell corpses was scored at indicated developmental stages and presented as the mean ± SD (n≥30). The *rrf-3(pk1426)* mutant was used to enhance the RNAi effect in RNAi experiments. Mutants were compared to wild-type, and RNAi treatment of individual genes was compared to control RNAi (*$P<0.05$ and **$P<0.001$, two-tailed *t* test).

(B) The DIC images of the wild-type and *lin-3(e1417)* mutant embryos at approximately 270 min after fertilization. The white arrowheads indicate ABpl/rpppapp cell corpses and the hollow arrowheads indicate excretory cells. The percentage of embryos that did not have ABpl/rpppappcell corpse is shown in the bottom left corner. *$P=0.048$ when compared to wild-type (Fisher's exact test). Twenty one and thirteen embryos were scored for wild-type and *lin-3* mutants, respectively. Scale bar: 10 μm.

(C) The GFP and DIC images of the wild-type, *lin-3(e1417)*, and *egl-1(n1084n3082)* worms expressing *sur-5::gfp* at the L1 stage. The arrowheads indicate the nuclei of hyp8, hyp9, hyp10, and hyp11. The hyp10 cell is binuclear. The hollow arrowheads indicate a surviving ABpl/rpppapp. The percentage of worms with surviving ABpl/rpppapp is shown in the bottom right corner. *indicates $P<0.05$ and **$P<0.001$ when compared to wild-type (Fisher's exact test). More than thirty worms were scored for each genotype. Scale bar: 10 μm. The GFP protein expressed from the *sur-5::gfp*
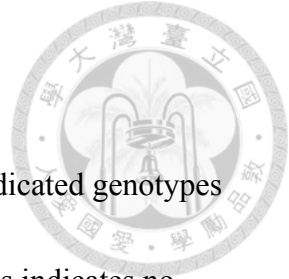
transgene is localized to almost all somatic nuclei [86].

(D) The percentage of worms with surviving ABpl/rpppapp of the indicated genotypes was shown. *indicates *P*<0.05 and **P*<0.001 (Fisher's exact test). ns indicates no statistical difference (p>0.05). Alleles used here are *lin-3(e1417), let-23(sy1)*, and *egl-1(n1084n3082)*. More than thirty worms were scored for each genotype.

(E) Analysis of surviving cells in the pharyngeal region (n=20). Alleles used here are *lin-3(e1417)* and *let-23(n1045)*.

(F) The g1 and g2 gland cells in the pharynx are shown in the illustration. The white circles indicate the five gland cells (g1P, g1AL, g1AR, g2L, and g2R) that normally survive and the gray circles the sister cells of g1AL, g1AR, g2L, and g2R that are destined to die. Monomeric red fluorescent protein (mRFP) images of the wild-type, *lin-3(e1417)*, and *ced-3(n717)* worms expressing $P_{B0280.7}::4Xnls::mrfp$ are shown. The arrowheads indicate cells expressing mRFP. The percentage of animals that have extra gland cell(s) is shown in the bottom right corner. *indicates *P*<0.05 and **P*<0.001 when compared to wild-type (Fisher's exact test). One hundred L4 animals were scored for each genotype. The image stacks were merged by maximum intensity projection using Image J. Scale bar: 10 μm.

(G) The percentage of worms with extra gland cells of the indicated genotypes was shown. *indicates *P*<0.05 and **P*<0.001 (Fisher's exact test). ns indicates no statistical

difference (p>0.05). Alleles used here are *lin-3(e1417)* and *ced-3(n717)*. More than

forty worms were scored for each genotype.
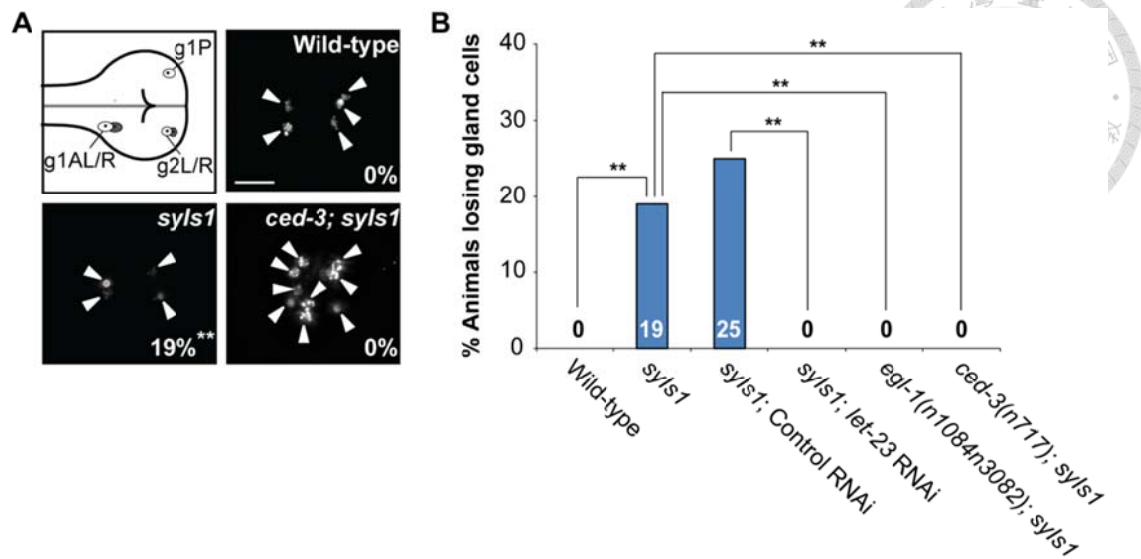
Figure 2. Overexpression of *lin-3* induces ectopic gland cell death(s) through *let-23* and the core PCD pathway.

(A) Monomeric red fluorescent protein (mRFP) images of the wild-type, *syIs1*, and *ced-3(n717); syIs1* worms expressing $P_{B0280.7}::4Xnls::mrfp$ are shown. The arrowheads indicate cells expressing mRFP. The percentage of animals losing gland cell(s) is shown in the bottom right corner. **indicates $P<0.001$ when compared to wild-type (Fisher's exact test). One hundred L4 animals were scored for each genotype. The image stacks were merged by maximum intensity projection using Image J. Scale bar: 10 μm.

(B) The percentage of worms losing gland cell(s) of the indicated genotypes was shown. **indicates $P<0.001$ (Fisher's exact test). More than forty worms were scored for each genotype.
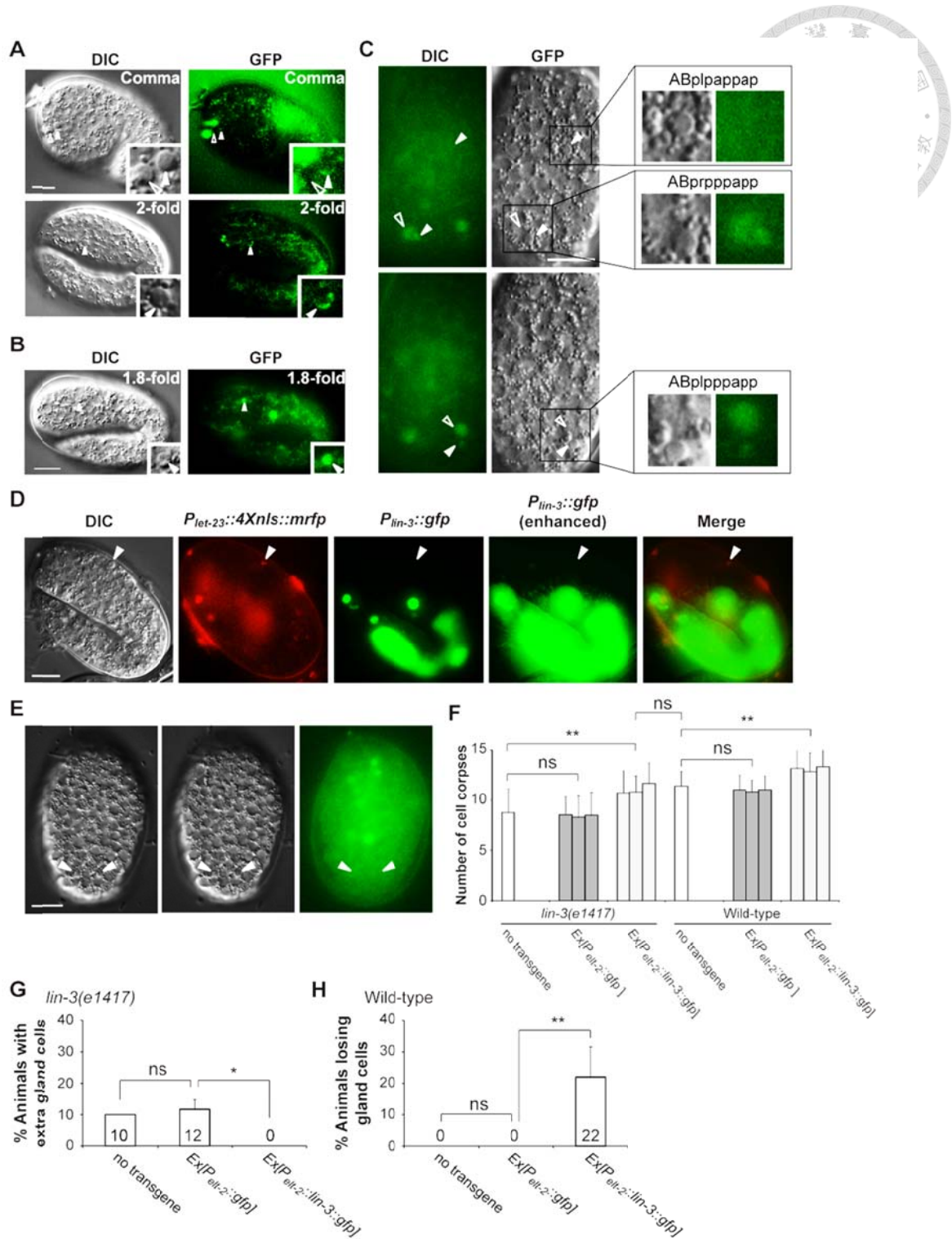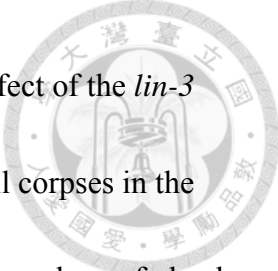
Figure 3. let-23 is expressed in dying cells, whereas lin-3 acts in a cell-nonautonomous manner to promote PCD.

(A and B) Representative DIC and GFP images of embryos carrying (A) the *syEx234[P_{let-23}::let-23::gfp]* transgene or (B) the *P_{let-23}::4Xnls::gfp* transgene. The white arrowheads indicate cell corpses expressing LET-23::GFP and the hollow arrowheads cell corpses not expressing LET-23::GFP. Scale bar: 10 μm. The insets show a dying cell at a three-fold higher magnification.

(C) The DIC and GFP images of an embryo carrying the *P_{let-23}::4Xnls::gfp* transgene. Two different focal planes of the same embryo are shown in the upper and lower panels. The white arrowheads indicate ABpl/rpppapp corpses and ABplpappap and the hollow arrowheads sister cells of ABpl/rpppapp. Scale bar: 10 μm. The insets show the indicated cells at a higher magnification.

(D) The expression pattern of *P_{lin-3}::gfp* and *P_{let-23}::4Xnls::mrfp* transgenes in a wild-type embryo. The white arrowheads indicate the same cell corpse expressing *P_{let-23}::4Xnls::mrfp*. The image stacks of *P_{lin-3}::gfp* were merged by maximum intensity projection using Image J. The strong GFP expression is from the co-injection marker *P_{elt-2}::gfp*. Scale bar: 10 μm.

(E) *P_{lin-3}::gfp* is not expressed in ABpl/rpppapp corpses. The image stacks of *P_{lin-3}::gfp* were merged by maximum intensity projection using Image J. Scale bar: 10 μm.

(F-H) Intestine-specific expression of LIN-3 rescues the cell death defect of the *lin-3* mutant and causes ectopic cell deaths in the wild-type. Embryonic cell corpses in the indicated genotypes were scored at the 1.5-fold stage (n≥30), and the numbers of gland cells were scored at the L4 stage (n≥40). Three independent stable transgenic lines were analyzed.

*indicates $P<0.05$ and **$P<0.001$ in a two-tailed *t*-test (F) or fisher's exact test (G and H). ns indicates no statistical difference ($p>0.05$).
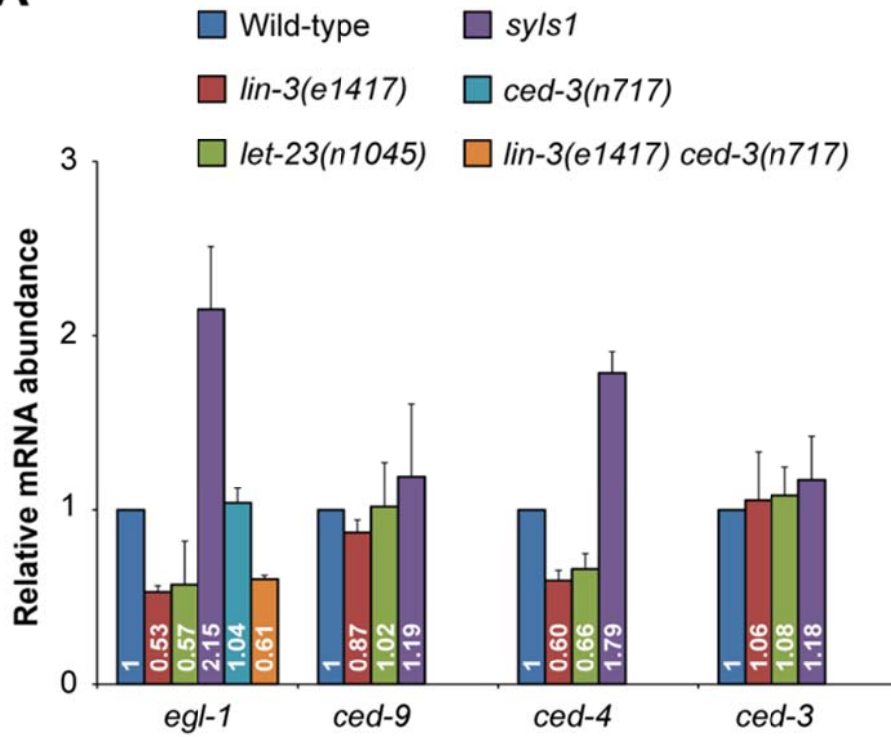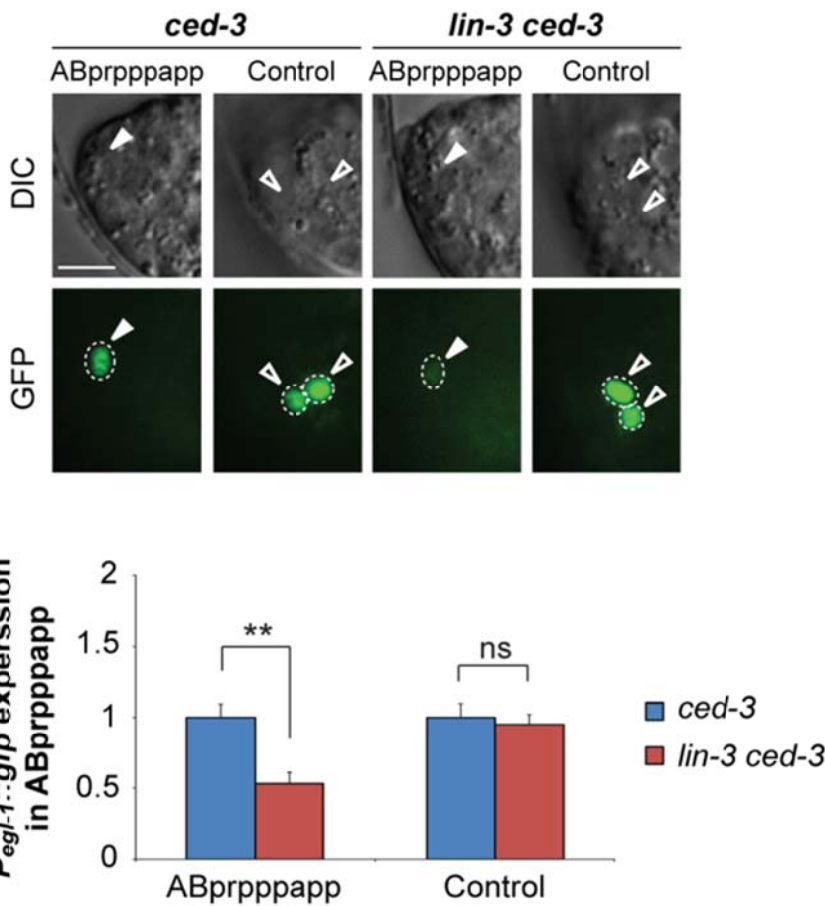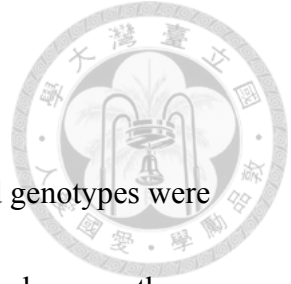
Figure 4. *lin-3* promotes *egl-1* transcription.

(A) *egl-1*, *ced-9*, *ced-4*, and *ced-3* transcripts in embryos of indicated genotypes were measured by quantitative RT-PCR. The relative mRNA abundance is shown as the mean and SD of the results from at least two independent experiments, each performed in triplicates.

(B) The DIC and GFP images of *ced-3* (left) and *lin-3 ced-3* (right) embryos expressing the P_{egl-1}::*gfp* transgene. Arrowheads indicate ABprpppapp, and hollow arrowheads indicate two cells that also express *egl-1* near ABprpppapp (Control experiment). The bottom figures show the P_{egl-1}::*gfp* expression level of the indicated cells in the *ced-3* single mutant (blue) and the *lin-3 ced-3* double mutant (red). The expression level of P_{egl-1}::*gfp* in ABprpppapp of *ced-3(n717)* (n=44) and *lin-3(e1417) ced-3(n717)* (n=40) mutants was analyzed as described in Materials and Methods. Error bars represent the SEM. **indicates $P<0.001$ (two-tailed *t* test). Scale bar: 5 μm.
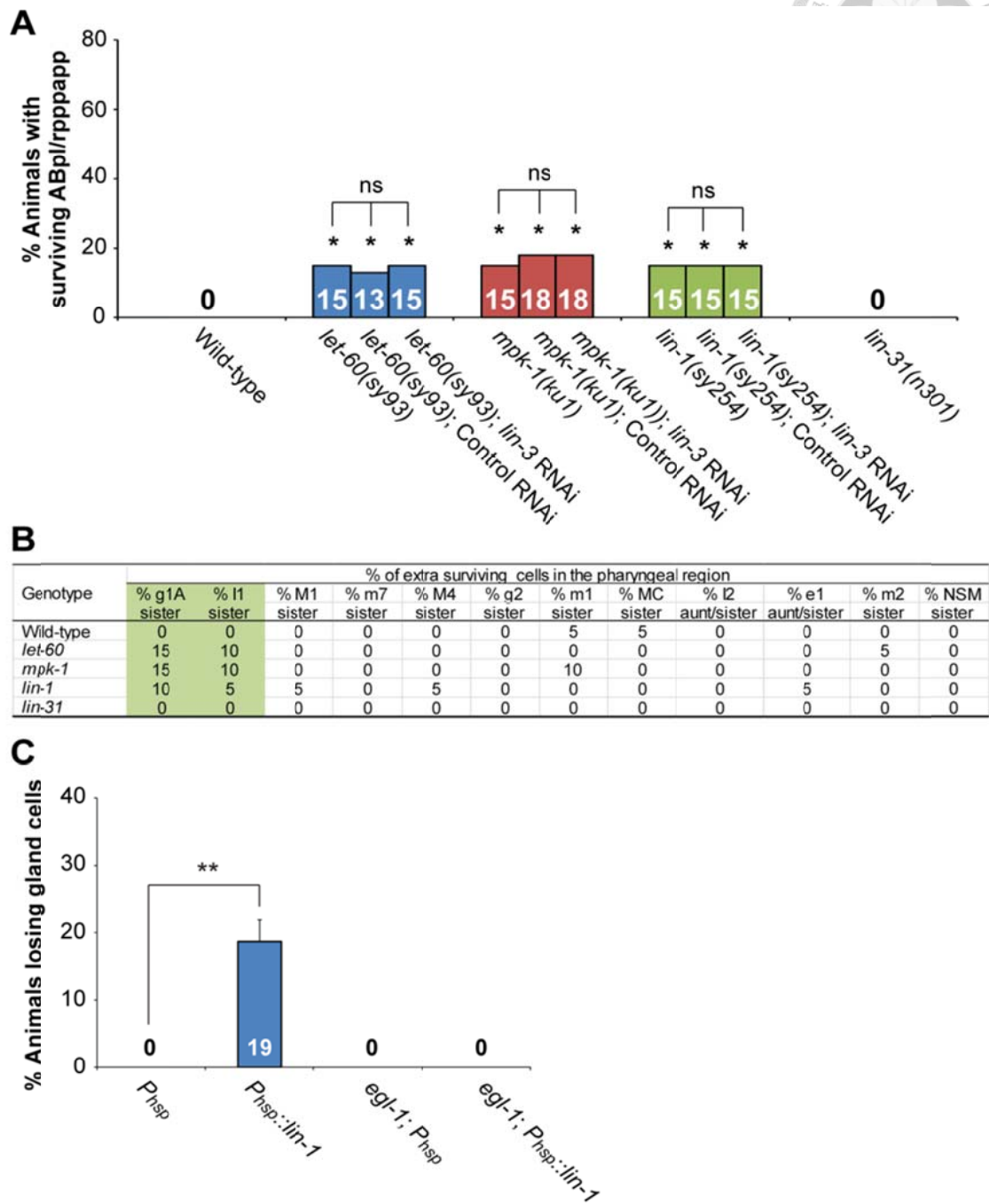
Figure 5. *lin-3*, *lin-1* and the LET-60-MPK-1 pathway act in the same pathway to promote PCD.

(A) The percentage of worms with surviving ABpl/rpppapp of the indicated genotypes

Panel B table:

Genotype	% of extra surviving cells in the pharyngeal region											
	% g1A sister	% I1 sister	% M1 sister	% m7 sister	% M4 sister	% g2 sister	% m1 sister	% MC sister	% I2 aunt/sister	% e1 aunt/sister	% m2 sister	% NSM sister
Wild-type	0	0	0	0	0	0	5	5	0	0	0	0
let-60	15	10	0	0	0	0	0	0	0	0	5	0
mpk-1	15	10	0	0	0	0	10	0	0	0	0	0
lin-1	10	5	5	0	5	0	0	0	0	5	0	0
lin-31	0	0	0	0	0	0	0	0	0	0	0	0

was shown. *indicates *P*<0.05 when compared to the wild-type (Fisher's exact test). ns indicates no statistical difference (p>0.05). More than thirty worms were scored for each genotype.

(B) Analysis of extra surviving cells in the pharyngeal region (n=20). Alleles used here are *let-60(sy93), mpk-1(ku1), lin-1(sy254), and lin-31(n301)*.

(C) The percentage of wild-type or *egl-1(n1084n3082)* worms carrying the indicated transgene that lost gland cell(s) in the pharynx was shown. **P*<0.001 (Fisher's exact test). The gland cells were scored using the *tpIs8* transgene, and the worms were treated with heat shock as described in Materials and Methods. *P*~*hsp*~*::lin-1* or *P*~*hsp*~ indicate the transgenes, in which *lin-1* or no cDNA was expressed under the control of the heat-shock promoter, respectively. More than forty worms were scored for each genotype.
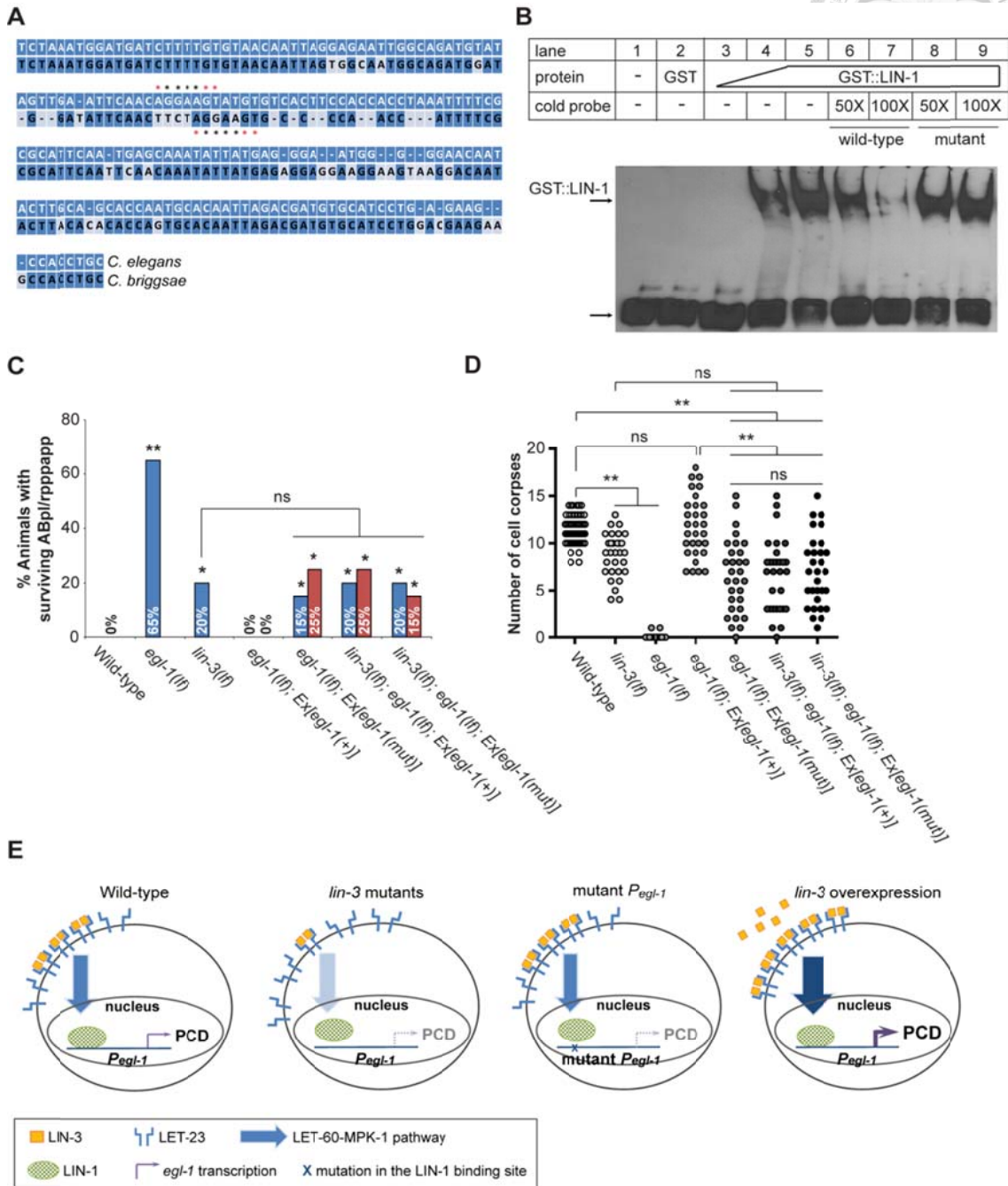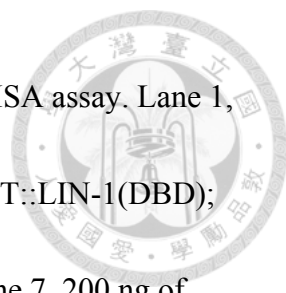
Figure 6. *lin-3* promotes PCD through transcriptional activation of *egl-1* by LIN-1.

(A) The alignment between the *C. elegans* and *C. briggsae* genomic sequences near the

P3 fragment. *indicates the LIN-1 minimal recognition sequence GGAA/T.

(B) GST::LIN-1(DBD) directly binds to the *egl-1* promoter in an EMSA assay. Lane 1, no protein; lane 2, 200 ng of GST; lanes 3-5, 10, 50, or 200 ng of GST::LIN-1(DBD); lane 6: 200 ng of GST::LIN-1(DBD) + 50X wild-type cold probe; lane 7, 200 ng of GST::LIN-1(DBD) + 100X wild-type cold probe; lane 8, 200 ng of GST::LIN-1(DBD) + 50X mutant cold probe; lane 9, 200 ng of GST::LIN-1(DBD) + 100X mutant cold probe. The bottom arrow indicates non bound probe and the top arrow DNA bound to GST::LIN-1(DBD) and displaying retarded mobility.

(C) The percentage of animals with surviving ABpl/rpppapp of the indicated genotypes was scored (n≥30). *Ex[egl-1(+)]* and *Ex[egl-1(mut)]* indicate wild-type and mutant *egl-1* transgenes, respectively, as described in the text. The surviving ABpl/rpppapp was scored using the *sur-5::gfp* reporter as described in Figure 1B. Two independent stably transmitted lines were analyzed for each transgene. Alleles used: *lin-3(e1417)* and *egl-1(n1084n3082)*. *indicates *P<0.05* and **P<0.001 when *egl-1(lf)* and *lin-3(lf)* were compared to wild-type or the transgenic strains were compared to *egl-1(lf); Ex[egl-1(+)]* (Fisher's exact test). ns, no significance.

(D) Cell corpses in the embryos of the indicated genotypes carrying the wild-type or mutant *egl-1* gene were scored at the 1.5-fold stage (n≥30). Each circle represents a single embryo. At least three independent stably transmitted lines were analyzed for each transgene. Alleles used: *lin-3(e1417)* and *egl-1(n1084n3082)*. **indicates *P<0.001*

in a two-tailed *t*-test. ns indicates no statistical difference (p>0.05).

(E) Proposed model of how *lin-3* promotes PCD (see text for details).

APPENDIX

A

Dying Cell	Disappearance ratio
ABalaapapa	0/13
ABalaappaa	0/13
ABalapapaa	0/13
ABalappaaa	0/13
ABalppaaaa	0/13
ABalppaapa	0/13
ABaraaaapp	0/13
ABarpaaapp	0/13
ABplpappap	0/13
ABplppaaap	0/13
ABplpppapp	1/13
ABprppaaap	0/13
ABprpppapp	2/13
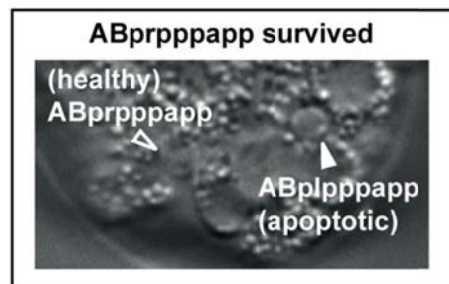
Appendix 1. Loss of *lin-3* causes the disappearance of ABpl/rpppapp corpse(s).

The first 13 cells that die in the AB lineage during embryogenesis were examined by four-dimensional DIC microscopy in thirteen *lin-3(e1417)* mutant embryos as described in Materials and Methods.

(A) The ratio of embryos that did not have the indicated cell corpse was shown.

(B) A representative DIC image of a *lin-3 ((e1417)* embryo showing apoptotic ABpl/rpppapp (indicated by arrow heads).

(C) A representative DIC image of a *lin-3 ((e1417)* embryo showing healthy ABprpppapp (indicated by open arrow head) and apoptotic ABplpppapp (indicated by arrow head).
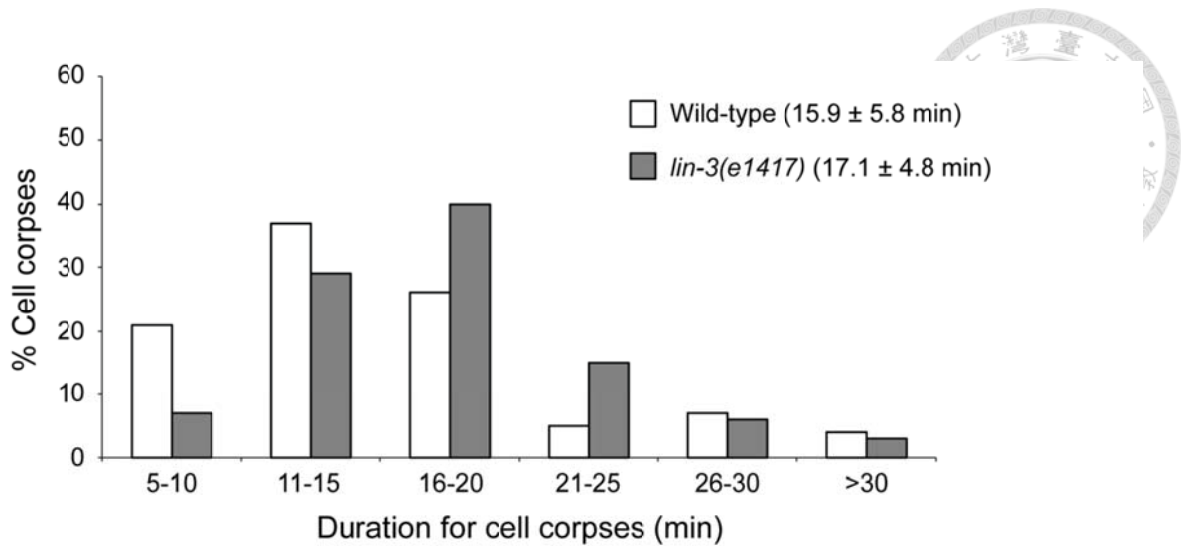
Appendix 2. The *lin-3(e1417)* mutation does not affect the duration of the first 13 cell corpses derived from the AB lineage.

The duration of cell corpses in the wild-type (white bars) and *lin-3(e1417)* mutant (gray bars) embryos was measured by a four-dimensional DIC microscopy analysis. More than 13 embryos were analyzed for each genotype. The y axis represents the percentage of cell corpses in a specific duration range (shown on the x axis). Numbers in parentheses indicate the average duration time of cell corpses (mean ± SD) for each genotype. There is no significant difference between the wild-type and *lin-3(e1417)* mutant embryos (*P*=0.24, two-tailed *t* test).

Appendix 3. Analysis of extra surviving cells in the pharyngeal region in the *ced-3(n2427)* sensitized background.

Genotype	% of extra surviving cells in the pharyngeal region											
	% g1 sister	% l1 sister	% M1 sister	% m7 sister	% M4 sister	% g2 sister	% m1 sister	% MC sister	% l2 aunt/sister	% e1 aunt/sister	% m2 sister	% NSM sister
ced-3	10	10	30	15	5	55	20	15	10	0	15	0
lin-3 ced-3	35	40	60	35	15	70	35	35	10	0	20	5
let-23; lin-3	40	40	70	20	10	70	40	20	15	5	10	0

Extra surviving cells were counted in the anterior and posterior pharynx of L4 hermaphrodites using Nomarski optics (n=20). Alleles used: *lin-3(e1417)*, *let-23(n1045)*, and *ced-3(n717)*.

Appendix 3. Analysis of extra surviving cells in the pharyngeal region in the *ced-3(n2427)* seneitized background.

Appendix 4. *lin-3* requires *let-23* and the core PCD pathway to increase numbers of embryonic cell corpses.

| Genotype | Number of embryonic cell corpses[a] | | | | |
	Comma	1.5-fold	2-fold	3-fold	4-fold
Wild-type	10.0 ± 1.6	11.4 ± 1.5	10.0 ± 1.9	2.1 ± 1.7	0.5 ± 0.7
syIs1	12.4 ± 2.4**	13.2 ± 2.2**	13.1 ± 2.1**	2.5 ± 1.8	0.5 ± 0.6
let-23(n1045); syIs1	9.9 ± 2.4[††]	10.8 ± 1.9[††]	9.3 ± 2.6[††]	2.2 ± 1.5	0.6 ± 0.6
egl-1(n1084n3082)	0.1 ± 0.3	0.1 ± 0.3	0.1 ± 0.3	0.0 ± 0.0	0.0 ± 0.2
egl-1(n1084n3082); syIs1	0.1 ± 0.3	0.0 ± 0.0	0.0 ± 0.0	0.0 ± 0.0	0.0 ± 0.2
ced-9(n1950)	0.1 ± 0.3	0.4 ± 0.5	1.2 ± 1.1	0.5 ± 0.6	0.4 ± 0.6
ced-9(n1950); syIs1	0.3 ± 0.5	0.4 ± 0.6	0.8 ± 0.8	0.7 ± 0.7	0.7 ± 0.7
ced-4(n1162)	0.1 ± 0.3	0.1 ± 0.3	0.0 ± 0.0	0.0 ± 0.0	0.0 ± 0.0
ced-4(n1162); syIs1	0.1 ± 0.3	0.1 ± 0.3	0.0 ± 0.0	0.0 ± 0.0	0.0 ± 0.0
ced-3(n717)	0.1 ± 0.3	0.1 ± 0.3	0.1 ± 0.3	0.0 ± 0.0	0.0 ± 0.0
ced-3(n717); syIs1	0.1 ± 0.3	0.1 ± 0.3	0.1 ± 0.3	0.0 ± 0.0	0.0 ± 0.0

[a]Cell corpses scored at the indicated developmental stages are presented as the mean ± SD. (n≥30). *syIs1* is a chromosomal integrant of a repetitive *lin-3* transgene. *syIs1* was compared to wild-type (**P*<0.05 and ***P*<0.001, two-tailed *t* test) and *let-23(n1045); syIs1[lin-3(+)]* were compared to *syIs1[lin-3(+)]* ([†]*P*<0.05 and [††]*P*<0.001, two-tailed *t* test).

Appendix 4. *lin-3* **requires** *let-23* **and the core PCD pathway to incerase numbers of embryonic cell corpses.**

Appendix 5. Mutants defective in the LET-60-MPK-1 pathway have reduced numbers of cell corpses.

Genotype	Number of cell corpses[a]									
	Comma		1.5-fold		2-fold		3-fold		4-fold	
Wild-type (at 20℃)	10.0	± 1.6	11.4	± 1.5	10.0	± 1.9	2.1	± 1.7	0.5	± 0.7
Wild-type (at 25℃)	10.1	± 2.5	11.1	± 2.1	10.0	± 1.9	2.2	± 1.9	0.5	± 0.7
let-60(n1046gf)	9.5	± 2.3	10.7	± 3.1	9.7	± 2.4	2.0	± 1.7	0.6	± 0.7
unc-32(e189)	9.7	± 1.6	10.9	± 1.8	9.8	± 2.0	1.7	± 1.5	0.5	± 0.7
unc-79(e1068)	9.3	± 2.2	11.3	± 1.7	10.0	± 2.1	2.5	± 1.5	0.5	± 0.7
sem-5(n1779)	7.6	± 1.6**	9.5	± 1.5**	6.3	± 2.3**	1.5	± 1.4	0.3	± 0.5
sos-1(cs41) (at 25℃)[b]	7.7	± 2.7**	10.9	± 3.5	8.9	± 2.8	2.0	± 1.7	0.3	± 0.5
let-60(sy93)	6.5	± 3.0**	8.5	± 2.4**	6.2	± 3.3**	2.3	± 1.7	0.4	± 0.7
lin-45(n2506)[c]	6.7	± 2.6**	8.2	± 2.0**	6.3	± 3.4**	1.5	± 1.6	0.4	± 0.6
mek-2(ku114)[c]	7.1	± 2.6**	7.9	± 2.6**	5.6	± 3.0**	1.7	± 1.6	0.5	± 0.8
mpk-1(ku1)[d]	7.7	± 2.5**	9.0	± 1.1**	6.5	± 2.5**	2.2	± 1.7	0.4	± 0.6
mpk-1(n2521)[e]	6.9	± 2.3**	8.0	± 2.4**	5.9	± 2.2**	1.9	± 1.5	0.5	± 0.7
mpk-1(n2521)[c]	7.3	± 2.3**	8.4	± 2.0**	7.0	± 3.5**	2.4	± 2.0	0.5	± 0.9
Control RNAi	9.2	± 2.9	10.2	± 3.7	9.7	± 1.8	2.1	± 1.8	0.5	± 0.7
let-60 RNAi	7.3	± 1.8*	8.5	± 2.2*	6.4	± 3.0**	1.8	± 2.0	0.4	± 0.6

[a]Cell corpses scored at the indicated developmental stages are presented as the mean ± SD. (n≥30). The *rrf-3(pk1426)* mutant was used to enhance the RNAi effect in RNAi experiments. Mutants embryos were compared to wild-type, and *let-60* RNAi treatment was compared to control RNAi treatment (*P<0.05 and **P<0.001, two-tailed *t* test). [b]*sos-1(cs41)* is temperature-sensitive and its cell corpse profile was scored at 25℃. [c]Mutants also contain *let-60(n1046gf)*. [d]Mutants also contain *unc-32(e189)*. [e]Mutants also contain *unc-79(e1068).*

Appendix 5. Mutants defective in the LET-60-MPK-1 pathway have reduced numbers of cell corpses.

79

Appendix 6. The PI3K pathway and PLC genes are not involved in embryonic PCD.

A. Mutants defective in the PI3K pathway have normal numbers of cell corpses.

Genotype	Number of cell corpses[a]				
	Comma	1.5-fold	2-fold	3-fold	4-fold
Wild type (at 20℃)	10.0 ± 1.6	11.4 ± 1.5	10.0 ± 1.9	2.1 ± 1.7	0.5 ± 0.7
Wild type (at 25℃)	10.1 ± 2.5	11.1 ± 2.1	10.0 ± 1.9	2.2 ± 1.9	0.5 ± 0.7
aap-1(ok282)	10.3 ± 1.4	11.8 ± 2.0	10.6 ± 1.6	2.3 ± 1.2	0.6 ± 0.7
aap-1(m889)	10.3 ± 1.8	11.4 ± 1.9	10.5 ± 1.9	2.5 ± 1.3	0.7 ± 0.6
age-2(yw23); age-1(hx546) (at 25℃)[b]	10.4 ± 1.9	11.2 ± 1.0	10.5 ± 1.6	2.9 ± 1.1	0.5 ± 0.6
daf-16(m26); age-1(m333)	10.1 ± 2.2	11.1 ± 1.6	10.0 ± 1.7	2.1 ± 1.0	0.5 ± 0.6

B. Mutants defective in PLC genes have normal numbers of cell corpses.

Genotype	Number of cell corpses[a]				
	Comma	1.5-fold	2-fold	3-fold	4-fold
plc-1(rx1)[c]	10.5 ± 1.3	11.0 ± 2.3	10.5 ± 2.3	2.5 ± 2.0	0.7 ± 0.8
plc-2(ok1761)	10.0 ± 2.4	10.8 ± 1.9	10.5 ± 2.8	2.0 ± 1.1	0.6 ± 0.7
plc-3(tm1340)[d]	10.4 ± 2.0	11.7 ± 1.9	10.9 ± 1.9	2.7 ± 1.6	0.5 ± 0.6
plc-4(ok1215)	10.6 ± 1.8	11.9 ± 2.6	10.5 ± 1.6	2.3 ± 1.6	0.7 ± 0.7

[a]Cell corpses scored at the indicated developmental stages are presented as the mean ± SD (n≥30).
[b]The *age-2(yw23); age-1(hx546)* strain is temperature-sensitive and its cell corpse profile was scored at 25℃.
[c]GFP-negative progeny of *plc-1(rx1); kfEx2[plc-1(+); sur-5::gfp]* adult worms.
[d]GFP-negative progeny of *plc-3(tm1340)/mIn1[mIs14 dpy-10(e128)]* adult worms.

Appendix 6. The PI3K pathway and PLC genes are not involved in embryonic PCD.

Appendix 7. *lin-1* **mutants, but not** *lin-31* **mutants, have reduced numbers of cell corpses.**

Genotype	Number of cell corpses[a]									
	Comma		1.5-fold		2-fold		3-fold		4-fold	
Wild-type	10.0	± 1.6	11.4	± 1.5	10.0	± 1.9	2.1	± 1.7	0.5	± 0.7
lin-3(e1417)	6.8	± 2.0**	8.8	± 2.3**	6.3	± 2.4**	1.5	± 1.8	0.2	± 0.6
lin-1(sy254)	6.7	± 2.6**	8.9	± 2.0**	6.3	± 2.3**	1.5	± 1.6	0.3	± 0.6
lin-1(n1047)	6.7	± 1.7**	9.0	± 3.0**	6.7	± 2.3**	1.5	± 1.3	0.5	± 0.6
lin-1(n303)	7.7	± 1.8**	8.5	± 2.2**	7.0	± 2.5**	1.8	± 1.7	0.4	± 0.7
lin-1(n1761)	8.0	± 2.4**	8.4	± 2.5**	5.8	± 2.8**	1.6	± 2.0	0.3	± 0.5
lin-31(n301)	9.6	± 2.4	10.8	± 3.3	10.2	± 2.7	2.3	± 1.9	0.5	± 0.7
lin-31(n1053)	10.4	± 1.6	11.4	± 2.3	10.7	± 2.1	2.3	± 1.3	0.7	± 0.7
lin-31(gk569)	10.1	± 1.9	11.5	± 2.4	10.6	± 2.4	2.0	± 1.8	0.7	± 0.8
lin-1(sy254) lin-3(e1417)	7.2	± 1.5**	9.3	± 1.4**	7.1	± 1.3**	2.3	± 1.8	0.4	± 0.6

[a]Cell corpses scored at the indicated developmental stages are presented as the mean ± SD. (n≥30). Mutant embryos were compared to wild-type (*P<0.05 and **P<0.001, two-tailed *t* test). The cell corpse numbers of *lin-1(sy254) lin-3(e1417)* double mutants showed no significant difference when compared to the *lin-1(sy254)* or *lin-3(e1417)* single mutant (P>0.05, two-tailed *t* test).

Appendix 7. *lin-1* **mutants, but not** *lin-31* **mutants, have reduced numbers of cell corpses.**

Chapter 2

Identify New Genes Involved in Programmed Cell Death

in *C. elegans*
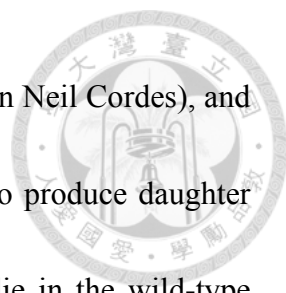
INTRODUCTION

The four genes, *egl-1*, *ced-9, ced-4*, and *ced-3*, are regulated for most programmed cell

death (PCD) in *C. elegans* [1-3]. These core PCD genes need to be precisely regulated

so that PCD can occur at the right time and in the right location. Despite of extensive

studies of these core PCD genes, how they are regulated remains largely unknown.

Moreover, although CED-3 is the most well-known cell-killing caspase, few CED-3

substrates are described, remaining a gap between CED-3 activation and downstream

cell death execution events.

Cells undergoing PCD are generated by asymmetric cell divisions in *C. elegans* [4]. The

mother of apoptotic cell divides asymmetrically to generate one large cell and one small

cell. The large cell differentiates or further divides, whereas the small cell undergoes

PCD (Figure 1A). When doomed cells fail to die in *ced-4* or *ced-3* mutants, they adopt

their sister cell fates, differentiate, and function [2]. However, dying cells that

inappropriately survive do not adopt their sister cell fates, if the latter cells undergo cell

division and the resulting descendent cells then differentiate (Figure 1C) [2].

Several genes that regulate asymmetric cell divisions during PCD have been identified.

They include *ham-1* (HSN abnormal migration) [5,6], *pig-1* (*par-1*-like gene) [7], *grp-1*

(general receptor for phosphoinositides) (Doctoral dissertation, Shaun Neil Cordes), and

cnt-2 (CeNTaurin) [8]. In these mutants, the affected cells divide to produce daughter

cells that are in equal or reversal size and cells that destined to die in the wild-type

transform to their sister cells. However, these doomed cells still undergo PCD and the

fate transformation is masked (Figure 1B). Only when a mutation disrupts PCD, such as

egl-1 or *ced-3*, the mask is removed and the underlying transformation is revelaed,

leading to the production of extra differentiated cells (Figure 1D).

We observed that the *grp-1; ced-3* double mutant, but not *grp-1* or *ced-3* single mutant,

had a ventral ridge in the tail. The ridge contains extra hyp8/9 and additional hyp8/9 is

sufficient to cause the tail defect. Based on these observations, we performed a genetic

screen in the *grp-1* background and tried to isolate new genes involved in PCD. Several

known PCD genes, such as *egl-1*, *ced-4*, *ced-3*, and *ced-8*, were isolated from this

screen. A *C. elegans* CAD (carbamoyl phosphate synthetase, aspartate transcarbamylase,

and dihydroorotase) gene, *pyr-1*, was also isolated and demonstrated to regulate the

PCD of the aunt cells of hyp8/9 and excretory cell. The pro-apoptotic function of *pyr-1*

is independent of its CAD activity. More importantly, we show that PYR-1 is a CED-3

substrate *in vitro*. These results show that our screen is feasible to find new PCD genes.

MATERIALS AND METHODS

General Methods and Strains

C. elegans strains were maintained at 20°C as described previously [9]. The N2 Bristol

strain was used as the wild-type strain. Alleles used:

Linkage group (LG)I: *ced-1(e1735), ced-12(bz187),* and *cps-6(ok1718).*

LGII: *pyr-1(cu8), pyr-1(tp12),* and *syIs107[P$_{lin-3}$::pes-10::gfp].*

LGIII: *ced-4(n1162), ced-9(n1950),* and *grp-1(gm350).*

LGIV: *ced-3(n2427), ced-3(n2923), ced-3(n717),* and *jcIs1[ajm-1::gfp].*

LGV: *egl-1(n1084n3082).*

LGX: *ced-8(n1891)* and *arIs99[P$_{dpy-7}$::2xnls::yfp].*

All alleles are described in WormBase (http://www.wormbase.org/). The *grp-1(gm350)*

mutant is a kind gift from Gian Garriga.

Transgenic animals

Germline transformation experiments were performed as described previously [10]. To

examine the number of PHsh, *P$_{ver}$::4Xnls::gfp* (50 ng/μl) was injected into different

mutants with the coinjection markers *sur-5::rfp* (30 ng/μl) . To observe the expression

pattern of *pyr-1*, *P$_{pyr-1}$::pyr-1::gfp* (50 ng/μl) was injected into the *pyr-1(tp12)* mutant

with the coinjection markers *P$_{myo-2}$::rfp* (5 ng/μl). To evaluate whether additional hyp8/9
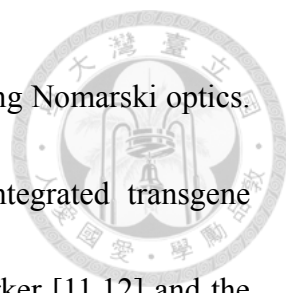
could result in the tail defect, *P~lin-26~::mcherry* or *P~lin-26~::ced-9(gf)* (200 ng/μl) was injected into the *grp-1(gm350); arIs99* mutant with the coinjection markers *sur-5::rfp* (30 ng/μl).
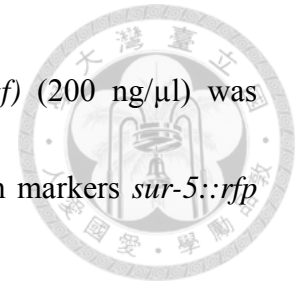
Molecular biology

Standard methods of cloning, sequencing, and PCR amplification were used. To generate *P~ver-1~::4xnls::gfp*, the *ver-1* promoter was amplified by PCR using primers 5'-ggctgcagcaatgcactggaatactccagag-3' and 5'-ccggatccaactctacaaactttccaattttttg-3' and the resulting PCR fragment was inserted into the pPD122.56 vector to generate pYW1562. To generate *P~lin-26~::mcherry*, the *lin-26* promoter was amplified by PCR using primers 5'-gatcaagcttctcttctaaccatcaattttag-3' and 5'-gatcaagcttggaagagaggtgtgaagggatc-3' and the resulting PCR fragment was inserted into the mcherry version of pPD95.75 vector to generate pYW1058. The *ced-9(gf)* cDNA was obtained by RT-PCR using worm total RNA prepared from the *ced-9(n1950)* mutant and the primers 5'-ttggtaccatgacacgctgcacg-3' and 5'-ggggtaccgacttcaagctgaacatc-3'. To generate *P~lin-26~::ced-9(gf)*, the *ced-9(gf)* cDNA was inserted into pYW1058 to generate pYW1218.

Cell death assays

Cell corpses were counted at the indicated developmental stages using Nomarski optics. To examine the number of hypodermal cells in the tail, the integrated transgene *jcIs1[ajm-1::gfp]* and *arIs99[P_{dpy-7}::2Xnls::yfp]* were used as a marker [11,12] and the number of hypodermal cells was scored at L1 stage by fluorescence microscopy. To count the number of PHsh, the extrachromosomal transgene *tpEx436[P_{ver-1}::4Xnls::gfp]* [13] was used as a marker and the number of PHsh was scored at L4 stage by fluorescence microscopy. To analyze the number of excretory cell(s), the integrated transgene *syIs107[P_{lin-3}::pes-10::gfp]* [14,15] was used as a marker and the number of excretory cell(s) was scored at 1.5-fold by fluorescence microscopy.

Mutagenesis screen

The mutagenesis was conducted as previously described [9]. Briefly, the *grp-1(gm350)* mutant was grown to the L4 or young adult stage and washed off from plates with M9 buffer into a 15 ml tube. Worms were centrifuged at low speed for 30 second and the supernatant was romoved. The pellet was washed with M9 buffer for three times to remove the bacteria. Worms were then suspended in 3 ml M9 buffer and transferred into 1 ml M9 buffer containing 0.2M EMS (ethyl methane sulfonate). The tube was placed on a shaker for 4 hours at room temperature. Following the mutagenesis protocol, worms were washed with M9 buffer for three times to remove EMS and transferred to a

NGM plate. Healthy looking L4 or young adult hermaphrodites were picked and incubated at 20°C. F1 progeny were randomly selected and F2 progeny were screened to isolate mutants with tail defects.

Statistical analysis

In histograms, the values are shown as the mean and standard deviation (SD). Data derived from different genetic backgrounds at a specific developmental stage were compared using Student's two-tailed unpaired t-test. Data were considered statistically different at $P<0.05$. Fisher's exact test was used when comparing the percentages of surviving cells in different genetic backgrounds. Data were considered statistically different at $P<0.05$.

RESULTS

Defects in the activation, execution, or kinetics of PCD cause the tail defect in the

***grp-1* background**

When examining the *grp-1(gm350); ced-3(n717)* double mutant under a dissecting

microscope, we noticed that they possessed an abnormal tail which had a ball- or

rod-like structure at the tip (Figure 2, Jo-Hao Ho). This abnormal tail morphology

(referred to as tail defect hereafter) was observed in almost all *grp-1(gm350);*

ced-3(n717) double mutants but rarely seen in either the *grp-1* or *ced-3* single mutant

(Table 1). Therefore, the *grp-1* and *ced-3* mutations act synergistically to cause the tail

defect. In addition, the *egl-1(n1084n3082)* or *ced-4(n1162)* loss-of-function (*lf*)

mutation as well as the *ced-9(n1950)* gain-of-function (*gf*) mutation also resulted in a

high penetrant tail defect in the *grp-1* background (Table 1). Besides the four core PCD

genes, *ced-8*, when mutated, also caused a high penetrant tail defect in the *grp-1* mutant

(Table 1). CED-8 is a homologue of the XK family proteins in *C. elegans*, has been

implicated in controlling the kinetics of PCD with unknown mechanism [16-18]. In

contrast, mutations disrupting the engulfment of cell corpses, such as *ced-1(e1735)* and

ced-12(bz187), and or those reducing DNA degradation, such as *cps-6(ok1718)*, did not

cause tail defects in the *grp-1* background (Table 1). These observations show that
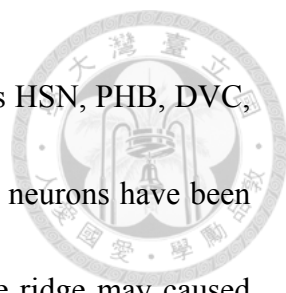
mutations that impair the activation, execution, or kinetics of PCD cause tail defects in the *grp-1* background.
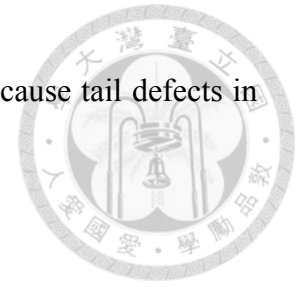
It is worthy of note that the weak *ced-3* allele *n2427* also caused a high penetrant tail defect and even the weakest *ced-3* allele identified thus far *n2923* caused a median penetrant tail defect in the *grp-1* background. *ced-3(n2923)* suppresses the embryonic lethality resulted from the *ced-9(lf)* mutation but does not change the cell corpse profile [19]. The median penetrance observed in the *grp-1(gm350); ced-3(n2923)* double mutant suggests that the affected cells in the tail are sensitive to impaired PCD machinery.

Extra hyp8/9 results in the tail defect

To investigate the cause of tail defects in the *grp-1;ced-3* double mutant, we first observed tail defects under Nomarski microscope. One, or occasionally two, ventral ridges posterior to the anus were frequently observed in the abnormal tail (Figure 3). The fact that defects depend on *ced-9(gf), ced-4(lf), ced-3(lf),* or *ced-8(lf)* mutation suggests that the tail defect may be caused by additional surviving cells. There are five cell lineages that generate apoptotic cell(s) in the tail on each side of the animal (Figure 4A). These lineages also generate hypodermal cells and neurons. Hypodermal cells,

such as hyp8/9 and hyp10, are relatively larger than neurons, such as HSN, PHB, DVC, PLM, and ALN, in *C. elegans*. Additional hypodermal cells but not neurons have been shown to cause abnormal body morphology. We speculated that the ridge may caused by additional hypodermal cells but not neurons. To test this possibility, we examined the tail of the *grp-1; ced-3* mutant using the *jcIs1[ajm-1::gfp]* transgene. AJM-1::GFP is localized to the adherens junction and outlines the apical border of hypodermal cells. We found that the *grp-1; ced-3* mutant had one or two additional hyp8/9 in the ridge of the tail (Figure 4B and E). Consistantly, when using the *arIs99[P$_{dpy-7}$::2xnls::yfp]* transgene to label the nuclei of hypodermal cells, we also found one or two additional hyp8/9 nuclei in the *grp-1; ced-3* mutant (Figure 4C and E). These observations indicate that the tail defect in the *grp-1; ced-3* mutant is resulted from additional hyp8/9. To further confirm the attribution of extra hyp8/9 to the tail defect, we microinjected *ced-9(gf)* cDNA under the control of *lin-26* promoter, which expresses in hyp8/9 and PHsh [20], into the *grp-1; arIs99[P$_{dpy-7}$::2xnls::yfp]* mutant. This construct could cause the tail defect (Figure 5), showing that the tail defect is resulted from additional hyp8/9. We also observed that the *grp-1; ced-3* mutant had extra phasmid sheath cell(s) (PHsh) (Figure 4D and E). Interestingly, we often observed one extra hyp8/9 boundary (80%) (Figure 4B and E) but two extra hyp8/9 nuclei and PHsh (77%) (Figure 4C-E). As shown in Figure 6, we propose that ABplpppapp and ABprpppapp (referred to as

95

ABpl/rpppapp hereafter), the aunt cells of hyp8/9, survive, divide and differentiate to

hyp8/9 but only one of them expresses AJM-1 in the *grp-1; ced-3* mutant. Alternatively,

the additional hyp8/9 cells may fuse when inappropriately survive.

Identify new genes involved in PCD by a genetic screen in the *grp-1* background

Based on the observation that defects in the activation, execution, or kinetics of PCD

cause tail defects in the *grp-1* background, we thought to conduct a genetic screen using

the *grp-1(gm350)* mutant to screen new genes involved in PCD (Figure 7). From about

12000 haploid genomes, 182 mutants with a penetrant tail defect higher than 20% were

isolated (Table 2-7). Among them, four mutants were demonstrated to be allelic to *egl-1*,

four *ced-4*, six *ced-3*, and five *ced-8* (Table 2), showing that this screen is feasible to

isolate mutants defecctive in PCD. Interestingly, we also isolated three *ced-11* alleles

(Table 2). *ced-11* has been reported to be important in the morphological appearance of

cell corpses without affecting PCD (International *C. elegans* Meeting, 1997). Recently,

however, it is shown that *ced-11* mutations can enhance the cell death defect of weak

alleles of other PCD mutants in the ventral cord, indicating that *ced-11* plays a role in

PCD but this pro-apoptotic activity can be revealed only when the PCD machinery is

compromised [International *C. elegans* Meeting, 2013]. Therefore, our screen is

sensitive enough to isolate moderate or weak PCD mutation(s). By counting the

numbers of embryonic cell corpses, we classified these mutants into three groups: reduced or delayed cell corpse profiles (Table 3), increased numbers of cell corpses (Table 4), and unchanged numbers of cell corpses (Table 5-7).

45 mutants with reduced or delayed cell corpse profiles are isolated.

We isolated 45 mutants which either contain less cell corpses at 1.5-fold and/or 4-fold or present delayed cell corpse profiles (Table 3). The cell corpse profiles and the *grp-1* dependent nature of the tail defect suggest that they are mutations affecting PCD. We analyzed these mutants and two of them are demonstrated be be defective in the *pyr-1* and *klp-11* genes. The *pyr-1* mutant is undergoing further characterization (see below).

16 mutants with increased numbers of cell corpses are isolated

To our surprise, we also isolated 16 mutants which contain more cell corpses at 1.5-fold and/or 4-fold (Table 4). Several reasons come into our mind to explain the phenomena. First, there are other mutations affecting the numbers of cell corpses in these mutants. Second, like *ced-8*, these mutations may affect both PCD and engulfment [16-18]. Third, these mutations may alter the cell fate of grandmother of hyp8/9 and result in extra hyp8/9 and cell corpses (Appendix 1).

99 mutants with normal cell corpse numbers are isolated

We isolated 99 mutants whose cell corpse numbers are undistinguishable from the wild-type (Table 5-7) and 63 mutants with a higher penetrant tail defect ($\geqq 40\%$) (Table 5 and 6) are undergoing further characterization. Among the 63 mutants, 39 mutants requires the *grp-1* mutation to cause the tail defect (Table 5), suggesting that these mutations may affect the PCD of the aunt cells of hyp8/9 specifically and have no influence on other PCDs. Consistant with this hypothesis, HS0128 was shown to contain a mutation being allelic to *egl-1* and had normal cell corpse numbers (Table 2). We are trying to find the mutation site of *egl-1* in HS0128 and it might be an important element for transcriptional activation of *egl-1* in the aunt cells of hyp8/9 specifically.
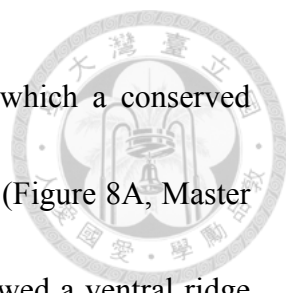
Remaining 24 mutants present tail defects in the absence of *grp-1* mutation (Table 6), suggesting that these mutations may not cause tail defects by affecting PCD. From these mutants, we isolated one *vab-9* allele (JS0004) and three *K02E10.4* alleles (CH6041, JS0006, and HS1096) (Table 6, Master thesis, Fei-Man Hsu). VAB-9 is a claudin-like junction protein and is localized to the adherens junction of all epithelial cells by HMR-1/cadherin [21]. Mutations in *vab-9* cause disorganized F-actin at the adherens junction and enhance adhension defects through functional loss of AJM-1 and DLG-1 [21], implying that the tail defect observed in JS0004 might be resulted from abnormal

cell adhesion. K02E10.4 is a hypothetical protein with unknown functions. Using online

bioinformatic tools, TMHMM2 program and SMART (Simple Modular Architecture

Research Tool), K02E10.4 is predicted to be a transmembrane protein with two WR1

(worm-specific repeat type 1) domains (Master thesis, Fei-Man Hsu). Different from the

tail defect observed in the *grp-1; ced-3* double mutant, the K02E10.4 mutants have

blunt tails (Master thesis, Fei-Man Hsu). The tail defect predominantly resides in hyp10

and the tail tip could not elongate properly (Master thesis, Fei-Man Hsu). Interestingly,

we found that the cuticle surrounding the tail spike seems to be shed off when molting

and the tail tip is shrunken progressively, leaving a thin tail spike behind (Master thesis,

Fei-Man Hsu). Therefore, the tail defect observed in the K02E10.4 mutants may come

from the failed maintenance of cell adhesion or morphology.

***pyr-1* is isolated as a new PCD gene**

Mutants presenting both tail defects and reduced/delayed cell corpse profiles are

candidates of animals with impaired PCD. We further characterized these mutants. On

of these mutant strains, HS0190, has been demonstrated to be defective in the *pyr-1*

gene (Table 3, Master thesis, Hung-Tsai Kan). *pyr-1* encodes *C. elegans* CAD

(carbamoyl phosphate synthetase, aspartate transcarbamylase, and dihydroorotase),

which has been shown to control the rate-limiting step during pyrimidine biosynthesis

[22,23]. The HS0190 strain possesses a *pyr-1(tp12)* mutation, in which a conserved

glycine residue in the CPS-A domain is replaced with glutamic acid (Figure 8A, Master

thesis, Hung-Tsai Kan). The *pyr-1(tp12); grp-1(gm350)* mutant showed a ventral ridge

posterior to the anus, as observed in the *grp-1; ced-3* mutant, whereas the *pyr-1(tp12)*

mutant did not (Figure 8B and C, Master thesis, Hung-Tsai Kan). The *pyr-1(cu8)*

mutation, in which a histidine residue in the DHO domain is replaced with glutamine,

and the *pyr-1(ok2391)* mutation, which results in a truncated form of PYR-1, also

caused the tail defect in the *grp-1* background (Figure 8A-C, Master thesis, Hung-Tsai

Kan). Interestingly, adding uracil as the pyrimidine supplement rescued the embryonic

lethality of the *pyr-1(cu8)* mutant (data not shown) but failed to recover the tail defect

of the *pyr-1; grp-1* mutants (Figure 8B and C, Master thesis, Hung-Tsai Kan), showing

that the tail defect caused by the *pyr-1* mutations is independent of the CAD activity.

Using the *arIs99[P_{dpy-7}::2xnls::yfp]* and *tpEx436[P_{ver-1}::4xnls::gfp]* transgenes as

specific cell markers, we found that the *pyr-1; grp-1* mutant had extra hyp8/9 (Figure

8D, Master thesis, Wan-Ying Lin) and PHsh (Figure 8E), as observed in the *grp-1;

ced-3* mutant. Additionally, we also found that the *pyr-1; grp-1* mutant had an extra

excretory cell (Figure 8F, Master thesis, Wan-Ying Lin). To examine the cause of the

extra cells in the *pyr-1; grp-1* mutants, we analyzed the first 13 PCDs in the AB

lineages. The cell coprses of the aunt cells of hyp8/9 and excretory cell are sometimes

absent (data not shown, Master thesis, Wan-Ying Lin). These data show that *pyr-1* is

important for the death of the aunt cells of hyp8/9 and excretory cell.

It has been reported that the mammalian CAD is the substrate of caspase [24]. In

collaboration with Dr. Ding Xue group, we found that the *C. elegans* PYR-1 was

cleaved in the addition of CED-3 *in vitro* and the cleavage sites were in the CPS-A and

DHO domain (Figure 8G, Yu-Zen Chen). Therefore, PYR-1 may be a substrate of

CED-3. To ask whether PYR-1 is a substrate of CED-3 in vivo, we first examined the

expression pattern of *pyr-1* by microinjecting $P_{pyr-1}::pyr-1::gfp$ into the *pyr-1(tp12)*

mutant. $P_{pyr-1}::pyr-1::gfp$ was observed in most, if not all, cells with a stronger

expression in the gut precursors from early embryogenesis and progressively declined

after 2-fold (Figure 9). The GFP expression reappeared in the gut and head muscles

after hatching and continued throughout adults (Figure 9). This expression pattern is

consistent with previous observations [22]. Importantly, $P_{pyr-1}::pyr-1::gfp$ was also

observed in ABplpappap (the aunt cell of excretory cell) and ABpl/rpppapp (the aunt

cells of hyp8/9) corpses (Figure 9), suggesting that PYR-1 could be a substrate of

CED-3 *in vivo*. We are continuing to find out the exact cleavage sites and test if the

cleavage is important for the pro-apoptotic function of *pyr-1*.

DISCUSSION

Extra hyp8/9 causes the tail defect in the *grp-1; ced-3* mutants

Under a dissecting microscope, we observed that the *grp-1; ced-3* mutant had a tail defect. Using specific cell markers and ectopic expression of *ced-9(gf)* in hyp8/9, we show that extra hyp8/9 causes the tail defect in the *grp-1; ced-3* mutant. In the *grp-1* mutant, the aunt cells of hyp8/9 transforms to its sister cell fate but still undergoes PCD, resulting no additional hyp8/9 in the tail. In the *ced-3* mutant, the aunt cells of hyp8/9 survives but fails to further divide and differentiate, remaining a small undead cell in the tail. Therefore, both survival and transformation of the aunt cells of hyp8/9 are required for the tail defect.

Extra PHsh is also observed in the *grp-1; ced-3* mutant but may be not the cause of tail defect by reason of the smaller cell size and distant localization from the tail defect. Tail-spike cell also survives and exists in the tail in the *ced-3* mutants [25,26]. Different from other PCDs, tail-spike cell differentiates and functions before death [27,28], suggesting that tail-spike cell does not require the *grp-1* mutation to further differentiate when inappropriately survives and we would observe the tail defect in the *ced-3* mutant if the survival of tail spike is the cause of tail defect. More importantly, it has been shown that *egl-1* plays a minor role in tail-spike cell death [25,26]. However, we
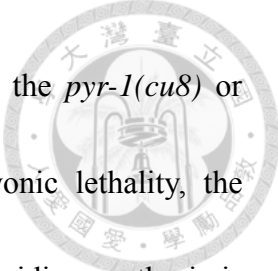
103

observed that the *grp-1; egl-1* mutant has a high penetrant tail defect, suggesting that the survival of tail-spike cell is not the cause of tail defect.

A genetic screen in the *grp-1* sensitized background can isolate PCD-defective mutations

Based on the observation that defects in PCD act synergistically with the *grp-1* mutation to cause tail defects, we performed a genetic screen to isolate mutants with tail defects in the *grp-1(gm350)* background and tried to identify new genes involved in PCD. This screen takes several advantages when compared to traditional genetics screens. First, the tail defect is easily observed under a dissecting microscope. Second, only mutants defective in the activation, execution, or kinetics of PCD can be isolated. Third, the tail defect is sensitive to PCD and this screen is able to identify weak regulators of PCD. Fourth, specific regulators of the PCD of the aunt cells of hyp8/9 can be revealed.

From this screen, we isolated several known *ced* genes and identified *pyr-1* as a new PCD gene. We showed that *pyr-1* is important in the PCD of the aunt cells of hyp8/9 and excretory cell. Moreover, PYR-1 is a substrate of CED-3 *in vitro*. It has been shown that the mammalian CAD is degraded by caspase-3 during apoptosis, resulting in the rapid decrease of pyrimidine [24]. However, our data imply that the pro-apoptotic

function of *pyr-1* is independent of its CAD activity. First, unlike the *pyr-1(cu8)* or *pyr-1(ok2391)* mutant, which shows a high penetrance of embryonic lethality, the *pyr-1(tp12)* mutant is superficially normal, suggesting that the pyrimidine synthesis is likely normal in this mutant. However, these *pyr-1* mutations are able to cause the tail defect in the *grp-1* background. Second, the uracil supplement rescued the embryonic lethality of the *pyr-1(cu8)* mutant but failed to rescue the tail defect of the three *pyr-1; grp-1* mutants. Therefore, *pyr-1* has a novel pro-apoptotic function in addition to its CAD activity. It has been reported that the CPSII domain of CAD can interact with the caspase recruitment domains (CARDs) of NOD2 [29]. The fact that CED-3 contains the CARD domain and PYR-1 can be cleaved by CED-3 *in vitro* implies the direct interaction of PYR-1 and CED-3. The cleavage of PYR-1 may result in the change of protein function or localization, which can be analyzed by examining the effect on PCD and localization of different cleaved forms of PYR-1.

Mutants with abnormal tail morphogenesis independent of PCD can also be isolated from this genetic screen

Morphogenesis is a fundamental process during development but less is known about this event. By analyzing the requirement of *grp-1* mutation in the tail defect formation, we can isolate mutants defective in morphogenesis rather than PCD. Using this strategy,

two genes, *vab-9* and *K02E10.4*, are identified to be important in tail morphogenesis. While *vab-9* mutants show abnormal tail morphology, which is likely resulted from defective cell adhension, *K02E10.4* is required for the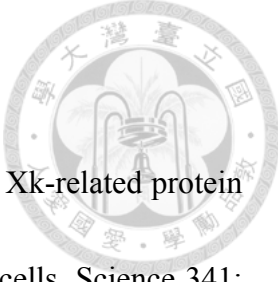 maintenance of tail morphology. Further characterization of these mutants can help us to understand the mechanism of formation and maintenance of morphology.

REFERENCES

1. Conradt B, Horvitz HR (1998) The *C. elegans* protein EGL-1 is required for programmed cell death and interacts with the Bcl-2-like protein CED-9. Cell 93: 519-529.

2. Ellis HM, Horvitz HR (1986) Genetic control of programmed cell death in the nematode *C. elegans*. Cell 44: 817-829.

3. Hengartner MO, Ellis RE, Horvitz HR (1992) *Caenorhabditis elegans* gene *ced-9* protects cells from programmed cell death. Nature 356: 494-499.

4. Hoeppner DJ, Hengartner MO, Schnabel R (2001) Engulfment genes cooperate with *ced-3* to promote cell death in *Caenorhabditis elegans*. Nature 412: 202-206.

5. Guenther C, Garriga G (1996) Asymmetric distribution of the *C. elegans* HAM-1 protein in neuroblasts enables daughter cells to adopt distinct fates. Development 122: 3509-3518.

6. Frank CA, Hawkins NC, Guenther C, Horvitz HR, Garriga G (2005) *C. elegans* HAM-1 positions the cleavage plane and regulates apoptosis in asymmetric neuroblast divisions. Dev Biol 284: 301-310.

7. Cordes S, Frank CA, Garriga G (2006) The *C. elegans* MELK ortholog PIG-1 regulates cell size asymmetry and daughter cell fate in asymmetric neuroblast divisions. Development 133: 2747-2756.

8. Singhvi A, Teuliere J, Talavera K, Cordes S, Ou G, et al. (2011) The Arf GAP CNT-2 regulates the apoptotic fate in *C. elegans* asymmetric neuroblast divisions. Curr Biol 21: 948-954.

9. Brenner S (1974) The genetics of *Caenorhabditis elegans*. Genetics 77: 71-94.

10. Mello C, Fire A (1995) DNA transformation. Methods Cell Biol 48: 451-482.

11. Myers TR, Greenwald I (2005) *lin-35* Rb acts in the major hypodermis to oppose ras-mediated vulval induction in *C. elegans*. Dev Cell 8: 117-123.

12. Mohler WA, Simske JS, Williams-Masson EM, Hardin JD, White JG (1998) Dynamics and ultrastructure of developmental cell fusions in the *Caenorhabditis elegans* hypodermis. Curr Biol 8: 1087-1090.

13. Procko C, Lu Y, Shaham S (2011) Glia delimit shape changes of sensory neuron receptive endings in *C. elegans*. Development 138: 1371-1381.

14. Hwang BJ, Sternberg PW (2004) A cell-specific enhancer that specifies *lin-3* expression in the *C. elegans* anchor cell for vulval development. Development 131: 143-151.

15. Denning DP, Hatch V, Horvitz HR (2012) Programmed elimination of cells by caspase-independent cell extrusion in *C. elegans*. Nature 488: 226-230.

16. Chen YZ, Mapes J, Lee ES, Skeen-Gaar RR, Xue D (2013) Caspase-mediated activation of *Caenorhabditis elegans* CED-8 promotes apoptosis and

phosphatidylserine externalization. Nat Commun 4: 2726.

17. Suzuki J, Denning DP, Imanishi E, Horvitz HR, Nagata S (2013) Xk-related protein 8 and CED-8 promote phosphatidylserine exposure in apoptotic cells. Science 341: 403-406.

18. Stanfield GM, Horvitz HR (2000) The *ced-8* gene controls the timing of programmed cell deaths in *C. elegans*. Mol Cell 5: 423-433.

19. Shaham S, Reddien PW, Davies B, Horvitz HR (1999) Mutational analysis of the *Caenorhabditis elegans* cell-death gene *ced-3*. Genetics 153: 1655-1671.

20. Landmann F, Quintin S, Labouesse M (2004) Multiple regulatory elements with spatially and temporally distinct activities control the expression of the epithelial differentiation gene *lin-26* in *C. elegans*. Dev Biol 265: 478-490.

21. Simske JS, Koppen M, Sims P, Hodgkin J, Yonkof A, et al. (2003) The cell junction protein VAB-9 regulates adhesion and epidermal morphology in *C. elegans*. Nat Cell Biol 5: 619-625.

22. Franks DM, Izumikawa T, Kitagawa H, Sugahara K, Okkema PG (2006) *C. elegans* pharyngeal morphogenesis requires both de novo synthesis of pyrimidines and synthesis of heparan sulfate proteoglycans. Dev Biol 296: 409-420.

23. Huang M, Graves LM (2003) De novo synthesis of pyrimidine nucleotides; emerging interfaces with signal transduction pathways. Cell Mol Life Sci 60:

321-336.

24. Huang M, Kozlowski P, Collins M, Wang Y, Haystead TA, et al. (2002) Caspase-dependent cleavage of carbamoyl phosphate synthetase II during apoptosis. Mol Pharmacol 61: 569-577.

25. Chiorazzi M, Rui L, Yang Y, Ceribelli M, Tishbi N, et al. (2013) Related F-box proteins control cell death in *Caenorhabditis elegans* and human lymphoma. Proc Natl Acad Sci U S A 110: 3943-3948.

26. Maurer CW, Chiorazzi M, Shaham S (2007) Timing of the onset of a developmental cell death is controlled by transcriptional induction of the *C. elegans ced-3* caspase-encoding gene. Development 134: 1357-1368.

27. Sulston JE, Horvitz HR (1977) Post-embryonic cell lineages of the nematode, *Caenorhabditis elegans*. Dev Biol 56: 110-156.

28. Sulston JE, Schierenberg E, White JG, Thomson JN (1983) The embryonic cell lineage of the nematode *Caenorhabditis elegans*. Dev Biol 100: 64-119.

29. Richmond AL, Kabi A, Homer CR, Marina-Garcia N, Nickerson KP, et al. (2012) The nucleotide synthesis enzyme CAD inhibits NOD2 antibacterial function in human intestinal epithelial cells. Gastroenterology 142: 1483-1492 e1486.
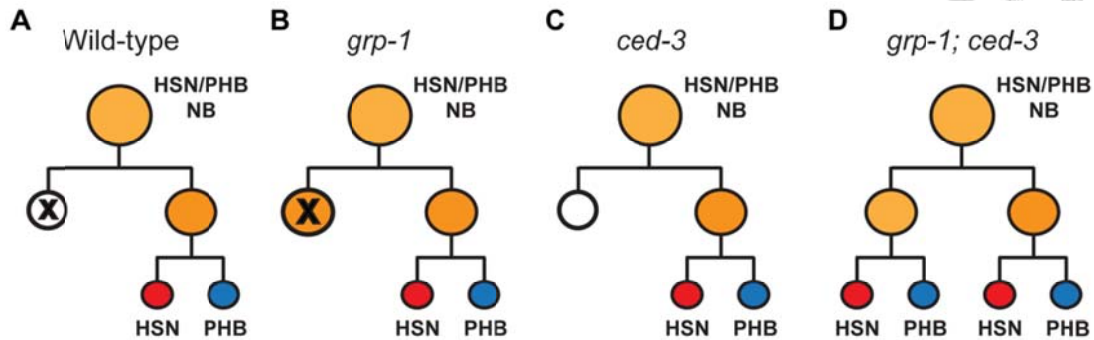
FIGURES AND TABLES

Figure 1. A model illustrates how the *grp-1* and *ced-3* mutations may act synergistically to result in extra neurons.

Diagrams depicting the cell lineage in the wild-type, *grp-1*, *ced-3*, and *grp-1; ced-3* animals are shown when using the HSN/PHB lineage as an example. (A) In the wild-type, the HSN/PHB neuroblast (NB) divides to generate a small anterior cell that undergoes PCD (**X**) and a large posterior cell that further divides to generate a HSN and PHB. (B) In the *grp-1* mutant, the anterior cell transforms to its sister cell fate but still undergoes PCD. (C) In the *ced-3* mutant, the anterior cell survives but does not divide. (D) In the *grp-1; ced-3* double mutant, the anterior cell survives and further divides to generate an extra HSN and PHB.

Wild-type   grp-1(gm350); ced-3(n717)

Jo-Hao Ho
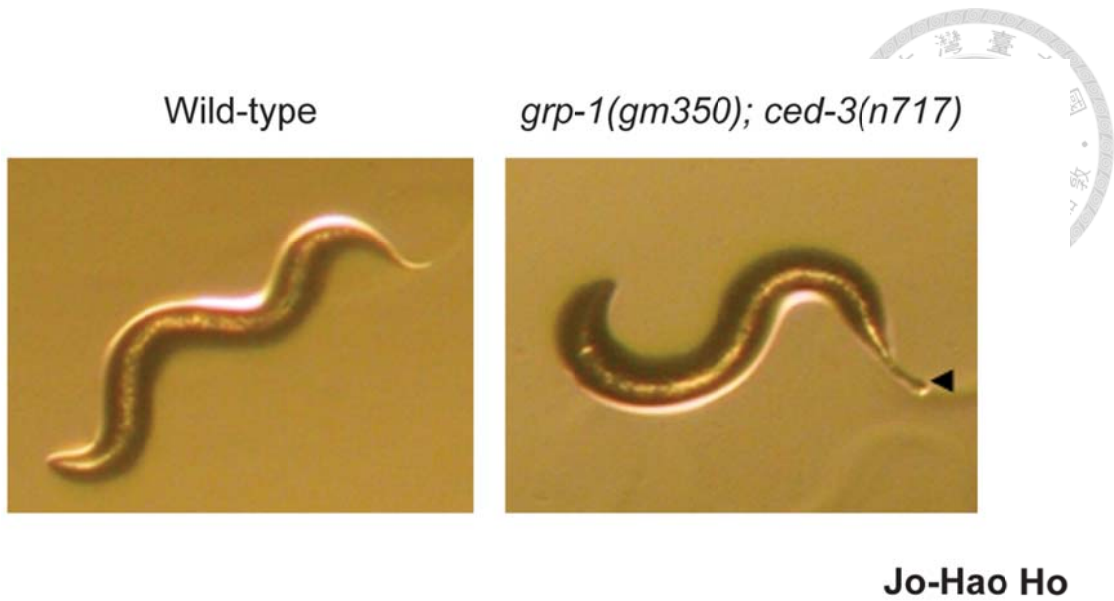
Figure 2. The *grp-1(gm350); ced-3(n717)* double mutant displays abnormal tail morphology.

The images of wild-type (left) and *grp-1(gm350); ced-3(n717)* double mutant (right) under a dissecting microscope are shown. The wild-type exhibits a smooth tail, whereas the *grp-1(gm350); ced-3(n717)* double mutant has a ball- or rod-like structure at the tip of the tail (indicated by an arrowhead).

Figure 3. The *grp-1; ced-3* double mutant has ventral ridge(s) posterior to the anus.

The DIC images of wild-type, *grp-1*, *ced-3*, and *grp-1; ced-3* animals are shown. *

indicates the anus and arrowheads ventral ridges. Alleles used here: *grp-1(gm350)* and

ced-3(n717). Scale bar: 10 μm.
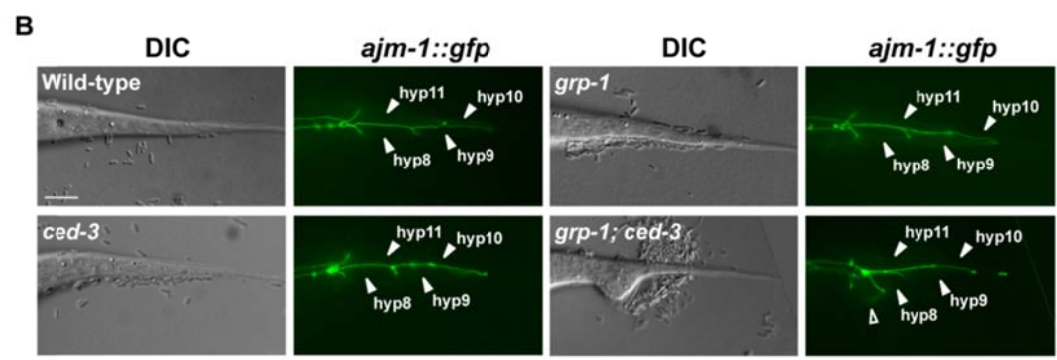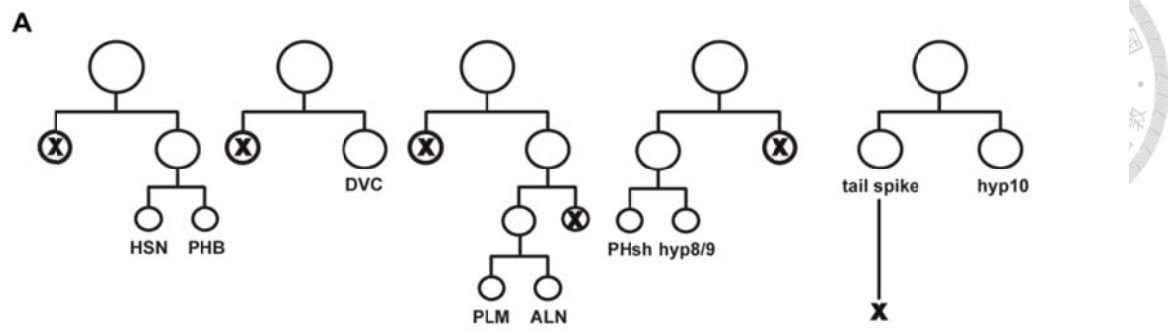
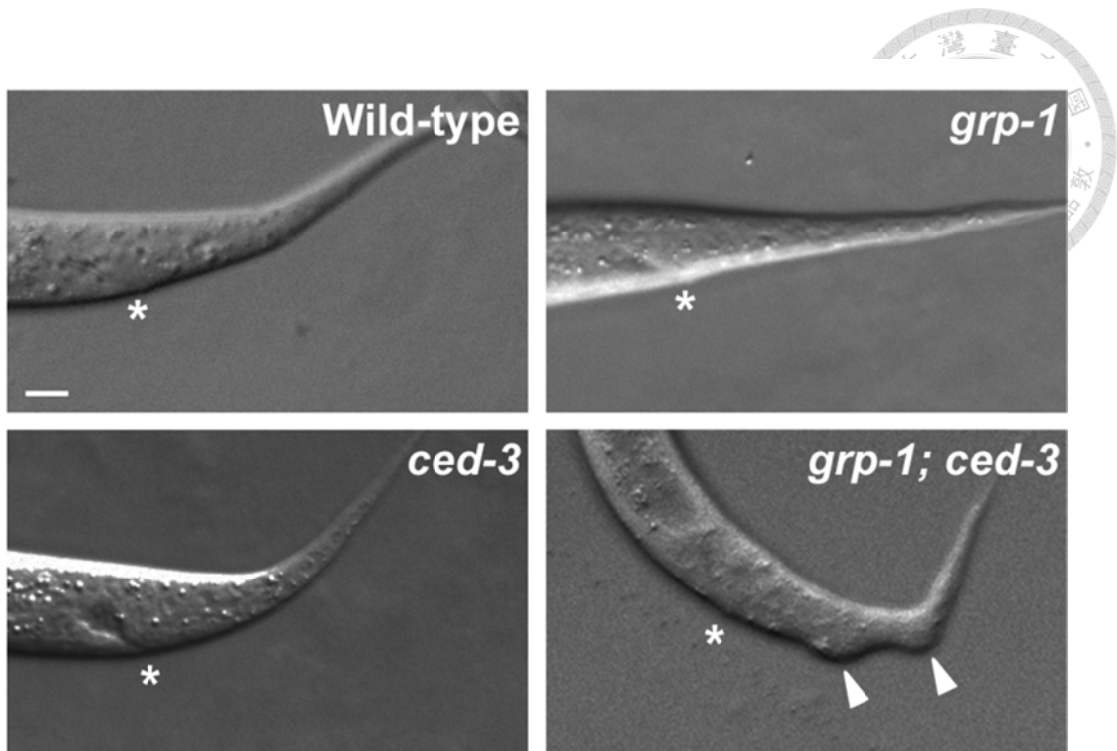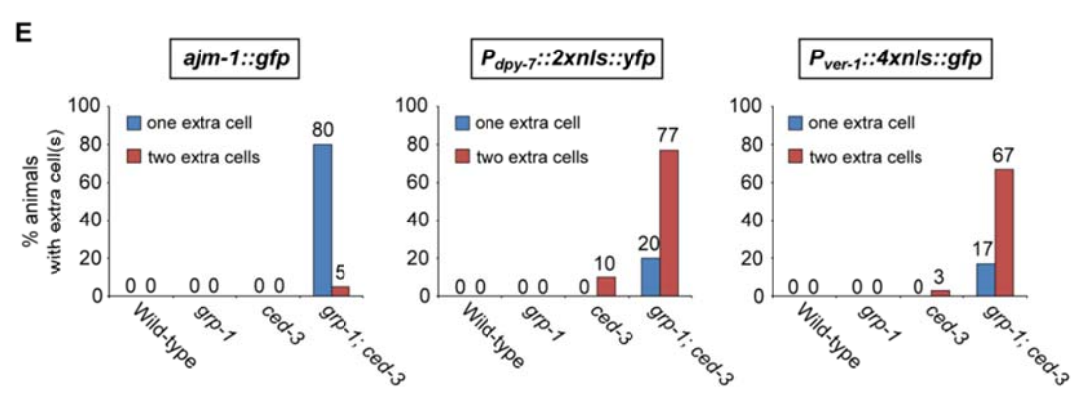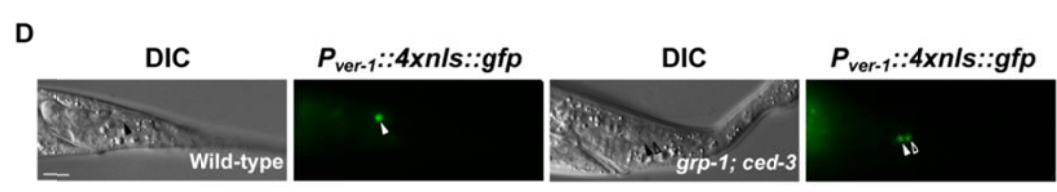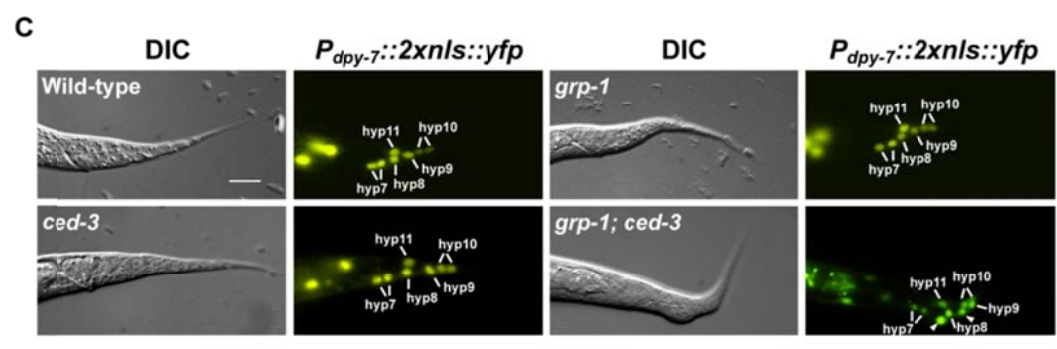**Figure 4. The *grp-1; ced-3* mutant has extra hyp8/9 and PHsh.**

(A) Diagrams depicting the cell lineages containing apoptotic cell(s) (**X**) in the tail. (B)

The DIC and GFP images of wild-type, *grp-1*, *ced-3*, and *grp-1; ced-3* worms carrying

the *jcIs1[ajm-1::gfp]* transgene. The arrowheads indicate hyp8, hyp9, hyp10, and hyp11

(hyp8-11) and the hollow arrowhead an extra hypodermal cell. (C) The DIC and YFP

images of wild-type, *grp-1*, *ced-3*, and *grp-1; ced-3* worms carrying the

arIs99[P$_{dpy-7}$::2xnls::yfp] transgene. The nuclei of hyp7 and hyp8-11 are indicated.

There are two hyp7 cells in the ventral side behind the anus. hyp10 is binuclear. The

arrowheads indicate extra hyp8/9 cells. (D) The DIC and GFP images of wild-type and

grp-1; ced-3 worms carrying the *tpEx436[P$_{ver-1}$::4xnls::gfp]* transgene. The arrowheads

indicate PHshL and hollow arrowheads extra PHshL. PHshR is on the other side and

therefore out of focus. (E) Quantification of the percentage of animals with extra cells

when analyzed by *ajm-1::gfp*, *P$_{dpy-7}$::2xnls::yfp*, or *P$_{ver-1}$::4xnls::gfp* (n≥30).

Alleles used here: *grp-1(gm350)* and *ced-3(n717)*. Scale bar: 10 μm.
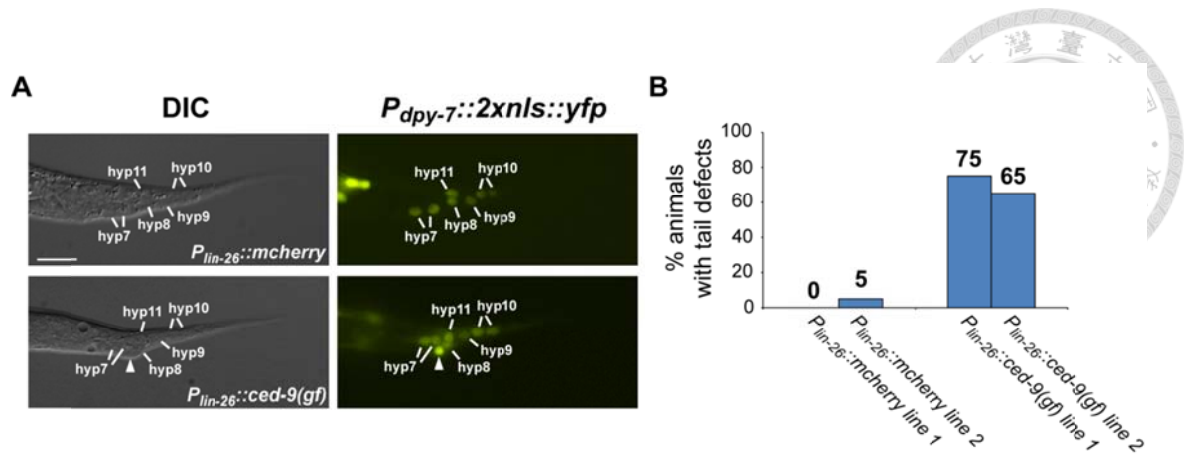
Figure 5. Extra hyp8/9 is sufficient to cause the tail defect.

(A) The DIC and YFP images of *grp-1; arIs99[P_{dpy-7}::2xnls::yfp]* mutant carrying either the *P_{lin-26}::mcherry* or *P_{lin-26}::ced-9(gf)* transgene are shown. The nuclei of hyp7-11 are pointed out and the arrowhead indicates extra hyp8/9. Scale bar: 10 μm. (B) Quantification of the percentage of indicated transgenic animals with tail defects (n≥30).
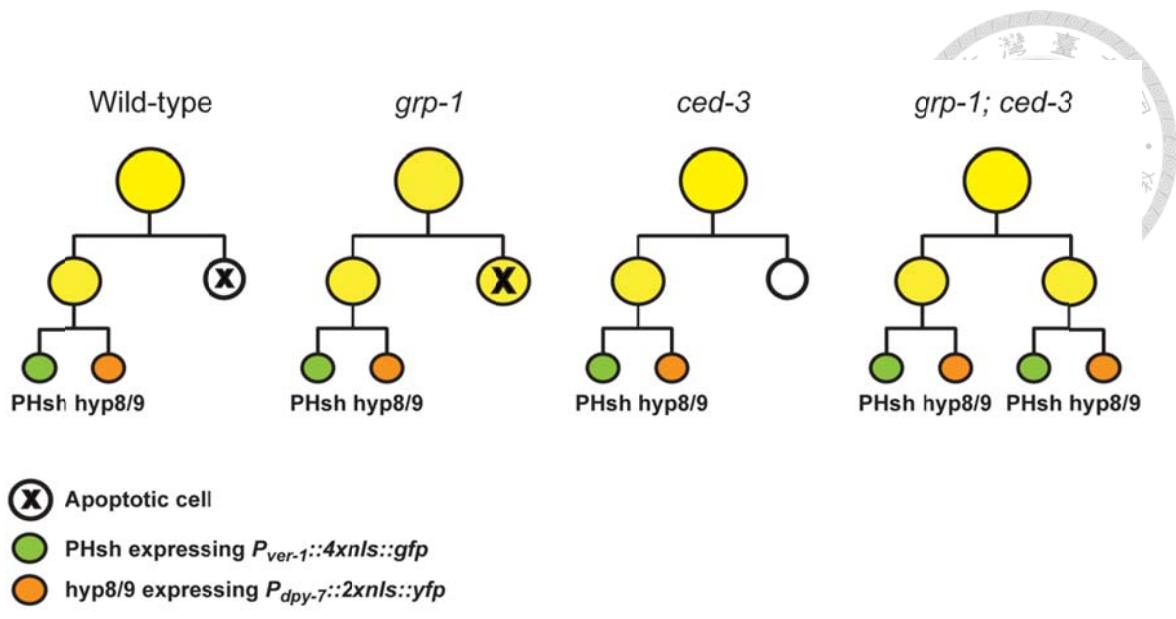
Figure 6. The proposed lineages in worms of the indicated genotypes.
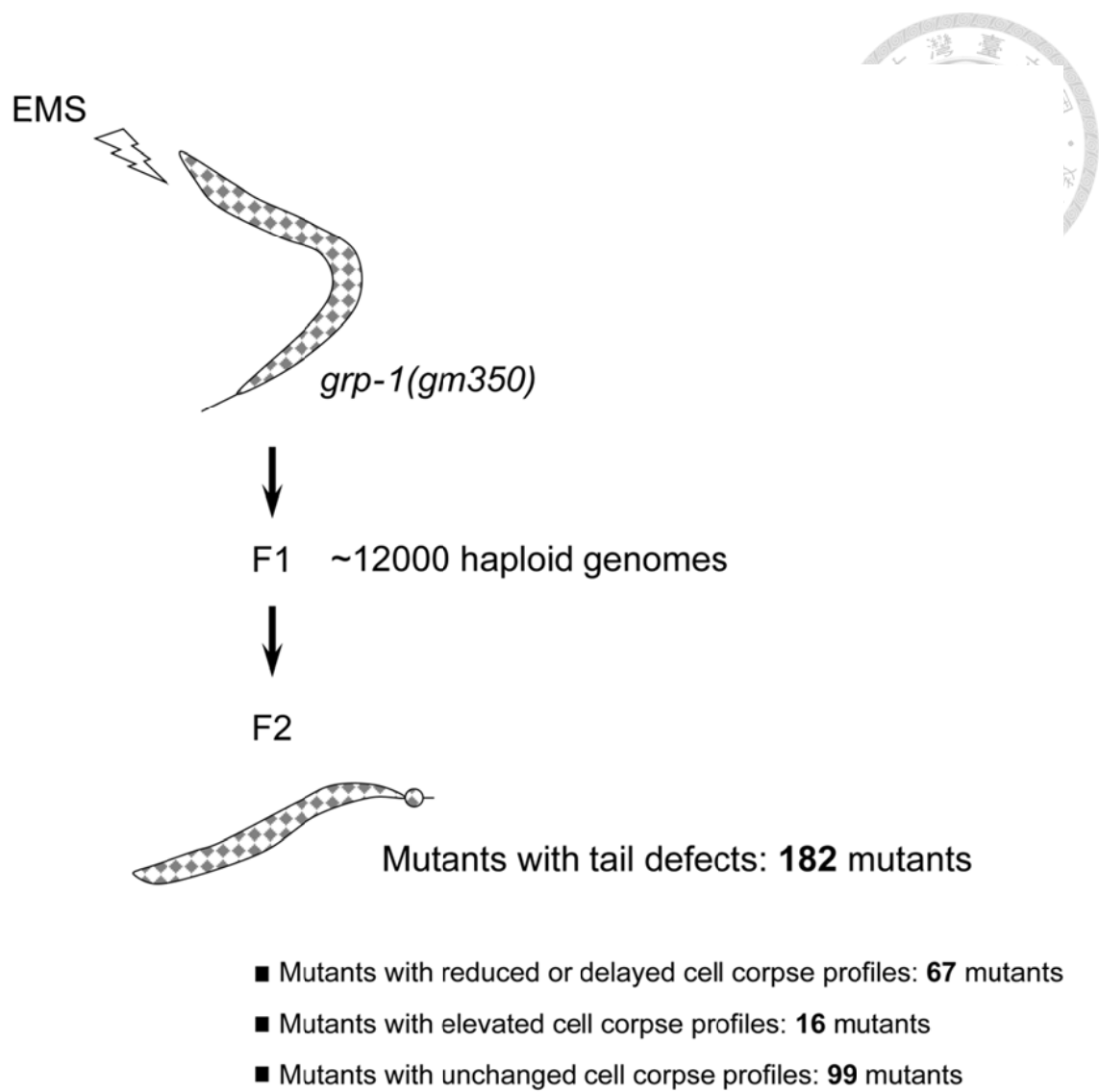
Figure 7. The flowchart and brief description of a genetic screen to isolate mutants with tail defects in the *grp-1* sensitized background.

See text and Materials and Methods for detail.
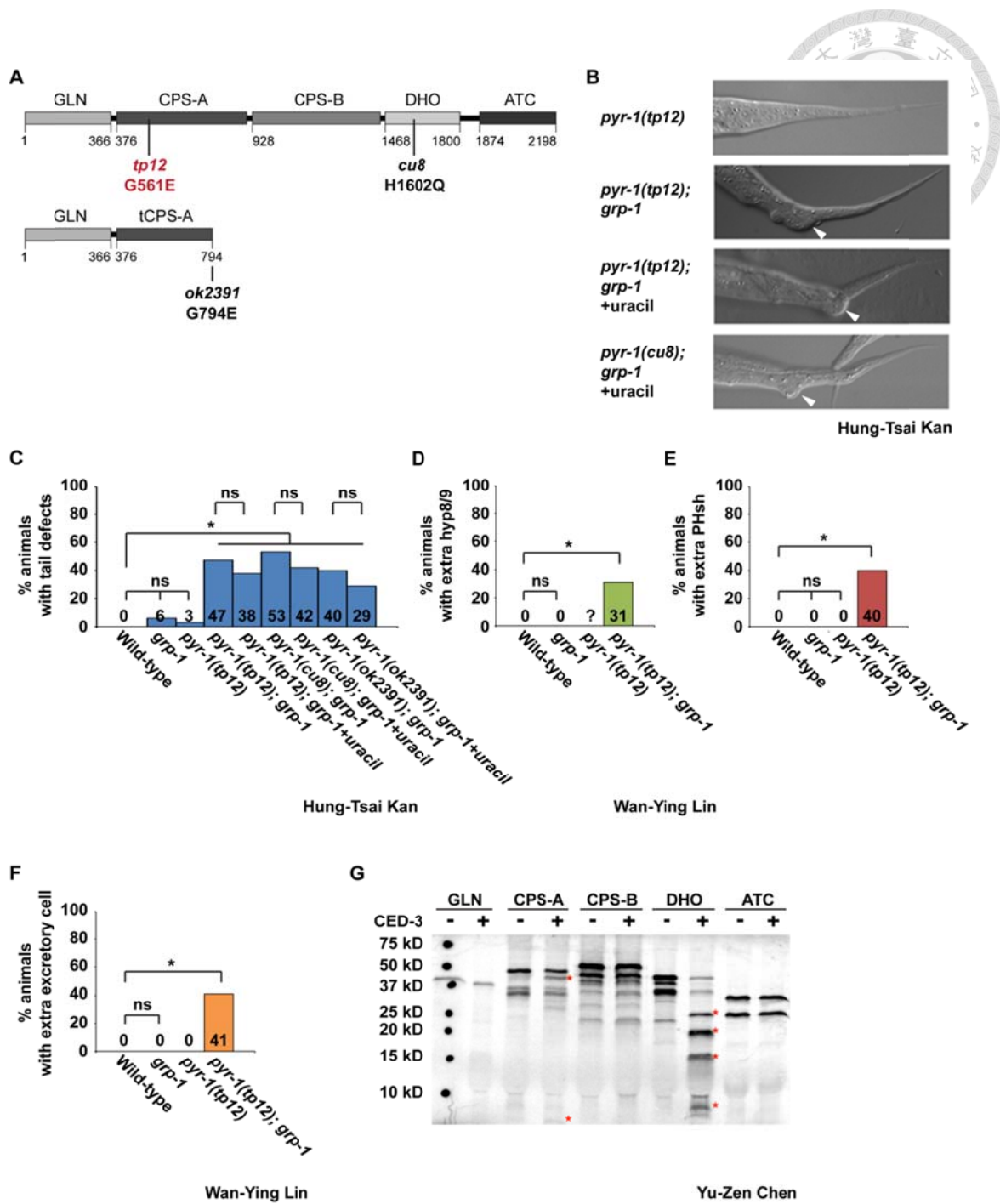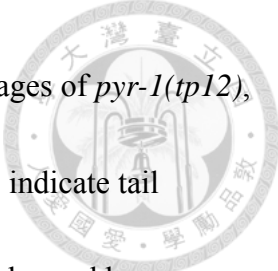
Figure 8. PYR-1 can be cleaved by CED-3 in vitro and is important in the PCD of the aunt cells of hyp8/9 and excretory cell.

(A) A schematic diagram of the PYR-1 domain structure. The numbers of amino acid

residues and mutations used in this study are shown. (B) The DIC images of *pyr-1(tp12)*,

pyr-1(tp12); grp-1, and *pyr-1(cu8); grp-1* are shown. The arrowheads indicate tail

defects. The uracil supplement does not rescue the tail defect. The allele used here:

grp-1(gm350). (C-F) The percentages of animals with tail defects (C), extra hyp8/9 (D),

extra PHsh (E), and extra excretory cell (F) of indicated genotypes are shown (n≥30). *

indicates $P<0.05$ (Fisher's exact test). ns indicates no statistical difference ($P>0.05$,

Fisher's exact test). The allele used here: *grp-1(gm350).* (G) PYR-1 can be cleaved by

CED-3 in *vitro*. Different domains of PYR-1 were synthesized and labelled with

[35]S-methionine using TNT Transcription/Translation coupled system (Promega) and

incubated without (-) or with (+) purified CED-3 at 30°C for 2 hours. The reactions

were then resolved by 15% SDS-PAGE.
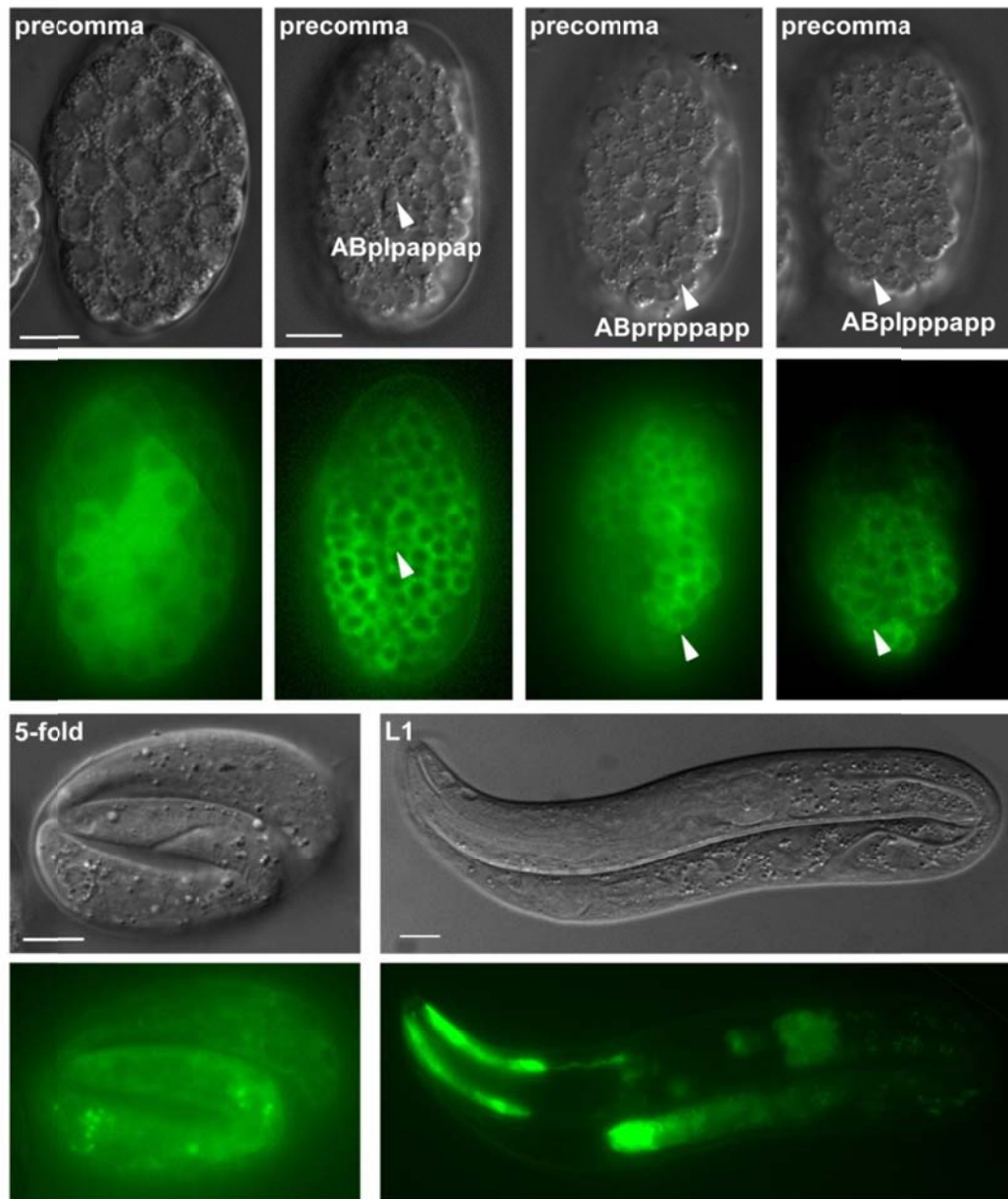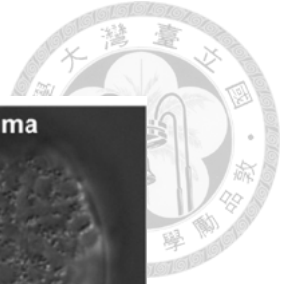
Figure 9. The expression pattern of *pyr-1*.

The DIC and GFP images of *pyr-1(tp12)* mutant carrying the *P~pyr-1~::pyr-1::gfp* transgene at indicated stages are shown. The arrowheads indicate ABplpappap (the aunt cell of excretory cell) or ABpl/rpppapp (the aunt cells of hyp8/9). Scale bar: 10 μm.

Table 1. Defects in the induction, execution, or kinetics of PCD cause tail defects in the *grp-1* background.

Genotype	% animals with tail defects
Wild-type	0
grp-1(gm350)	6
egl-1(n1084n3082)	2
grp-1(gm350); egl-1(n1084n3082)	87
ced-9(n1950)	5
grp-1(gm350) ced-9(n1950)	94
ced-4(n1162)	8
ced-4(n1162) grp-1(gm350)	94
ced-3(n717)	1
grp-1(gm350); ced-3(n717)	86
ced-3(n2427)	0
grp-1(gm350); ced-3(n2427)	92
ced-3(n2923)	1
grp-1(gm350); ced-3(n2923)	43
ced-8(n1891)	0
grp-1(gm350); ced-8(n1891)	80
ced-1(e1735)	0
ced-1(e1735); grp-1(gm350)	8
ced-12(bz187)	1
ced-12(bz187); grp-1(gm350)	8
cps-6(ok1718)	0
cps-6(ok1718); grp-1(gm350)	8

The tail defects of indicated genotypes were scored at L3-L4 stages under a dissecting microscope (n≥50).

Table 1. Defects in the induction, execution, or kinetics of PCD cause tail defects in the *grp-1* background.

Table 2. Mutants with known *ced* genes (22 mutants)

strains	% animals with tail defects	of cell corpses		chromosome	gene
		1.5-fold	4-fold		
grp-1(gm350)	6	11.70	0.30		
HS0128	76	13.30	0.90	V	*egl-1*
JH0003	66	8.10*	0.40	V	*egl-1*
JH0013	64	6.30*	0.10	V	*egl-1*
CH9361	28	7.90*	0.40	V	*egl-1*
CH4268	63	6.50*	0.60	III	*ced-4*
JH0024	59	8.40*	0.30	III	*ced-4*
JH0012	56	5.60*	0.30	III	*ced-4*
CH8006	25	9.50*	3.10*	III	*ced-4*
CH6317	97	6.40*	0.47	IV	*ced-3*
JH0002	92	6.30*	0.40	IV	*ced-3*
HS0813	90	1.30*	0.10	IV	*ced-3*
JH0030	90	0.30*	0.30	IV	*ced-3*
JH0020	90	5.10*	0.70	IV	*ced-3*
JH0063	84	2.60*	4.30*	IV	*ced-3*
CH9298	94	9.20*	0.63	X	*ced-8*
CH2055	77	2.00*	6.70	X	*ced-8*
JH0025	72	9.20*	0.30	X	*ced-8*
JH0054	58	7.40*	12.30*	X	*ced-8*
HS0751	43	4.20*	4.60*	X	*ced-8*
JH0035	46	8.00*	0.30	III	*ced-11*
JH0039	42	0.30*	0.00	III	*ced-11*
HS0078	38	0.30*	0.40	III	*ced-11*

All strains contain *grp-1(gm350)*. The percentage of animals with tail defects were scored under the dissecting microscope (n ≥ 30). The average numbers of cell corpses scored at the indicated developmental stages are presented (n ≥ 20). Mutant embryos were compared to *grp-1(gm350)* (*P<0.05, two-tailed t test).
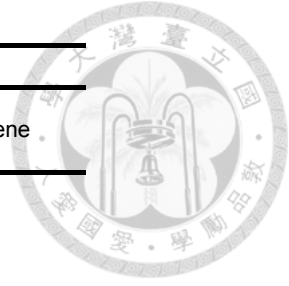
Table 2. mutants with known *ced* genes (22 mutants).

Table 3. Mutants with reduced or delayed cell corpse profiles (45 mutants)

strains	% animals with tail defects	No. of cell corpses		chromosome	gene
		1.5-fold	4-fold		
grp-1(gm350)	6	11.70	0.30		
CH2038	46	5.50*	0.40	I	
JH0056	30	8.70*	0.20	I	
JH0007	24	8.50*	0.50	I	
HS0190	74	7.30*	1.30*	II	*pyr-1*
CH2125	57	9.00*	0.40	II	
CH2121	27	9.30*	0.80	II	
CH8358	40	9.40*	0.40	III	
JH0052	38	7.70*	0.30	III	
HS0577	94	7.60*	0.00*	IV	
CH6168	45	3.30*	0.20	IV	
JH0016	42	9.10*	1.40*	IV	
JH0006	42	6.10*	0.70	IV	*klp-11*
CH1066	39	7.50*	0.70	IV	
HS0414	33	9.70*	0.80	IV	
CH2295	23	7.60*	0.40	IV	
KY6012	77	8.30*	0.20	V	
JH0062	61	7.30*	0.20	X	
HS0538	53	8.60*	0.20	X	
CH2526	49	7.00*	0.50	X	
CH2519	37	7.90*	0.70	X	
CH2326	31	5.20*	0.30	X	
CH2126	28	4.30*	0.20	X	
JS0010	32	5.50*	0.40	V?	
CH4095	33	8.00*	0.80*	I and V	
CH9436	61	8.20*	1.20*	II or V	
CH2535	58	9.50*	0.50	III or IV	
CH2018	42	8.20*	0.40	III or V	
JS0009	19	9.33*	0.50	III or V	
JH0019	59	9.20*	0.30		
CH9438	47	9.00*	0.80		
JH0046	45	9.40*	0.50		
KY6011	43	3.50*	0.40		
CH7070	42	8.30*	0.10		
CH9928	41	6.10*	0.50		
CH2431	38	8.10*	0.10		
CH8340	36	7.70*	0.30		
CH6172	36	9.70*	1.00*		
CH2004	33	7.80*	0.30		
CH7152	31	7.70*	0.30		
CH8400	31	7.70*	0.30		
JH0009	27	7.70*	0.30		
CH9160	27	9.60*	0.20		
KY7029	26	10.00*	0.50		
CH2096	24	9.40*	0.40		
CH2112	20	7.50*	0.20		

All strains contain *grp-1(gm350)*. The percentage of animals with tail defects were scored under the dissecting microscope (n ≥ 30). The average numbers of cell corpses scored at the indicated developmental stages are presented (n ≥ 20). Mutant embryos were compared to *grp-1(gm350)* (*P < 0.05, two-tailed t test).

Table 3. mutants with reduced or delayed cell corpse profiles (45 mutants).

Table 4. Mutants with increased numbers of cell corpses (16 mutants)

strains	% animals with tail defects	No. of cell corpses		chromosome	gene
		1.5-fold	4-fold		
grp-1(gm350)	6	12.00	0.60		
CH9476	57	13.70*	0.30	II	
CH8121	60	11.90	3.90*	III	
JS0008	51	16.50*	1.40*	III	
CH8037	30	14.50*	0.80	III	
HS0127	21	20.50*	4.80*	III	
JS0013	73	14.00*	0.60	IV	
KY6015	86	16.30*	0.30	V	
HS1245	77	16.60*	0.90	X	
HS0199	97	16.40*	0.60	II	
JH0064	46	11.70	1.90*	X	
HS0013	55	15.90*	0.50		
CH2524	49	11.70	1.70*		
JH0021	48	15.20*	0.60		
HS1067	38	15.60*	0.90		
HS0100	36	13.10	1.70*		
JH0040	32	12.00	1.30*		

All strains contain *grp-1(gm350)*. The percentage of animals with tail defects were scored under the dissecting microscope (n≥30). The average numbers of cell corpses scored at the indicated developmental stages are presented (n≥20). Mutant embryos were compared to *grp-1(gm350)* (*P<0.05, two-tailed t test).

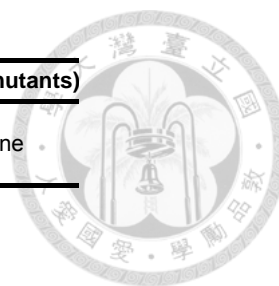**Table 4. Mutants with increased numbers of cell corpses (16 mutants).**

Table 5. Mutants with unchanged numbers of cell corpses (*grp-1*-dependent, 39 mutants)

strains	% animals with tail defects	No. of cell corpses		chromosome	gene
		1.5-fold	4-fold		
grp-1(gm350)	6	12.00	0.60		
JH0008	88	11.10	0.30	I	
HS0541	77	11.40	0.50	I	
JS0012	44	10.60	0.70		
JH0017	91	11.80	0.50	II	
JH0026	74	11.10	0.50	II	
CH2464	43	11.40	0.20	II	
KY1024	92	11.50	0.80	III	
CH4141	59	11.10	0.30	III	
KY4010	42	12.30	0.50	III	
JS0002	91	13.00	0.70	IV	
CH9158	88	10.80	0.20	IV	
JH0011	66	11.70	0.60	IV	
JH0051	43	13.30	0.40	IV	
JH0028	81	13.80	0.60	V	
JS0005	67	11.00	0.40	X	
CH2491	56	14.30	0.30	X	
HS0090	39	11.90	0.50	X	
CH8130	69	11.50	0.10	I?	
CH9899	67	10.20	0.40	I?	
HS0196	95	13.80	0.60	X?	
HS0469	42	10.80	0.40	I or X	
JH0065	60	12.60	0.40	II or V	
KY7049	40	11.30	0.20	IV or X	
CH9533	55	11.90	0.40	V or X	
JH0023	73	11.90	0.30		
JH0042	72	11.10	0.30		
JH0031	56	10.50	0.70		
JH0053	55	11.20	0.40		
KY8082	50	11.20	0.30		
CH8043	49	11.10	0.30		
HS0188	47	10.60	0.50		
JH0061	45	11.10	0.30		
HS0053	44	11.80	0.40		
JH0014	44	10.80	0.50		
CH2368	43	11.10	0.40		
CH6318	43	11.00	0.20		
CH2083	42	11.00	0.50		
CH4088	42	13.30	0.60		
CH6264	42	12.30	0.30		

All strains contain *grp-1(gm350)*. The percentage of animals with tail defects were scored under the dissecting microscope (n≥30). The average numbers of cell corpses scored at the indicated developmental stages are presented (n≥20). Mutant embryos were compared to *grp-1(gm350)* (*P<0.05, two-tailed t test).

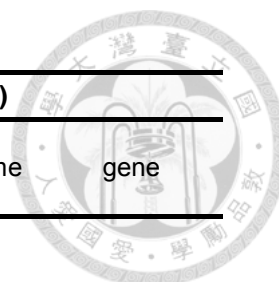**Table 5. Mutants with unchanged numbers of cell corpses (*grp-1*-dependent, 39 mutants).**

Table 6. Mutants whose tail defects are *grp-1*-independent (24 mutants)

strains	% animals with tail defects	No. of cell corpses		chromosome	gene
		1.5-fold	4-fold		
grp-1(gm350)	6	12.00	0.60		
JH0018	83	11.10	0.20	I	
JS0004	99	10.00	0.40	II	*vab-9*
JS0003	90	8.40*	0.30	II	
JH0060	61	9.70	0.20	II	
JH0055	41	11.30	0.30	II	
JH0057	67	11.10	0.50	III	
JH0029	83	8.60*	0.20	IV	
CH8386	44	9.70	0.20	IV	
HS0157	56	10.20	0.10	V	
KY8018	44	11.20	0.70	V	
CH6041	100	9.70*	0.20	X	*K02E10.4*
JS0006	99	12.50	0.50	X	*K02E10.4*
HS1096	97	10.60	0.40	X	*K02E10.4*
CH2251	81	11.90	0.20	X	
HS0325	77	9.50*	0.90	X	
HS0513	71	11.80	0.20	X	
JH0041	75	14.40	0.60	II or IV	
HS0045	99	10.20	0.20	III or IV	
JS0007	77	11.30	0.50		
JH0066	67	12.10	1.00		
HS0439	64	10.60	0.40		
HS1187	57	11.80	0.50		
HS1117	45	16.80*	0.60		
HS1172	41	14.80*	0.90		

All strains contain *grp-1(gm350)*. The percentage of animals with tail defects were scored under the dissecting microscope (n≥30). The average numbers of cell corpses scored at the indicated developmental stages are presented (n≥20). Mutant embryos were compared to *grp-1(gm350)* (*P<0.05, two-tailed t test).

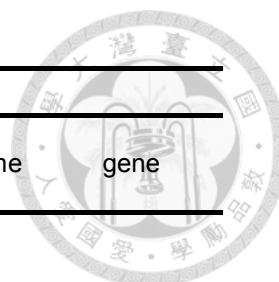**Table 6. Mutants whose tail defects are *grp-1*-independent (24 mutants).**

Table 7. Unanalyzed mutants (36 mutants)

strains	% animals with tail defects	No. of cell corpses		chromosome	gene
		1.5-fold	4-fold		
grp-1(gm350)	6	12.00	0.60		
JH0004	38	13.40	0.20		
JH0027	38	11.60	0.60		
JS0011	38	11.20	0.50		
CH4067	38	10.30	0.50		
JH0001	37	10.80	0.40		
CH2402	37	10.80	0.40		
CH2514	37	11.70	0.20		
CH8267	37	10.90	0.20		
HS0032	36	10.30	0.80		
KY1037	36	11.90	0.30		
JH0059	35	11.10	0.60		
JH0037	33	11.80	0.50		
JH0048	32	12.30	0.30		
JH0044	31	11.50	0.30		
JH0058	31	11.80	0.30		
KY6023	31	11.80	0.50		
JH0045	30	10.80	0.20		
CH8381	29	12.00	0.30		
JS0001	28	11.50	0.30		
CH8182	28	11.30	0.50		
CH8215	28	11.10	0.60		
JH0038	27	12.10	0.40		
JH0033	27	10.00	0.30		
CH4138	27	10.90	0.70		
CH6401	27	11.20	0.50		
HS0070	26	12.10	0.60		
CH9610	26	10.50	0.70		
JH0015	25	10.20	0.20		
CH2293	24	10.60	0.30		
CH8301	24	12.10	0.40		
CH8406	24	11.50	0.40		
CH6392	23	11.50	0.30		
CH4256	21	10.50	0.50		
CH7443	22	11.40	0.80		
CH8156	22	11.50	0.30		
CH2071	20	11.00	0.40		

All strains contain *grp-1(gm350)*. The percentage of animals with tail defects were scored under the dissecting microscope (n ≥ 30). The average numbers of cell corpses scored at the indicated developmental stages are presented (n ≥ 20). Mutant embryos were compared to *grp-1(gm350)* (*P<0.05, two-tailed t test).

Table 7. Unanalyzed mutants (36 mutants).

APPENDIX
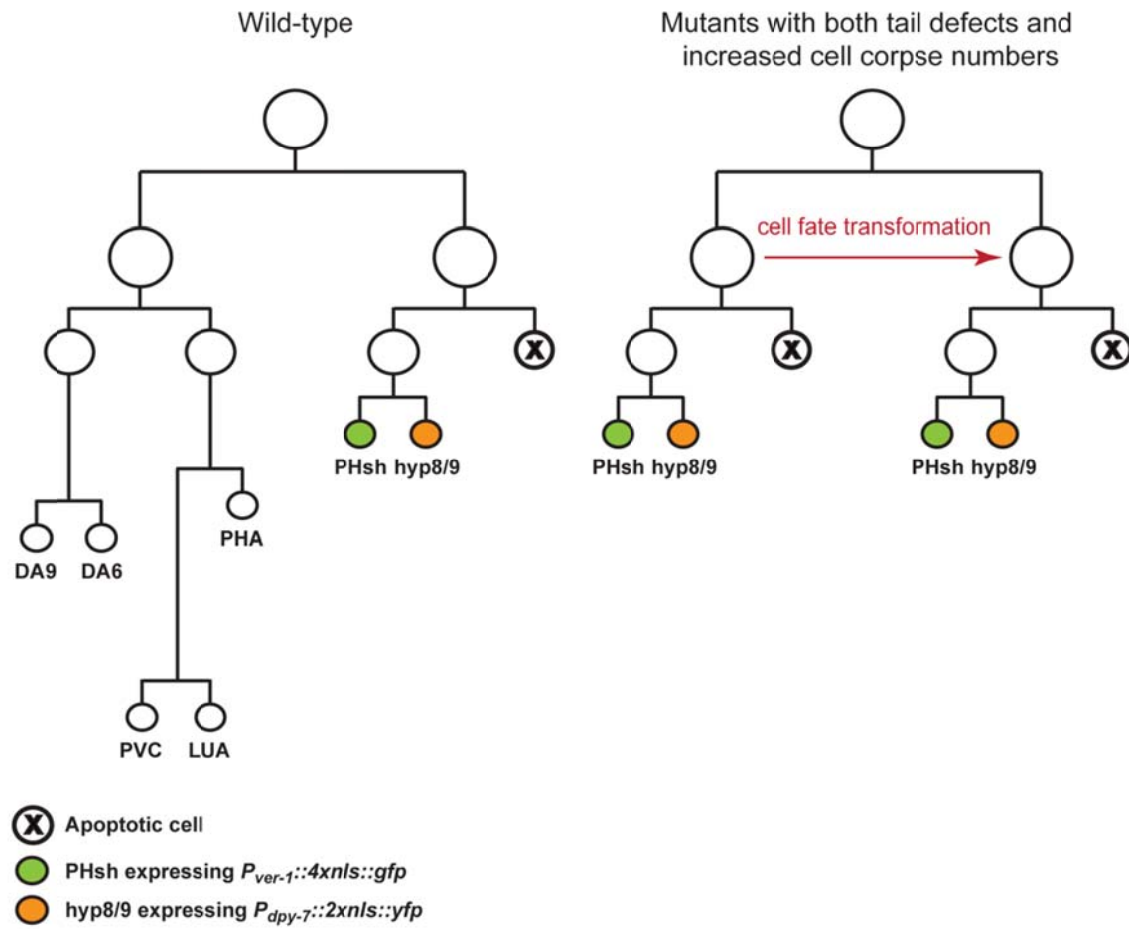
Appendix 1. A proposed lineage in the mutants with both tail defects and increased numbers of cell corpses.